REPORT DOCUMENTATION PAGE

Form Approved
OMB No. 0704-0188

1. AGENCY USE ONLY (Leave blank)	2. REPORT DATE	3. REPORT TYPE AND DATES COVERED
		FINAL REPORT - 30 Sep 92 - 31 Oct 95

4. TITLE AND SUBTITLE
High Frequency Optoelectronic Integrated Systems

5. FUNDING NUMBERS
61102F
2301/AS

6. AUTHOR(S)
Professor Fetterman

7. PERFORMING ORGANIZATION NAME(S) AND ADDRESS(ES)
Electrical Engineering Department
Univ of California, Los Angeles
Los Angeles, CA 90095-1594

AFOSR-TR-96
0138

9. SPONSORING / MONITORING AGENCY NAME(S) AND ADDRESS(ES)
AFOSR/NE
110 Duncan Avenue Suite B115
Bolling AFB DC 20332-0001

10. SPONSORING / MONITORING AGENCY REPORT NUMBER
F49620-92-J-0535

11. SUPPLEMENTARY NOTES

19960408 075

12a. DISTRIBUTION / AVAILABILITY STATEMENT
APPROVED FOR PUBLIC RELEASE: DISTRIBUTION UNLIMITED

12b. DISTRIBUTION CODE

13. ABSTRACT *(Maximum 200 words)*

In this high frequency optoelectronic program we have investigated the development of optical components and elements for integration of light into microwave and millimeterwave systems. This involved the development of new types of modulators, detectors and on wafer optical guides. Particular attention was paid to the requirements of integration and epitaxial liftoff was investigated as a means of incorporating different materials technologies. In combination with our polyimide optical guides, active polymer modulators, and microwave elements, this lift off technology has permitted the development of new unique systems. Both HEMT and HBT phototransistors were developed and tested in this effort using picosecond techniques and optical mixing. A unique traveling wave HBT, side coupled phototransistor has been designed and fabricated.

14. SUBJECT TERMS

15. NUMBER OF PAGES

16. PRICE CODE

17. SECURITY CLASSIFICATION OF REPORT	18. SECURITY CLASSIFICATION OF THIS PAGE	19. SECURITY CLASSIFICATION OF ABSTRACT	20. LIMITATION OF ABSTRACT
UNCLASSIFIED	UNCLASSIFIED	UNCLASSIFIED	

DISCLAIMER NOTICE

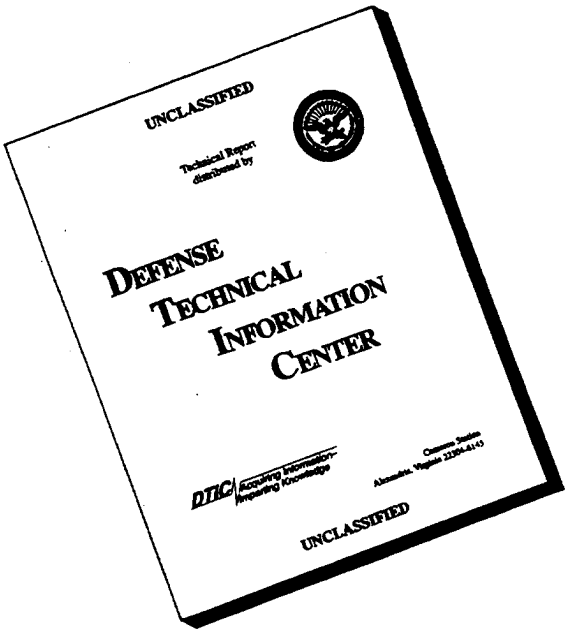

THIS DOCUMENT IS BEST QUALITY AVAILABLE. THE COPY FURNISHED TO DTIC CONTAINED A SIGNIFICANT NUMBER OF PAGES WHICH DO NOT REPRODUCE LEGIBLY.

FINAL REPORT

AIR FORCE OFFICE OF SCIENTIFIC RESEARCH

AWARD # F49620-92-J-0535

30 Sept. 92 - 31 Oct 95

HIGH FREQUENCY OPTOELECTRONIC INTEGRATED SYSTEMS

UCLA

HAROLD FETTERMAN

HIGH FREQUENCY OPTOELECTRONIC INTEGRATED SYSTEMS

HAROLD FETTERMAN
UCLA EE Department

In this high frequency optoelectronic program we have investigated the development of optical components and elements for integration of light into microwave and millimeterwave systems. This involved the development of new types of modulators, detectors and on wafer optical guides. Particular attention was paid to the requirements of integration and epitaxial liftoff was investigated as a means of incorporating different materials technologies. In combination with our polyimide optical guides, active polymer modulators, and microwave elements, this lift off technology has permitted the development of new unique systems. Both HEMT and HBT phototransistors were developed and tested in this effort using picosecond techniques and optical mixing. A unique traveling wave HBT, side coupled phototransistor has been designed and fabricated.

The effort, in addition to investigating new devices, also examined new application areas using this technology. This included optically controlled phase array radars and optically integrated microwave phase conjugation arrays. Both of these areas were investigated and novel configurations developed. These are in process of publication and preliminary versions are attached. The serial-feed phased array radar is particularly interesting since it reduces the complexity of the system to the point that it becomes economically viable. The phase conjugation effort brings the concept of nonlinear active surfaces into millimeterwave technology.

OPTICAL MODULATION

One of the major requirements in developing integrated (wafer scale) technology was to have a compatible, inexpensive, high frequency device for imposing modulation on optical signals. The method of choice that we concentrated upon was a polymer implementation and was developed in collaboration with Professor Steier's group at USC. The basic concept used a cross-linked polyurethane-Disperse Red polymer in a traveling wave structure as shown in figure 1.

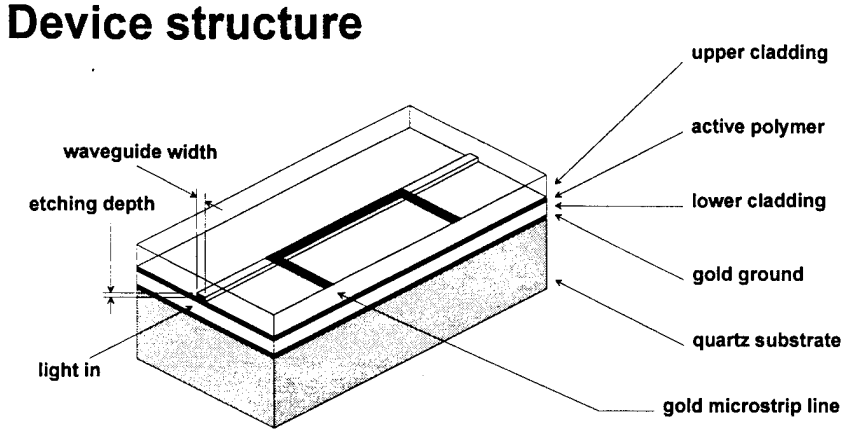

Figure 1

The initial measurements[1] in this approach showed excellent results up to 22 GHz, the limit of our spectrum analyzer. Using microwave mixers this work was then extended[2] up to 40 GHz as shown in figure 2.

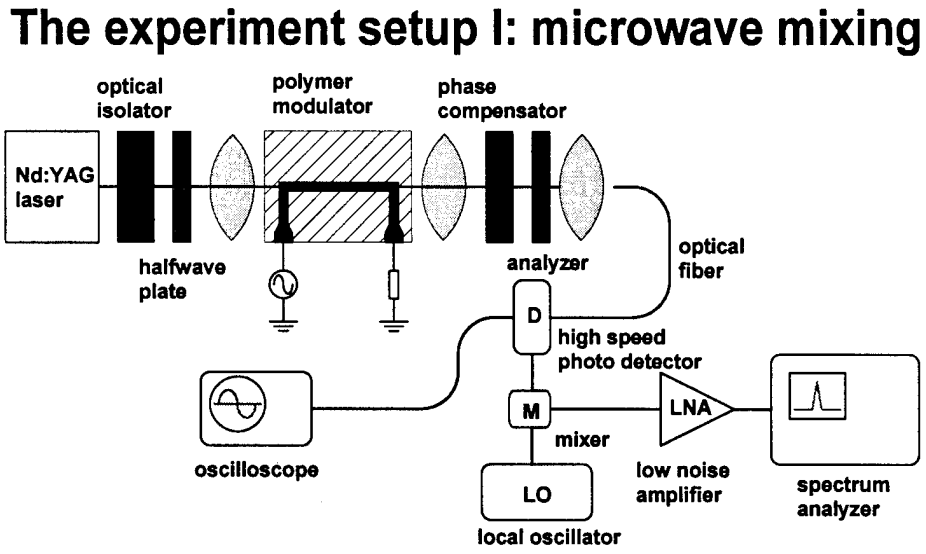

Figure 2

Finally, using a heterodyne approach with tunable 1.3micron lasers we reached 60 GHz with relatively[3] low loss (figures 3a & 3b). A similar technique using both mixing and optical heterodyne approaches has been incorporated into our 90 GHz measurement system. Higher frequency operation will be tested with tunable diode systems for heterodyne detection.

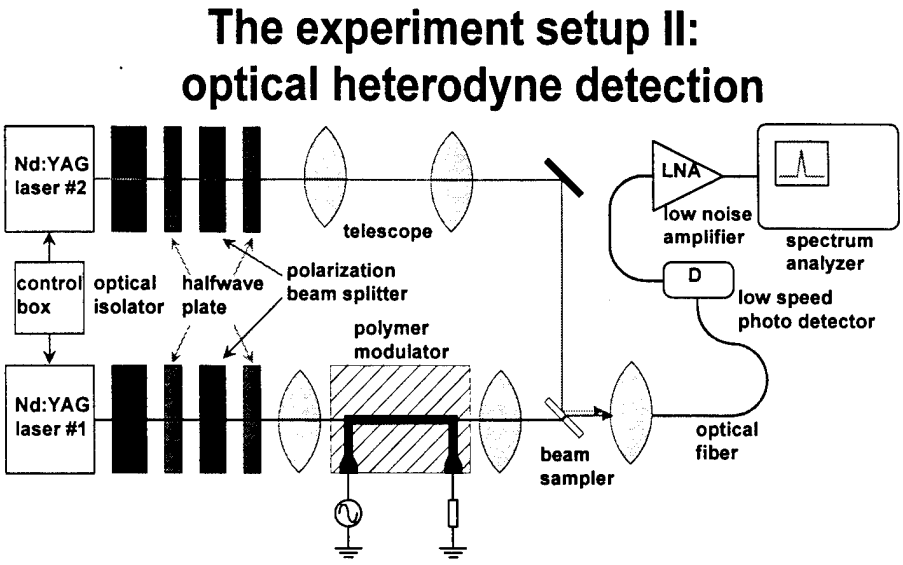

Figure 3a

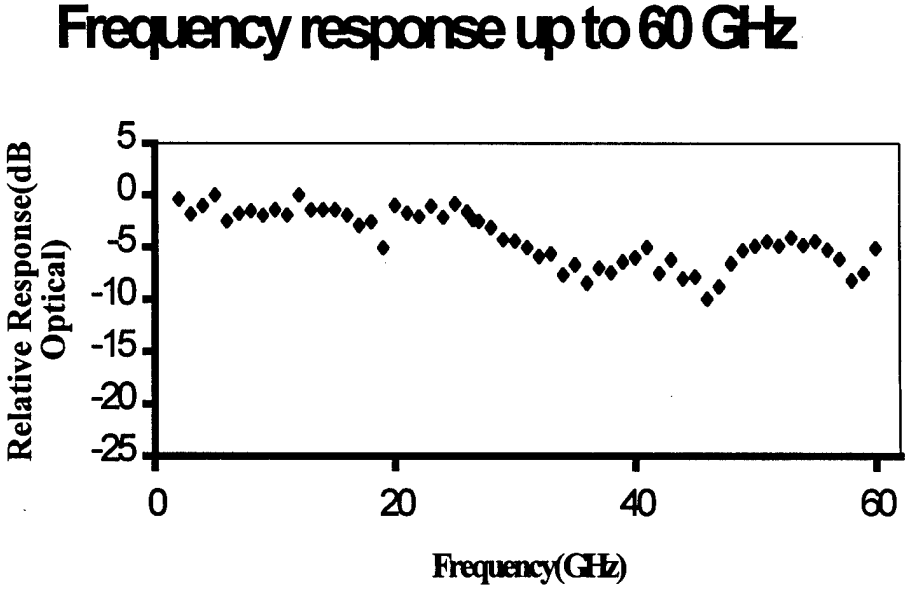

Figure 3b

This work was extended to 94 and 140 GHz with configurations having a lower Vπ. The systems we have designed uses a fin line approach with low impedance microstrip and is shown in figure 4. These modulators are compatible with all of our semiconductors, and with their active devices, and will be used as a basic element in our future systems. Prototype systems have been measured using our extended network

analyzers and show excellent microwave performance in the range of 75 to 100 GHz. This is largely a result of the extraordinary length-bandwidth product caused by the low dielectric constant.

$$(L\Delta f)_{\max} = \frac{c}{4\left|n - \sqrt{\varepsilon_{reff}}\right|}$$

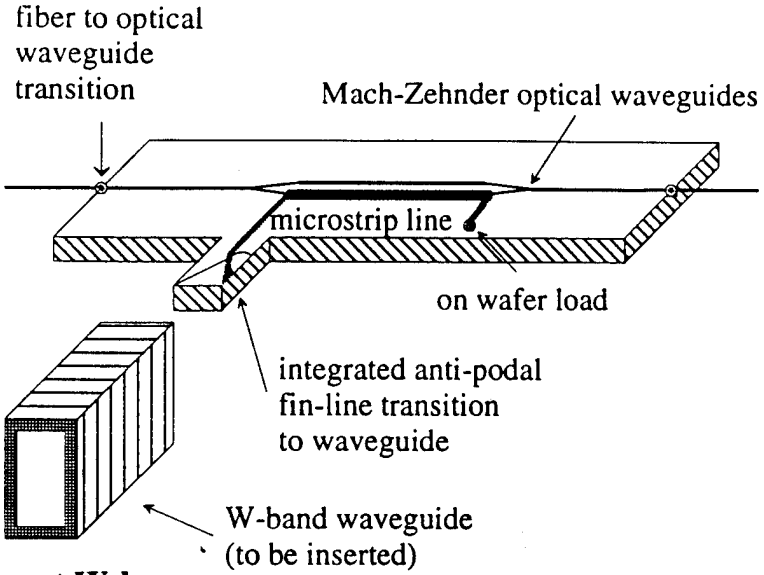

modulator at W-band

Figure 4a

The actual low loss S parameters are shown in figure 4b

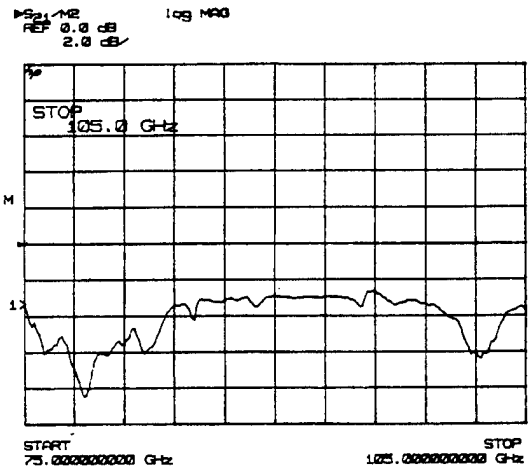

S_{21} of test circuit at W-band

4b

This basic device is expected to become the "standard" solution to the requirements of high speed modulation. Furthermore, the application in arrays looks very promising and will be continued in related contracts. The systems are stable, low loss and remarkable easy to incorporate into active systems involving photonics.

POLYIMIDE OPTICAL GUIDE AND GRAFTING

The key problem in using these devices is in bringing the radiation in and out of the guides. One of the ways we plan to investigate involves using our polyimide on wafer optical guide. This material has been used by us in making low loss guides, power splitters and delay lines[4] on a number of different types of wafers. The losses have been measured by us at visible and GaAs wavelengths and typically range about 0.3 dB/cm at 1.3 microns with single mode structures[5]. Complex structures have been fabricated using this technology and are extremely viable for systems integration. These results have also been extensively modeled using Beam Propagation software.

The polyimide and active polymer materials has now been connected on wafer in a low loss single mode approach. This has been demonstrated by a number of researchers in relatively simple structures. We have now incorporate our low loss 1.3 micron structures with our high frequency active materials using a serial grafting technique[6]. First our optical, filtered polyimide cladding is spin coated and baked. Then our EO polymer core layer is also spin coated and poled. Using O_2 RIE and a photoresist mask, channels of rectangular cross sections are then etched to define the active portion of the channel. The mask is then stripped and the grafted low loss polyimide to be grafted is spin coated and processed.

Finally, the passive polyimide channel core is formed using photolithography and RIE and integrated with the active guide. This basic concept of fabrication is indicated in figure 5. The problem which must now be addressed is the question of mode matching of the two systems. We are continuing to look at this problem. However an area that has also developed from this approach is coupling into our new traveling wave phototransistors from the side. This is discussed after our ELO section.

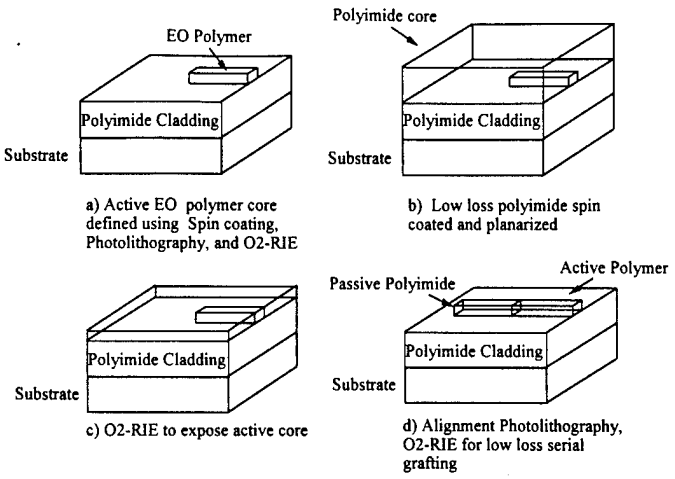

Fabrication of low loss connection between active polymer and low loss polyimide

Figure 5

PHOTOTRANSISTORS AND LIFTOFF

In addition to the work on guiding structures we have been studying the use of active phototransistors as detectors[7]. In figure 6a we show the optical gain of these devices which we measure by biasing the devices first as PIN devices and then as transistors. The figure indicates how the electrical and optical gains clearly track. In figure 6b we show the results of evanescent coupling using semiconducting guide into two serial devices.

$$\tau_{cd} = \frac{kT}{q} \frac{C_{be} + C_{bc}}{2I_{no}\left[\cosh\left(\frac{w_b}{L_{nb}}\right) - 1\right] + I_{peo} + I_{pco} + I_{bDC}}$$

As the equation shows the speed of the device is a strong function of the bias current and can be extremely fast.

In the figure I_c is plotted vs V_{ce} with I_b fixed at 2 μA. The optical power is changed from 1414 μW to 1200, 826, and 440. The powers coupled to the second HBT are down by a factor of approximately 20. These HBT with proper RF connections to the base and using appropriate bias connections to sweep out minority carriers have been tested to 60 GHz in our laboratories.

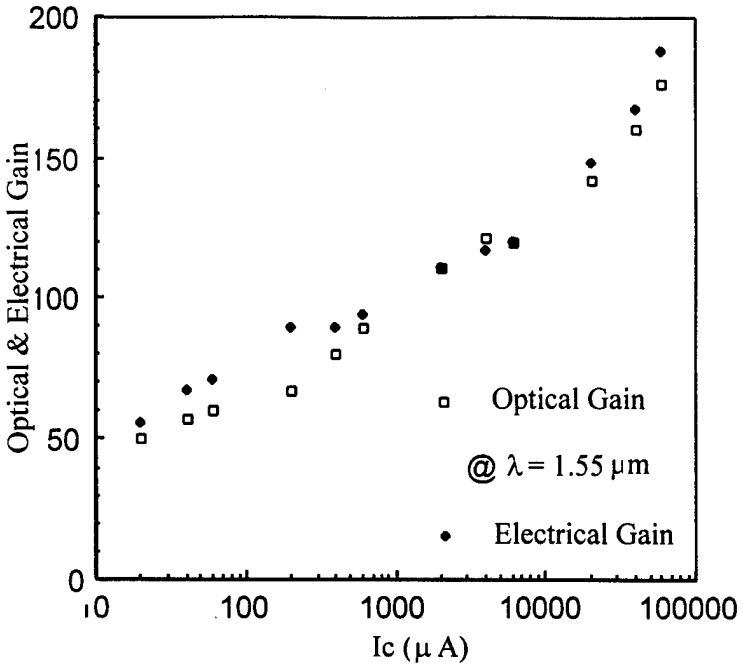

Figure 6a

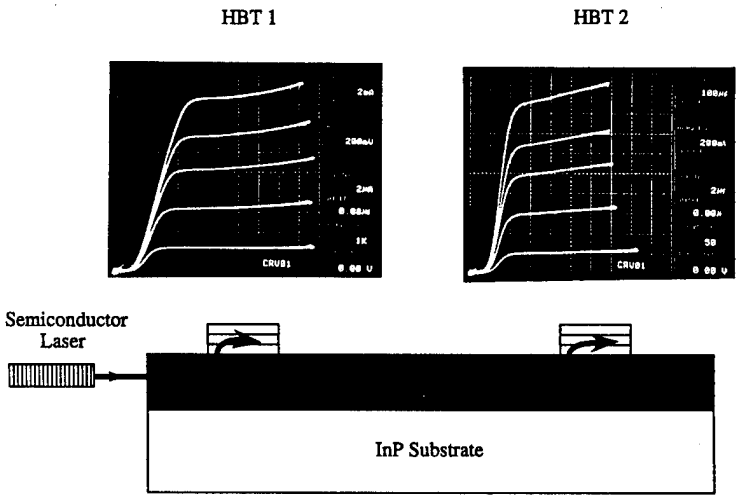

Figure 6b

The use of phototransistors, both HEMT and HBT, look extremely promising for our wafer integration approach except that there are certain material limitations. These can be avoided by using epitaxial lift off techniques. Recently we tested these concepts in lifting off a HEMT transistor and using it as a high frequency mixer[8]. Although the device was configured for relatively low frequencies it performed well (figure 7a) as an optical mixer up to 22 GHz (7b) and was limited by the range of the

spectrum analyzer we used. Our experiments have shown that there are consistently stronger signals (as much as a order of magnitude) obtained in this manner because of improved optical coupling efficiency, a decrease in substrate leakage, and an illumination-induced back gating effect.

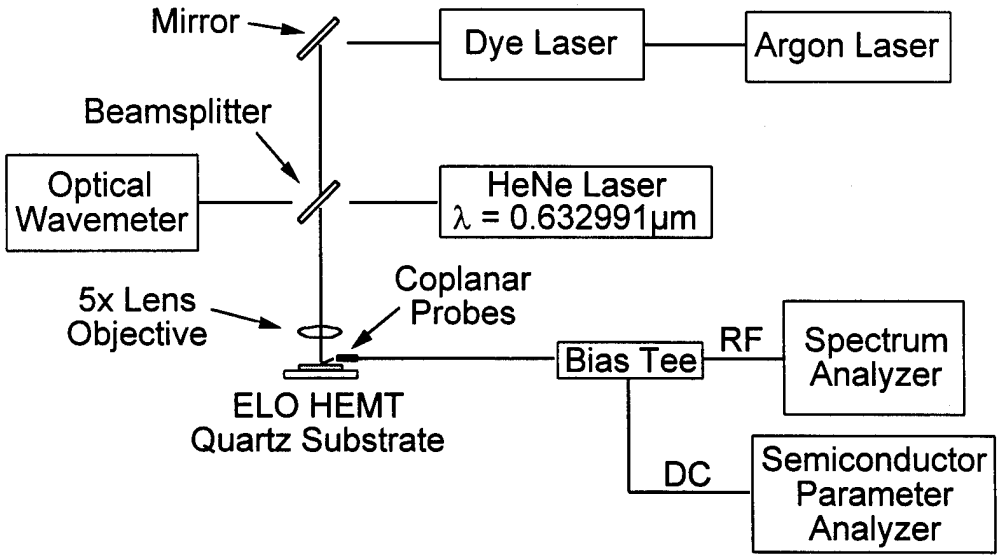

Figure 7a

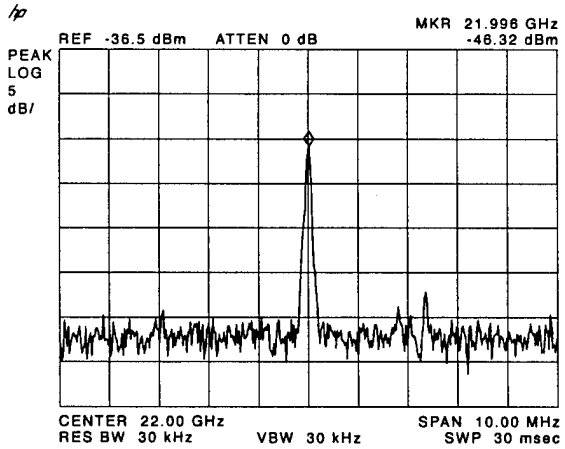

Figure 7b

Another technology that we have investigated involves a traveling wave Heterojunction Bipolar phototransistor. This has been extensively modeled and is shown in figure 8a. The modulated light is now injected into the polyimide guide and leaks into the base and collector regions along the length of the device. Figure 8b shows the simulation using the Beam Propagation Method (BPM) for this side coupling concept. Based upon these results , 90% of the light is absorbed in a device length of

800μm. Based upon of first generation of devices in this effort we expect that these devices will work well , with optical gain up to 100 GHz, and will become an important part of future millimeterwave optoelectronic systems. The final advanced devices are in the process of fabrication with the help of TRW.

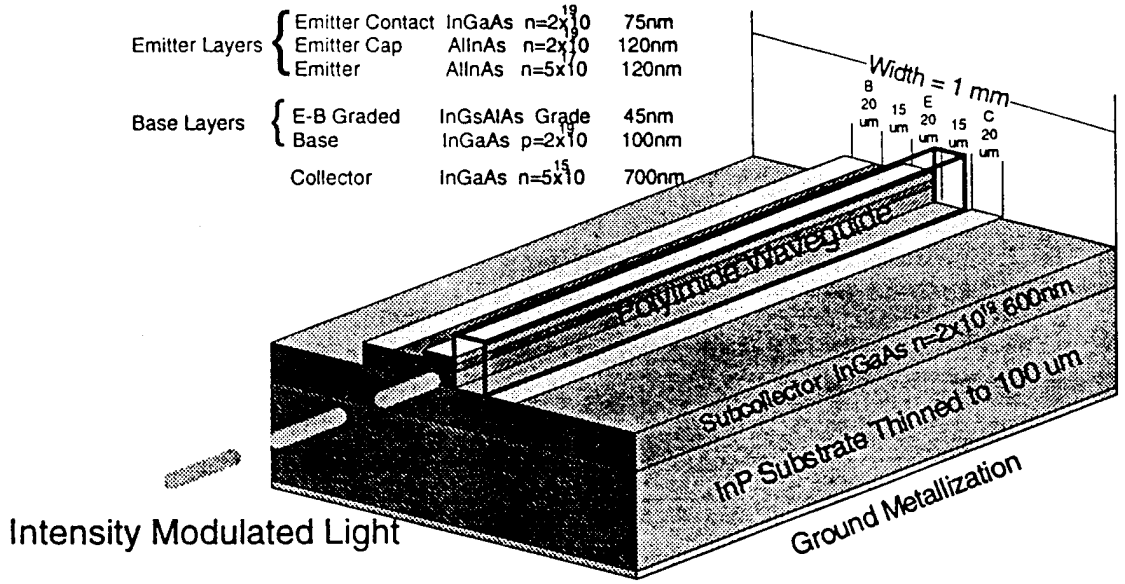

Schematic of TW-HPT utilizing the TRW baseline layer structure and an integrated polyimide optical waveguide

Figure 8a

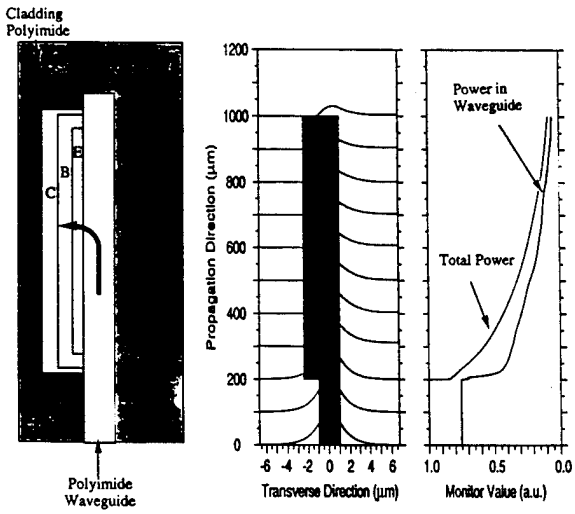

8b BPM simulation of side-coupled TW-HPT showing 800μm coupling length.

PHASE CONJUGATION

Microwave phase conjugation has been of interest to us for a number of years and we have been looking at the possibility of using nonlinear artificial materials based upon shaped microparticles. Recently we have found that mixing elements with antennas can be used to conjugate the wave at a given point. Then by using an array of elements it is possible to conjugate an entire wave front.

Efforts to examine this concept were made as much as 30 years ago and were largely abandoned because of the difficulties of bringing so many components together and controlling the microwave phase terms[9].[10] In the current work we propose to bring the microwave signal with the phase and frequency information to the mixing devices optically. An array of optically injected devices will then be used to generate the spatial conjugate waves.

To demonstrate the concept of using microwave devices in Three Wave Mixing to generate conjugate phase, a triple balanced mixer can be used as the nonlinear element. The mixer output signal can be written as:

$$V_{IF} = a(V_{LO} + V_{RF})^2 \qquad (1)$$

The conjugate phase arises from the term with the difference frequency: $\omega_{LO} - \omega_{RF}$. The incoming signal sending into the RF port of the mixer carries a phase factor $\omega t + \varphi$. It is mixed with $2\omega t$ (LO) to generate the conjugate phase: $\omega t - \varphi$ (IF). The other second-order terms can be filtered out by a bandpass filter.

It is also possible to implement this system using a system of mixing which closely resembles Four Wave Mixing. This would have the advantage of completely eliminating the original probe wave. It is important to note however that in three wave mixing the interaction takes place completely on a surface and does not require phase matching.

Our initial efforts to demonstrate optical injection used fiber optics feeds and eliminated the need of a frequency doubling amplifier for generating the pump signal (2ω), as shown in figure 9. The purpose of this first experiment was to validate that phase conjugation could be achieved at a particular element.

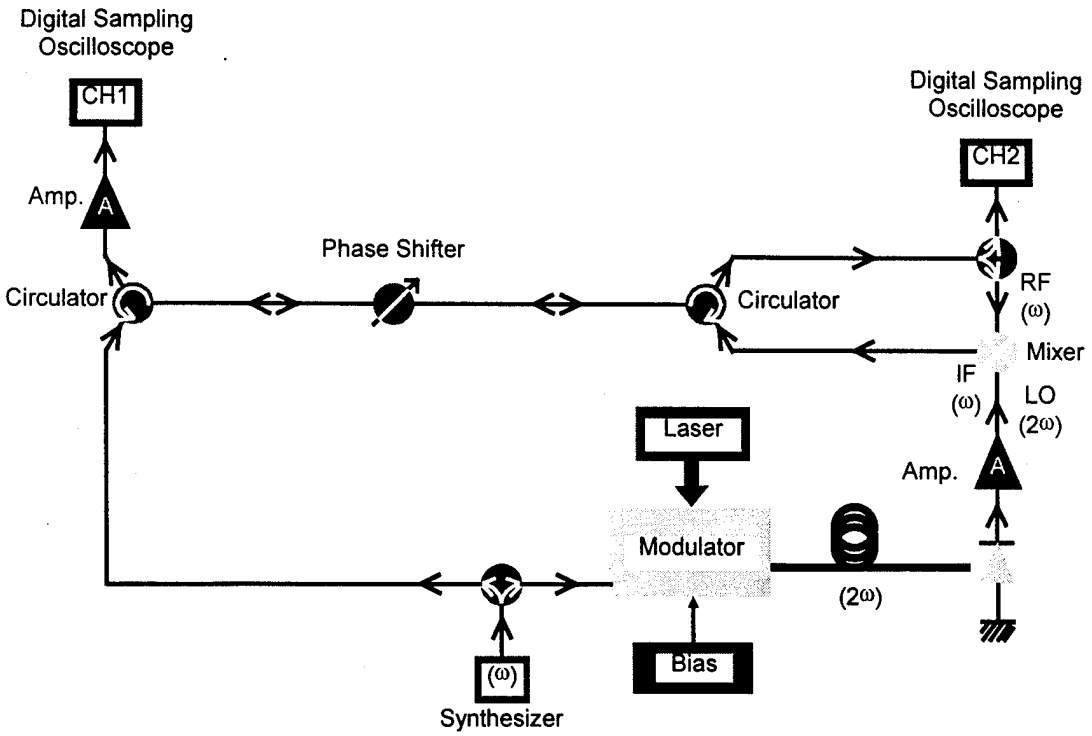

Figure 9. Initial experimental setup of optically injected conjugate phase conjugation.

A $LiNbO_3$ electro-optical modulator was biased at its transfer function extremum, therefore producing modulation at 2ω (20GHz) of the $1.3\mu m$ laser beam. After this the light was routed via optical fibers to a PIN diode and the microwave pump signal 2ω was extracted. The 2ω signal was then amplified and sent to the mixer to generate phase conjugate signal. The results are shown in figure 10. To prove the signal received at A in figure 9 is the phase conjugate signal of the input signal, a phase shifter was inserted in the microwave path. After the incoming signal passed through the phase shifter, it carried a phase shift $+\varphi$. TWM reversed this phase shift to $-\varphi$ and then sent the signal back. As this $-\varphi$ phase-shifted signal passed through the phase shifter, it picked up an additional phase shift $+\varphi$. Therefore at A the overall phase shift caused by the phase shifter was zero: $-\varphi + \varphi = 0$. It is clearly shown in figure 10 that the conjugate signal was virtually unchanged while the incoming signal was shifted due to the phase shifter change. This setup used only one element therefore it was an one dimensional experiment and could not be applied to reversing the wavefront. In order to extend to three dimensional phase conjugation, a two dimensional planar array must be used.

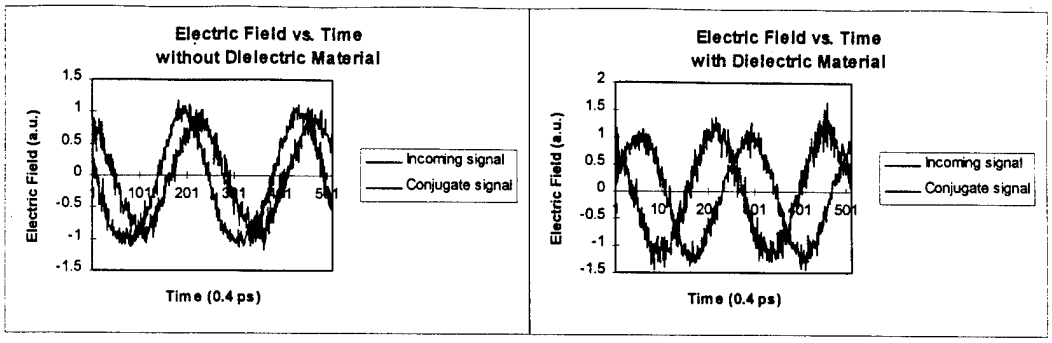

Figure 10. Incoming and conjugate signals of optically injected phase conjugation generation, monitored on the digital sampling oscilloscope. The incoming signals were recorded at B in figure 9 and the conjugate signals were recorded at A in figure 9.

In a microwave feed system, the field distribution can pose a significant design challenge. Optical injection of the pump signal can eliminate such problems. Another advantage of optical injection is that it relieves the need of a high power, high frequency (2ω) microwave source. Currently our study of this optical injection concentrated on using a single HBT as the phototransistor and the mixing device.

Up to this point, our discussion concentrated on generating phase conjugate signal at a single element. These one dimensional experiments would have little practical use if one could not extend this phase conjugate generation technique to higher dimensions. It can be proven that if the generated phase factor is conjugate to that of the incoming wave on a plane, it will be conjugate everywhere. Therefore an array of conjugate generation elements can provide the ability of generating phase conjugate waves. To demonstrate this concept, a eight-element system was built to show the directivity originated from phase conjugation. The setup is shown in figure 11. Both the transmitting horn and the receiving horn are mounted on rotational stages. The receiving horn is slightly higher and behind the transmitting one. After setting up the transmitting horn at an arbitrary angle, the receiving horn was moved around until the received signal was maximized on the sampling oscilloscope. The receiving horn was always able to follow the transmitting horn.

drawing are similar to the mixer circuit in figure 9.

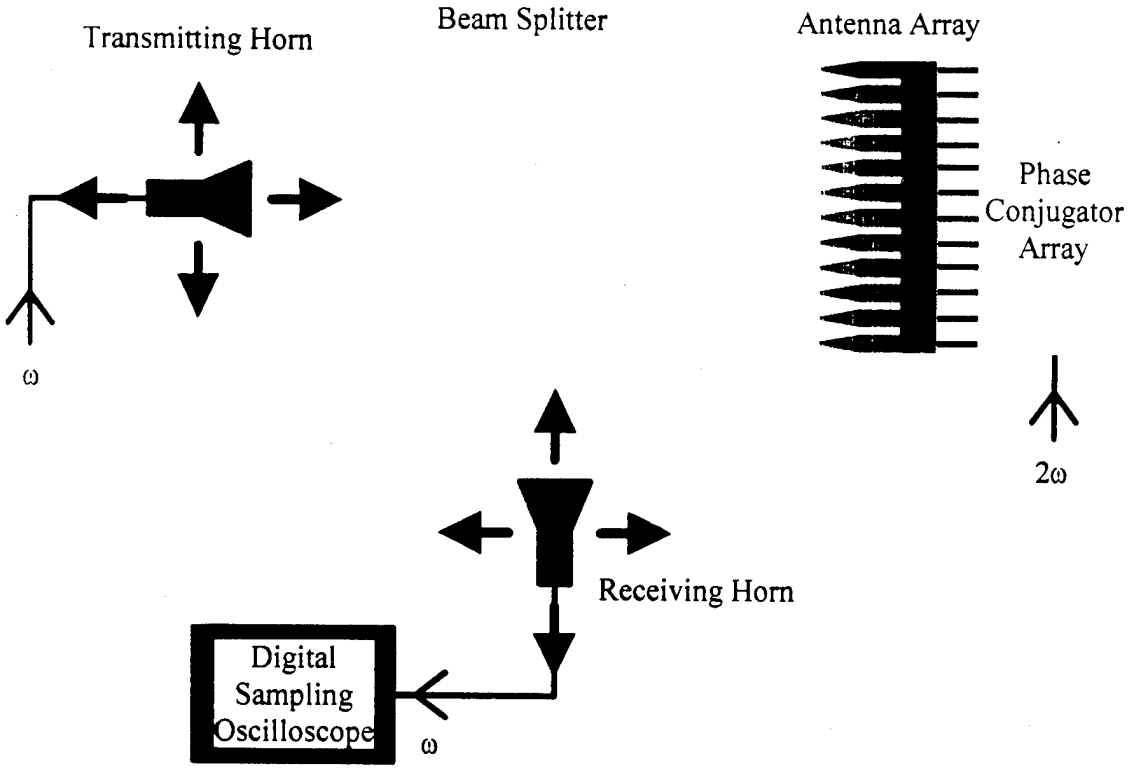

Figure 11. Experimental setup of the eight-element array phase

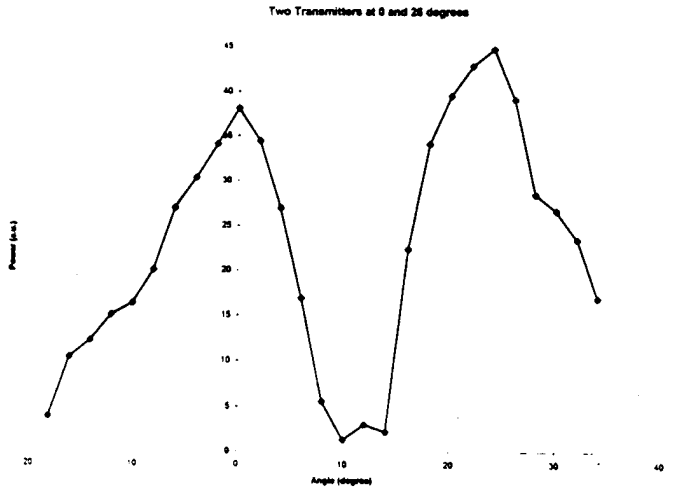

Figure 12 Results of the phase conjugation of two discrete sources from the eight element array.

SERIAL FED ANTENNA STRUCTURES

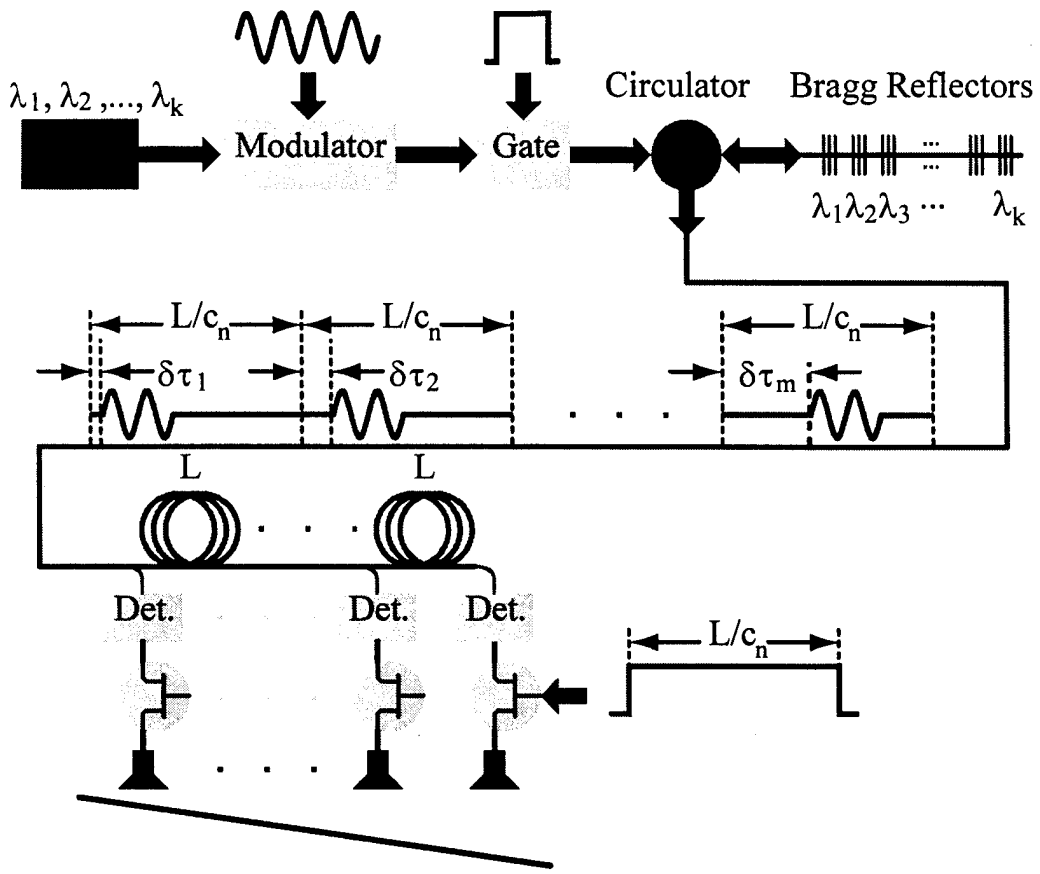

Figure 13
Serial - Feed Phased Array System with real time delays

Finally, as a result of our ongoing interest in phase array antenna structures[11] we have been looking at several configurations which relate to our optoelectronic integrated systems. One of these, developed in conjunction with USC, uses the concept of serially tuning the wavelength of a laser. A Millimeterwave signal is placed upon the optical carrier using our polymer modulator. It is important that the modulation frequency be an integral multiple of the frequency f_o determined by the fiber delay lines c_n/L. This makes the frequency discreet but broadly tunable. A gate is then used to clock the system at a repetition rate f_o. The length of the gate is equal to the desired radar pulse length.

The light from this system is fed to a circulator and then to a fiber with Bragg reflectors corresponding to the wavelengths that can be obtained from the tunable laser. Therefore, by tuning the laser it is possible to select different delays for the gate pulse that is generated using another polymer modulator. The light is then extracted via the circulator and is fed to the fiber optic delay lines as shown in the figure.

At each of the antenna elements there is a directional coupler, optical detector and microwave switch. After the entire delay line is loaded with the delayed gates the signal is detected and switched out to the antenna elements simultaneously. The cycle is then repeated with the laser used to tune specific wavelengths corresponding to particular delays. Again, after the delay line is serially loaded it is switched out in parallel to form the directional pulse of radiation.

By introducing the concept of an optoelectronic clock this system brings a dramatic simplification to the concept of optically controlled phased array radars. It uses but one laser and one delay line structure for all the radiating elements. There are several other ways of obtaining delays as a function of wavelength other than the Bragg fibers. These will also be examined for optimum performance capabilities. This effort will involve combining the on wafer optical circuitry we have developed with multiple fiber storage elements. This will be an important step in our development of optoelectronic systems. In many ways this concept is the inverse of frozen wave generators where the fields are established in parallel and radiated serially.

The basic idea is extremely interesting in terms of our wafer scale integration concepts in that it simplifies extremely complex systems down to a single source laser and fiber (or on-wafer) delay line with gratings. It has a natural extension to a receive system and can be modified for implementation as a cw imaging system. In the receive mode the system is essentially routed back through the system in reverse. Furthermore by increasing the number of wavelengths it can be extended to two dimensions with no added components. We feel that the extension of the concept of a clock to these optical/millimeter wave integrated systems is a major advance in the field of optically controlled phased arrays. We will use it here to demonstrate the capabilities of our integrated systems performing involved timing functions for new applications.

CONCLUSION

This effort has built upon the high frequency devices and structures that we were intitially developed as part of our Wafer Scale Union Grant. It has extended the range and performance of the individual components so that advanced systems can be fabricated at frequencies ranging up to at least 140 GHz. It has implemented integrated components which will demonstrate microwave phase conjugation, optoelectronic oscillation and a new form of phased array serial output stage. This work has shown the effectiveness and use of wafer scale integration as a major new building block in next generation systems. It has indicated, by experimentation and demonstration new capabilities at vastly reduced cost and weight. There are numerous systems in communications, IFF and imaging that will follow from these initial developments.

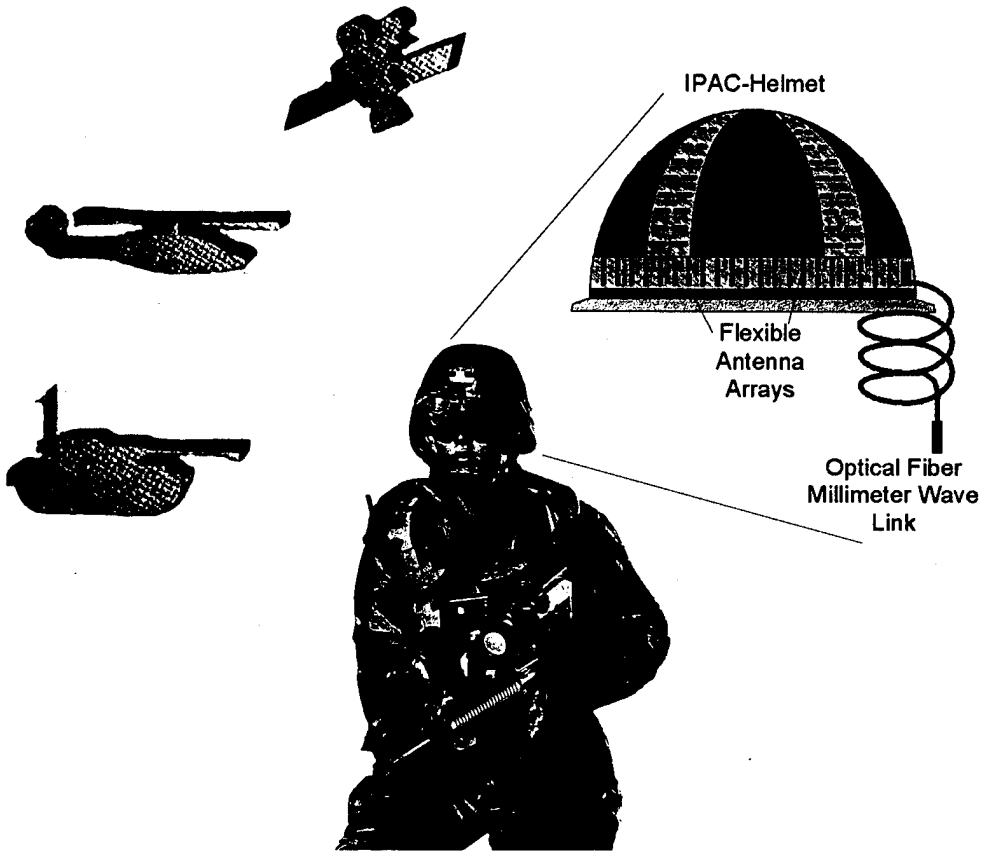

Integrated Phased-conjugated Array Communication Helmet

Figure 14

Based upon our previous grant we have established the basic technology now to make systems which will have the capability for important new tasks. The examples we have chosen accomplishes more than demonstrating simple systems. It establishes the basic concept of making a new class of structures which perform effectively as a macroscopic nonlinear surface. The use of combined optical-millimeterwave integrated on-wafer configurations have the potential of defining an entirely new approach to future systems. As an example of future IFF systems we show a optically integrated phase conjugation Helmet that could use this type of technology at millimeter wavelengths in figure 14. Such a system would be low power since it would respond only when contacted and send its conjugated signal only to the source. This concept indicates the future potential of integrated electro-optic systems for novel applications.

---

[1] W. Wang, D. Chen, H. Fetterman, Y Shi, W. Steier and L. Dalton, "Traveling wave electro-optic phase modulator using cross-linked nonlinear optical polymer,"Appl. Phys. Lett., vol 65, 8, 929, 1994

[2] W. Wang, D. Chen H. Fetterman et al, "40 GHz Polymer electrooptic phase modulators," IEEE Photonics Technology Letters, vol 7,638, 1995

[3] W. Wang et al. Heterodyne detection of 60 GHz electrooptical modulation , included in Appendix

[4] D.P. Prakash, D. Plant, D. Zhang, H. Fetterman, "Optical Transmission of MillimeterWave Signals through Polyimide Channel Waveguides using direct laser writing," SPIE, 1773, 20, 1992

[5] T. Matsurra, S. Ando, S. Matsui, S. Sasaki, and Yamamoto, Heat-resistant singlemode waveguides using fluorinated polyimides," Electronics Letters, vol 29, 2107,1993

[6] T. Watanabe et al. "Novel serially grafted connection between functional and passive polymer waveguides," Appl Phys. Lett. ,65,1205, 1994

[7] InP HBTs, editors B. Jalali, S. Pearton, Artech House 1995
Chapter: 10 Millimeterwave generation using InP Phototransistors, D. Scott, H. Fetterman

[8] D. Bhattacharya, P. Bal, H. Fetterman, D. Streit, "Optical mixing in epitaxial Lift-off Pseudomorphic HEMTs, Photonic Techn. Letts. Included in Appendix

[9] C. Cutler, R. Kompfer, and L. Tillotson, "A self-steering Array repeater," Bell Syst. Tech. J. vol 42, 2013, 1963

[10] Y. Chang, D. Scott, H. Fetterman, "Microwave Phase Conjugation using arrays of Nonlinear Optically Pumped Devices," SBMO/IEEEMTT-S Proceedings 909, 1995

[11] H. Fetterman, Y. Chang, D. Scott et al., "Optically controlled phased array radar receiver using SLM switched real time delays," IEEE Microwave and Guided Wave Lett. Included in Appendix

APPENDIX

SELECTED PAPERS

AFCEA PAPER

Demonstration of Ultrahigh Frequency Broadband Polymer Modulators

Harold Fetterman, Datong Chen, *UCLA EE Department*
Antao Chen, Srinath Kalluri, William H. Steier, Larry R. Dalton, *USC*
Wenshen Wang, Yongqiang Shi, *TACAN Corp.*

Abstract High frequency polymer modulators have been made and characterized up to 60 GHz. A new millimeter wave electrode design for higher speed devices is proposed and demonstrated. This high frequency effort is based upon the polymer material's low dispersion, our new traveling wave driving circuit design, and the use of optical heterodyne detection for effective high frequency electro-optic phase modulator measurement.

1. INTRODUCTION

Organic nonlinear optical polymer materials have many advantages over the traditional inorganic crystal materials. They have shown large nonlinearity, and a low and nondispersive dielectric constant. Very high frequency broadband traveling wave photonic devices can be made of these materials with simple planar circuit structures because of the close velocity match between the light wave and the microwave.

We have successfully fabricated the electro-optic polymer modulators using the cross-linked PUR-DR19 polymer. The intrinsic device bandwidth-length product is well above 100GHz•cm, which is significantly higher than devices based on current competing materials. We have characterized the devices from DC up to 60 GHz, and have now developed new millimeter wave circuits for W band operation.

2. FABRICATION

The device's structure is shown schematically in Fig. 1. The modulator has a typical triple layer stack structure. Commercial polyurethane polymers were used as the upper and lower cladding layers. All three polymer layers were spin-cast on a chromium-gold coated quartz substrate with thickness of about 5, 1, 9μm respectively. After the lower cladding layer was cured, the active polymer was spin-cast and kept in a vacuum oven at 60 °C for 12 hours drying and precuring. The sample was then heated to the glass transition temperature to perform corona poling and thermal setting. The channel waveguide structure was formed on the poled and cured active polymer by standard photolithography and oxygen reactive ion etching (RIE). The upper cladding layer was then spun on the active layer and cured at room temperature. After all the polymer layers were cross-linked, a 50Ω gold microstrip line was fabricated on top of the optical waveguide. The end surfaces of the device were sawed and polished because of the rubbery property of the material. Two Wiltron V connectors were used to launch and load the microwave signal through tapered contact pads. The DC resistance of the microwave circuit is 2Ω from connector to connector.

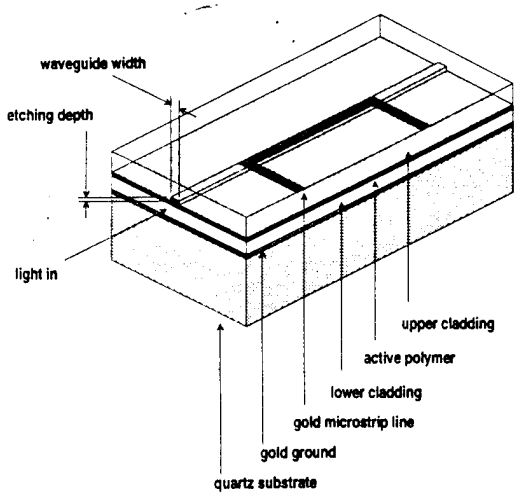

Fig. 1 Device structure

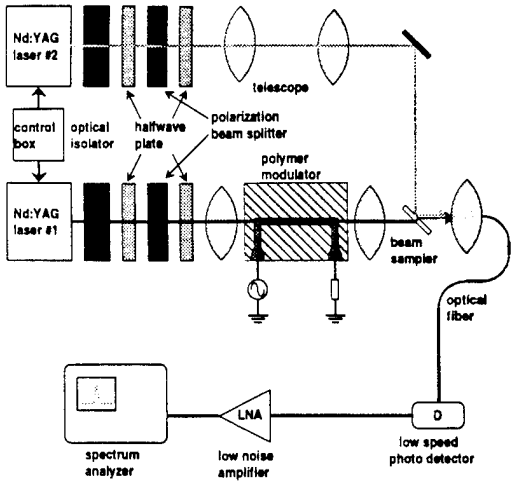

Fig. 2 Optical heterodyne detection setup

3. CHARACTERIZATION

To characterize our phase modulators at ultrahigh frequency, we used an optical heterodyne detection method. Our experimental setup is shown in Fig. 2. Two diode pumped Nd:YAG lasers at 1.319μm were used for the optical heterodyne detection of the phase modulation signal from these modulators. The power output of the lasers was controlled externally by a combination of polarization beam splitters and λ/2 waveplates. The beam of the laser 1 was end-fire coupled in and out of the modulator with a pair of 20× microscope objectives. The linearly polarized incident beam was rotated by another λ/2 waveplate to excite the transverse magnetic (TM) mode inside the waveguide. The output light from the modulator was directed to a multimode optical fiber through a 10× microscope objective, and finally connected to an photodetector of 6 GHz bandwidth. The beam of the laser 2 was aligned co-linearly with the output light from the modulator using a beam sampler. A telescope was used to control the beam divergence of laser 2. The frequencies of the lasers were adjusted by changing the crystal temperatures and cavity lengths and were stable to approximately 5 kHz.

The photo current in the detector can be written as

$$i_D \propto |E_1 + E_2|^2 \propto \sqrt{I_1 I_2}\{J_0(\phi_1')\cos(\Delta\omega t + \Delta\phi) - J_1(\phi_1')\sin[(\Delta\omega + \Omega)t + \Delta\phi] - J_1(\phi_1')\sin[(\Delta\omega - \Omega)t + \Delta\phi]\}.$$

where J_m is the *m*th order Bessel function of the first kind. Here the first term is the direct laser mixing, the other two terms are the optical heterodyne signals. Of particular importance is the last term in this expression which represents the down converted optical heterodyne signal with a $\Delta\omega$–Ω frequency component proportional to $\sqrt{I_1 I_2}$, where I_1, I_2 are the light intensities from each laser. This signal was transmitted through the multimode fiber and detected by the low frequency photodetector. It was then sent through a preamplifier and displayed on a spectrum analyzer. When the driving microwave voltage is small so that the modulation phase shift is much smaller than π, we have

$$i_D(\Omega) \propto J_1(\phi_1') \cong \frac{\phi_1'}{2} = \frac{\pi n^3 r_{33} l}{2 \lambda h} V \propto V$$

A linear relationship between the driving microwave voltage and the excited heterodyne current component is expected for small signal approximation.

As we can see that the optical heterodyne detection has several advantages over our previous microwave mixer testing system. $\Delta\omega$–Ω is a flexible frequency and can be adjusted so that the photodetector no longer needs to match the modulation frequency, and microwave pickup signal can be avoided. Further, using the second laser as the local oscillator can significantly improve the signal to noise ratio.

The frequency response curve was obtained by overlapping the measurements for the same modulation frequency at different laser detune settings. The curve has been calibrated to the driving microwave power and shown in Fig. 3. The response curve is about 4.7dB lower at 60GHz than that at 2GHz, and no identifiable rolling-off can be observed from 40 to 60GHz. This is an indication that an E-O modulator made of the polymer material can achieve high performance over a broad frequency band with only a simple planar microwave circuit design. The issue for our current design is the contact mismatch between the microstrip line and the Wiltron V coaxial transitions which causes the resonance in the measured frequency response curve. Our measurement also showed good repeatability with only about one half dB of fluctuation.

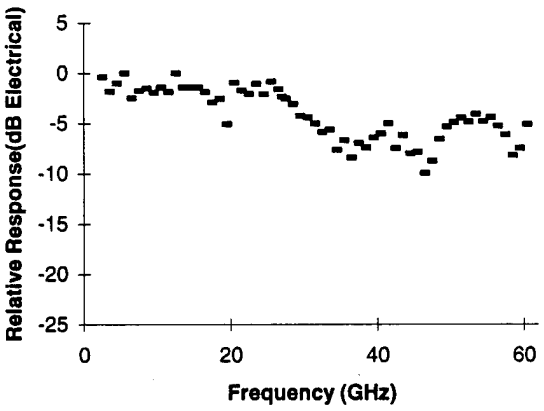

Fig. 3 Measured frequency response up to 60 GHz

4. NEW ELECTRODE DESIGN

For higher frequencies, the microwave driving power is usually transported through metallic rectangular waveguide. A transition from such microwave waveguides to the microstrip line electrode on the device is needed. We proposed to use anti-podal fin lines as an transition for such purpose since it has the advantages of both low loss and high dimensional fabrication tolerance.

Figure 4 is the overview of our higher frequency modulator design, it has an integrated anti-podal fin-line transition to W-band waveguide. Fig. 5 is the measured S_{21} of the tested circuit, which consists of two such transitions and a 9 mm long microstrip line. Since the fin lines does not need to be matched to 50 Ω, we can reduce ohmic losses by going to a lower impedance microstrip system. The observed loss of two transitions, around 3 dB, is much better than that of conventional coaxial to microstrip line. It is limited by contact resistance and the transition profile, and can be further improved.

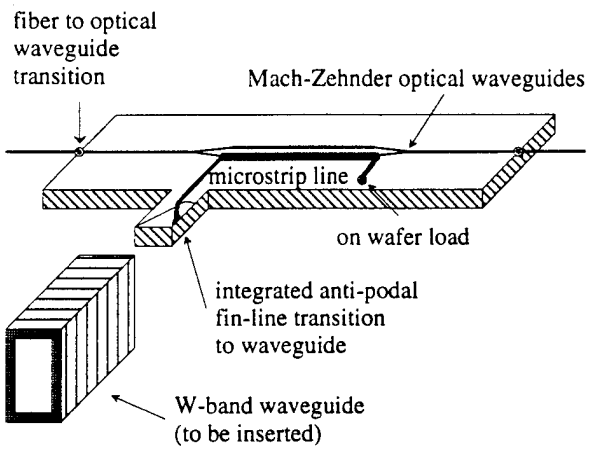

Fig. 4 Overview of proposed higher frequency modulator at W-band

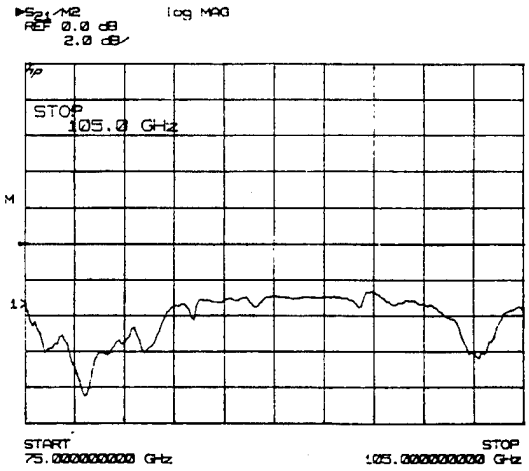

Fig. 5 S_{21} of test circuit at W-band

5. CONCLUSION

Polymers are an excellent material choice for ultrahigh frequency devices, and we have incorporated them into high speed optical modulators. These devices have recently been characterized as phase modulators up to 60 GHz. A high frequency driving circuit for W band modulator has been designed and tested. Efforts are now being made to extend this technology to 94 GHz using heterodyne detection and new microwave electrodes. This project has been sponsored in part by NCIPT and AFOSR.

Harold R. Fetterman: Professor of Electrical Engineering Department at University of California, Los Angeles, CA90095. Voice: (310) 825-3431 Fax: (310) 206-9497 E-mail: fetter@ee.ucla.edu.
Datong Chen: PhD. Student, Electrical Engineering Department, University of California, Los Angeles, CA90095. Voice: (310) 206-9457 Fax: (310) 206-9497 E-mail: datong@ucla.edu.
Antao Chen, Srinath Kalluri: PhD. Students, Electrical Engineering Department, University of Southern California, Los Angeles, CA90089-0483. Voice: (213) 740-8781 Fax: (213) 740-8684.
William H. Steier: Professor of Electrical Engineering Department at University of Southern California, Los Angeles, CA90089-0483. Voice: (213) 740-4415 Fax: (213) 740-8684.
Larry R. Dalton: Professor of Chemistry Department at University of Southern California, Los Angeles, CA90089-0483. Voice: (213) 740-8768
Wenshen Wang, Yongqiang Shi: Staff Scientists, TACAN Corp., Carlsbad, CA92008. Voice: (609) 438-1010 Fax: (609) 438-2412.

Optical heterodyne detection of 60 GHz electro-optic modulation from polymer waveguide modulators

Wenshen Wang, Datong Chen, and Harold R. Fetterman
Electrical Engineering Department, University of California, Los Angeles, Los Angeles, California 90025

Yongqiang Shi
TACAN Corporation, Carlsbad, California 92008

William H. Steier and Larry R. Dalton
Electrical Engineering Department and Chemistry Department, University of Southern California, Los Angeles, California 90089-0483

Pei-Ming D. Chow
TRW Electronics Systems and Technology Division, Redondo Beach, California 90278

(Received 23 May 1995; accepted for publication 20 July 1995)

An optical heterodyne technique has been used to demonstrate electro-optic modulation up to 60 GHz, the highest reported to date, in polymer waveguide modulators. The frequency response of the device from 40 to 60 GHz was obtained by measuring the frequency down converted modulation signal with a low frequency photodetector. No rolling-off was identifiable from the measured device response, indicating no fundamental material limitations in this frequency range for the polymer material which we used. Such an optical heterdyne system can be a powerful tool for modulator characterization at millimeter wave frequencies because of its high sensitivity and low frequency demands on photoreceivers. © *1995 American Institute of Physics.*

Nonlinear optical (NLO) polymer materials have been predicted to be a good candidate for very high frequency broadband photonic devices with a bandwidth-length product well above 100 GHz cm.[1] High frequency polymer electro-optic (E-O) modulators have been demonstrated with up to 40 GHz bandwidth.[2] We have made stable high frequency phase modulators using a cross-linked NLO polymer, and have tested them using external microwave mixers up to 40 GHz in a polarization modulator configuration.[3,4] Above 40 GHz, the measurement was limited by the bandwidths of our commercial photodetectors and microwave mixers. A number of techniques for high frequency modulator calibration have been developed to avoid the need of a high frequency detection system. A classical way is to use a scanning Fabry–Perot interferometer to display the frequency spectrum of the modulated light signal.[5] The swept frequency method was introduced by modulating the microwave driving field at a low frequency,[6] and optical downconversion has been used to determine the modulator response up to 40 GHz using a second Mach–Zehnder interferometric modulator of 20 GHz bandwidth.[7] Optical heterodyne detection using two lasers was demonstrated with high sensitivity and dynamic range for E-O modulator calibrations up to 26.5 GHz.[8] In this letter, we report our new measurement results, based on the optical heterodyne technique, of E-O modulation from our polymer modulators up to 60 GHz using two diode pumped Nd:YAG lasers. This is the highest modulation frequency reported to date on a device made of NLO polymer materials. Our measurements validate that polymer materials are a promising candidate for ultrahigh frequency broadband device applications. Our work has also demonstrated for the first time, to our knowledge, the use of optical heterodyne techniques for modulator calibration up to 60 GHz. The detection range can be further extended to beyond 100 GHz by combining the optical heterodyne method with currently available commercial photodetectors and microwave mixers. Further extension of the measurement range can be achieved by using tunable external cavity semiconductor lasers to virtually any frequency.

Our experimental setup is shown schematically in Fig. 1. The device tested was a polymer E-O phase modulator made of a cross-linked NLO polymer, PUR-DR19.[3,9] The modulator consists of a straight channel waveguide integrated with a microstrip line electrode. Two Lightwave Electronics 122 diode pumped Nd:YAG lasers at 1.319 μm were used for optical heterodyne detection of the phase modulation signal from these modulators. The power output of the lasers was controlled externally by a combination of polarization beam splitters and $\lambda/2$ wave plates. The beam of laser 1 was end-fire coupled in and out of the modulator with a pair of 20× microscope objectives. The linearly polarized incident beam was rotated by another $\lambda/2$ waveplate to excite the transverse

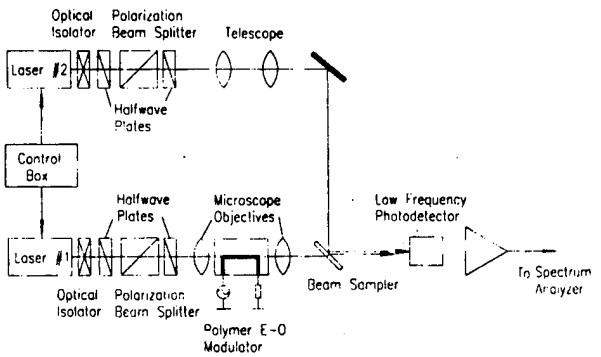

FIG. 1. The experiment setup for optical heterodyne detection of millimeter wave electro-optic modulation from a polymer phase modulator. Two diode pumped Nd:YAG lasers were in open loop running condition.

 0003-6951/95/67(13)/1806/3/$6.00

magnetic (TM) mode inside the waveguide. The output light from the modulator was directed to a multimode optical fiber through a 10× microscope objective, and finally connected to a 6 GHz bandwidth photodetector (Ortel RL W-50). The beam of laser 2 was aligned colinearly with the output light from the modulator using a beam sampler. A telescope was used to control the beam divergence of laser 2. The frequencies of the lasers were adjusted by changing the crystal temperatures and cavity lengths with no external feedback loop.

Turning the modulation field on, the beam from the modulator is phase modulated and can be written as

$$E_1 = E_{10}\cos[\omega_1 t + \phi_1(t)]$$

where

$$\phi_1(t) = \phi_{10} + \phi_1' \cos \Omega t$$

is the total phase delay, while

$$\phi_1' = k\Delta n l = \frac{\pi n^3 r_{\text{eff}}\, l}{\lambda h} V,$$

is the phase modulation amplitude at angular frequency Ω, k the light wave vector, n the index of refraction, l the interaction length, h the film thickness, V the magnitude of the applied modulation voltage. It should also be noticed that the effective $E-O$ coefficient $r_{\text{eff}} = r_{33}$ for the TM mode, is the largest $E-O$ coefficient for a poled NLO polymer film. If the second laser at frequency ω_2 is colinearly aligned to the photodetector and a small modulation voltage is applied, the excited photocurrent in the detector can be written as

$$\begin{aligned} i_D \propto |E_1 + E_2|^2 \cong E_{10}E_{20}\{&J_0(\phi_1')\cos(\Delta\omega t + \Delta\phi) \\ &- J_1(\phi_1')\sin[(\Delta\omega + \Omega)t + \Delta\phi] - J_1(\phi_1') \\ &\times \sin[(\Delta\omega - \Omega)t + \Delta\phi]\}, \end{aligned}$$

where J_m is the mth order Bessel function of the first kind, $\Delta\omega = \omega_1 - \omega_2, \Delta\phi = \phi_{10} - \phi_{20}$. Here, the first term is the direct laser mixing term while the last two are the optical heterodyne terms. Of particular importance is the last term which represents the downconverted optical heterodyne signal with a $\Delta\omega - \Omega$ frequency component proportional to $\sqrt{I_1 I_2}$, where I_1, I_2 are the light intensities from each laser. This signal was detected by the low frequency photodetector. It was then sent through a preamplifier and displayed on a spectrum analyzer. When the driving microwave voltage is small so that the modulation phase shift is much smaller than π, we have

$$i_D(\Delta\omega - \Omega) \propto J_1(\phi_1') \cong \frac{\phi_1'}{2} \propto V.$$

A linear relationship between the driving microwave voltage and the excited heterodyne current component is expected for small signal approximation.

As can be seen, the optical heterodyne detection has several advantages over our previous microwave mixer testing system. First, $\Delta\omega - \Omega$ is a flexible frequency and can be adjusted so that the photodetector no longer needs to match the modulation frequency, and microwave pickup can be avoided. Second, using the second laser as the local oscillator can significantly improve the signal to noise ratio. In addition, direct measurement of phase modulation can fully use our device's nonlinearity, since using a polarizer to detect TE and TM modes beating only uses two thirds of the maximum nonlinearity.[3] Moreover, although $\Delta\phi$ depends on the system alignment and is very sensitive to any environmental change, the amplitude of the heterodyne signal is very stable since it only depends on the phase modulation amplitude. Using optical heterodyne detection, microwave mixers are no longer needed within the tuning range of the lasers (>60 GHz) plus the detection range of the spectrum analyzer, yielding a direct measurement range over 80 for our 22 GHz spectrum analyzer. Using 40 GHz microwave mixers, the high frequency measurement capability can be extended to 120 GHz with photodetectors operating only up to 60 GHz. It is expected that this range can be further extended to higher frequencies when an external cavity tunable semiconductor lasers are used.

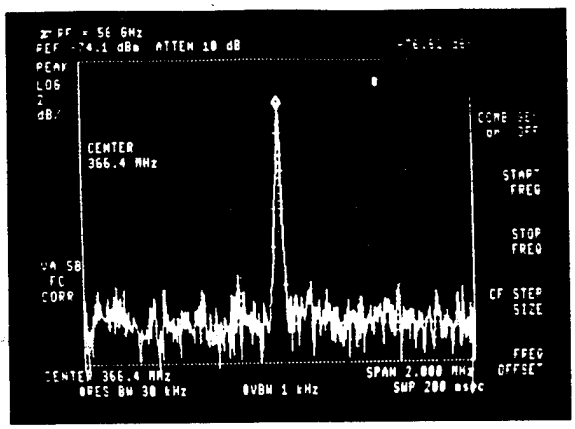

FIG. 2. The 60 GHz phase modulation signal from the polymer $E-O$ modulator downconverted by optical heterodyne mixing to less than 1 GHz and displayed on a spectrum analyzer. The driving microwave power was about 2.7 dBm.

In our experiment, the lasers were detuned to within about 500 MHz of the modulation frequency. The power level of the second laser was chosen to be near the saturation value of the photodetector. The signal from the photodetector

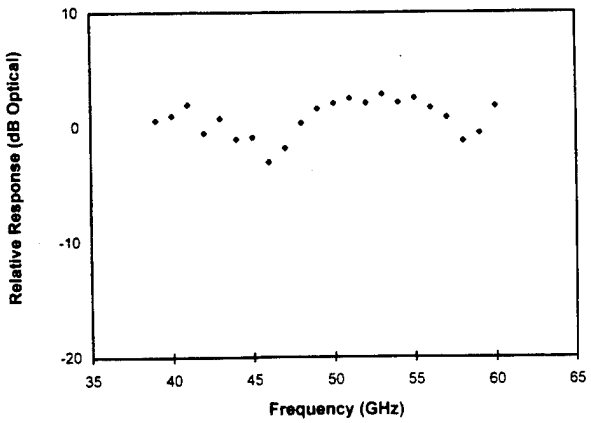

FIG. 3. The response curve of the polymer E–O modulator from 40 to 60 GHz. No rolling off is identifiable in this frequency range except resonances attributed to the microwave circuit contact mismatch. The accuracy of the measurement was about half dB.

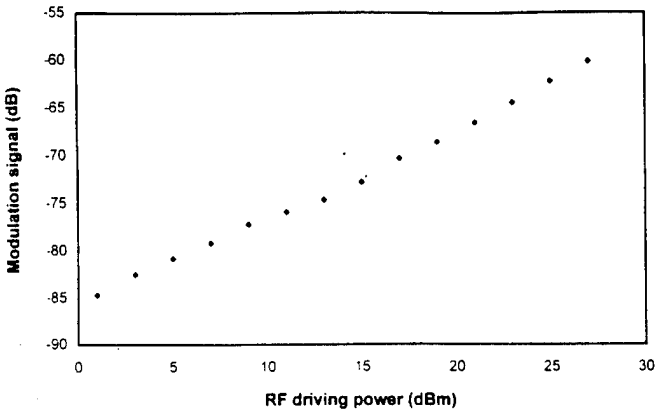

FIG. 4. The optical heterodyne signal dependence to the driving microwave power. The measurement was performed at 41 GHz using an InGaAs PHEMT power amplifier.

was sent through a preamplifier, and displayed on an HP 8592A spectrum analyzer. The 500 MHz observation frequency was chosen for convenience, and can be changed to a much lower frequency where detectors and preamplifiers are available. We drove the modulator with an Avantek 40–60 GHz (U band) quadrupler amplifier pumped by an HP 8350A sweep oscillator. The output power of the quadrupler over the frequency band is typically a few dBm (2.7 dBm at 60 GHz). Because of the significantly improved signal-to-noise ratios, we were able to obtain sizable signal above the noise level even with less than 0.05% of the driving power for π phase shift. Figure 2 shows the optical heterodyne signal at 60 GHz modulation frequency. This is the first reported demonstration of 60 GHz electro-optic modulation from a polymer device to date. Using this method, we were able to sweep the modulation frequency beyond 40 GHz and up to 60 GHz. For each modulation frequency, the frequency difference of the lasers were tuned to be about 500 MHz both lower and higher than the modulation frequency. The frequency response curve was obtained by overlapping the measurements for the same modulation frequency at different laser detune settings. The curve has been calibrated to the driving microwave power and shown in Fig. 3. The response curve is about 4.7 dB lower at 60 GHz than that at 2 GHz, and no identifiable rolling-off can be observed from 40 to 60 GHz. This is an indication that an E–O modulator made of the polymer material can achieve high performance over a broad frequency band with only a simple planar microwave circuit design. The issue for our current design is the contact mismatch between the microstrip line and the Wiltron V coaxial transitions which causes the resonance in the measured frequency response curve. Our measurement also showed good repeatability with only about one half dB of fluctuation.

In order to determine the microwave driving power dependence of the heterodyne signal, we have used a semiconductor power amplifier developed by TRW, Inc.[10] It is a pseudomorphic InGaAs high electron mobility transistor (PHEMT) microwave monolithic integrated circuit (MMIC) power amplifier with about 12 dB single stage gain from 38 to 44 GHz (Q band). Two such amplifiers were cascaded to form a two stage power amplifier having a saturated power output close to 30 dBm with about 20 dB associated gain. The amplifier was driven by the Avantek quadrupler which in turn was driven by an HP 8350A sweep oscillator. The measurement was performed at 41 GHz with the lasers beating at 41.5 GHz, while the driving power varied from 1 to 27 dBm. The measured curve is shown in Fig. 4, normalized to the half-wave voltage. A signal to noise ratio of over 40 dB can easily be obtained with higher driving microwave power. This has demonstrated the possibility of potential integration of solid-state microwave drivers with polymer photonic devices for system applications where compact size is a concern. We have already verified that the poling process is compatible with the semiconductor drivers.

In conclusion, 60 GHz E–O modulation has been demonstrated from a phase modulator made of a cross-linked NLO polymer PUR-DR19 using an optical heterodyne technique. Using two diode pumped Nd:YAG lasers and a photodetector of only a few GHz bandwidth, the millimeter frequency optical phase modulation was detected by measuring the heterodyne signal that had been frequency downconverted. The device response was obtained from 40 to 60 GHz with no measurable rolling-off, indicating no fundamental material limitations for device applications in this frequency band. An all-solid-state power driving system, including an InGaAs PHEMT MMIC Q band power amplifier with about 20 dB gain, has been used to demonstrate possible integration of polymer modulators with a compact driving system. This project was supported by the Air Force Office of Scientific Research (AFOSR) and National Center for the Integrated Photonic Technology (NCIPT).

[1] R. Lytel, Proc. SPIE **1216**, 30 (1990).
[2] C. C. Teng, Appl. Phys. Lett. **60**, 1538 (1992).
[3] W. Wang, D. Chen, H. R. Fetterman, Y. Shi, W. H. Steier, and L. R. Dalton, Appl. Phys. Lett. **65**, 929 (1994).
[4] W. Wang, D. Chen, H. R. Fetterman, Y. Shi, W. H. Steier, and L. R. Dalton, IEEE Photon Technol. Lett. **7**, 638 (1995)
[5] M. Izutsu, Y. Yamane, and T. Sueta, IEEE J. Quantum Electron. **QE-13**, 287 (1977).
[6] S. Uehara, Appl. Opt. **17**, 68 (1978).
[7] C. D. Watson, D. A. Humphreys, and M. G. F. Wilson, IEEE Photon. Technol. Lett. **5**, 1005 (1993).
[8] T. S. Tan, R. L. Jungerman, S. S. Elliott, IEEE Trans. Microwave Theory Tech. **37**, 1217 (1989).
[9] Y. Shi, W. H. Steier, M. Chen, L. P. Yu, and L. R. Dalton, Appl. Phys. Lett. **60**, 2577 (1992).
[10] J. C. L. Chi, J. A. Lester, Y. Hwang, P. D. Chow, and M. Y. Huang, IEEE Microwave Guided Wave Lett. **5**, 21 (1995).

40-GHz Polymer Electrooptic Phase Modulators

Wenshen Wang, *Student Member, IEEE,* Datong Chen, *Student Member, IEEE,* Harold R. Fetterman, *Fellow, IEEE,* Yongqiang Shi, William H. Steier, *Fellow, IEEE,* and Larry R. Dalton

Abstract— **A broad-band high-frequency traveling wave electrooptic phase modulator made from stable nonlinear optical polymers has been tested. Using a 1.319-μm light source, single-mode operation was achieved with high-input optical power, resulting in improved modulation depths and signal-to-noise ratios. The high-frequency optical modulation was observed up to 40 GHz using external microwave mixers. Direct optical-heterodyne detection of electrooptic phase modulation has also been demonstrated with high sensitivity at 40 GHz. The devices were tested with 10^5 W/cm^2 power density for 24 hours, and have showed no observable decay in nonlinearity.**

ORGANIC nonlinear optical (NLO) materials exhibit a low and nondispersive dielectric constant. Very high frequency broad-band traveling wave photonic devices can be made of these materials with simple planar circuit structures because of the close velocity match between the light wave and the microwave. Such a device has important applications in optical fiber communication network and optical interconnections where 1.3-μm or 1.55-μm light sources are commonly used. In an earlier paper [1], we reported fabrication of a high speed traveling wave electrooptic (EO) phase modulator from a cross-linked NLO polymer. The device showed good temporal and thermal stability, but was only characterized with 1.064 μm light source up to 18 GHz. In this paper, we report new measurement results using 1.3 μm sources with extended bandwidth and a detailed characteristics of the mode behavior. Single-mode operation was achieved at 1.3 μm wavelength with high input optical power (>20 mW), resulting in improved signal-to-noise ratios. Using external microwave mixers to display the modulation signal on a spectrum analyzer, we tested these devices up to 40 GHz, limited by our microwave sources. The modulation signal was also optically heterodyne detected at 40 GHz.

Traveling wave structures have been used to make high-frequency broad-band electrooptic modulators in various materials [2]–[9]. In these devices, light wave travels with the driving electromagnetic wave to avoid the transient-time induced frequency-length product limit in a lumped circuit configuration. The difference in velocity between light wave and microwave would result in a frequency-length product limit [10]:

$$(f \cdot l)_{\max} \cong \frac{c}{4|n_{\text{eff}} - \sqrt{\varepsilon_{\text{reff}}}|}$$

where f is the modulation frequency, l the interaction length, c the speed of light, n_{eff} the effective index of refraction, and $\varepsilon_{\text{reff}}$ the effective dielectric constant. Straightforward evaluation of this limit for $LiNbO_3$ and III–V modulators yields products less than 20 GHz · cm, with improvements obtainable at the cost of circuit and fabrication complexity. Since polymer materials have a low and nondispersive dielectric constant, this limit can be over 120 GHz · cm with a simple planar structure, making them natural candidates for high-frequency broad-band devices. Using low cost material and simple fabrication, polymer photonic devices can be made cheaply in mass production, and they are capable of integration with other electronic circuits or photonic devices on semiconductor surfaces.

Our devices have a three layer structure with a buried channel optical waveguide made of a thermoset polyurethane-Disperse Red 19 (PUR-DR19) NLO polymer with commercial polyurethane for the cladding layers. The material exhibited no decay in nonlinearity at room temperature for 4000 hours and a 30% decay at 90 °C for 3000 hours. The detailed material properties and poling techniques as well as device fabrication were reported earlier [1], [11]. All three polymer layers were spin-cast on a quartz substrate covered with a gold ground plane. The channel optical waveguides were defined on the poled active polymer layer by oxygen reactive ion etching. The end surfaces of the device were cut with a diamond saw and polished for end-fire coupling. A 50-Ω gold microstrip line was fabricated on top of the optical waveguide.

We have investigated the optical mode behavior using different waveguide parameters. The thickness of the active layer is about 1 μm, and the refractive indices of the guiding layer and cladding layers are 1.63 and 1.55 at 1.319 μm. The optical waveguides support single mode in the vertical direction while the number of modes along the surface is determined by the channel width and the etching depth. Using the effective index method, we calculated the relationship between the lateral modes and the waveguide dimension (Fig. 1). Optical waveguides of 3, 4, 5, 8, and 10 μm widths were fabricated experimentally with different etching depths. The modal behavior was compared to the theoretical prediction with good agreement. Although single-mode waveguides can be made of narrow width and shallow etching depth, they tend to have higher loss due to fabrication tolerances and the extension of more tail field in the high scattering loss

Manuscript received December 21, 1994; revised February 3, 1995. This work was supported by National Center of Integrated Photonic Technology (NCIPT) and Air Force Office of Scientific Research.

W. Wang, D. Chen, and H. R. Fetterman are with the Electrical Engineering Department, University of California, Los Angeles, CA 90024 USA,

Y. Shi is with TACAN Corporation, 2330 Faraday Avenue, Carlsbad, CA 92008 USA.

W. H. Steier and L. R. Dalton are with the Center for Photonic Technology, Electrical Engineering Department and Chemistry Department, University of Southern California, Los Angeles, CA 90089-0483 USA.

IEEE Log Number 9410673.

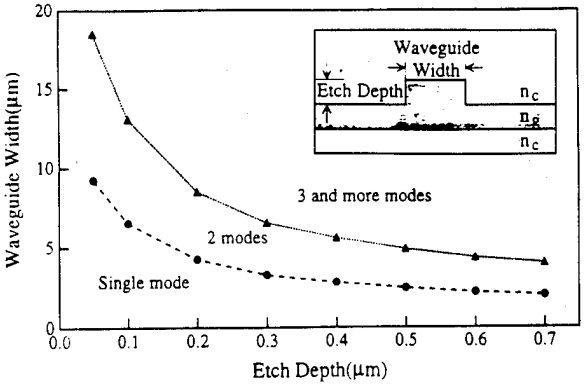

Fig. 1. The calculated relationship between the number of guiding lateral modes and the optical waveguide dimension. The indices of refraction are $n_g = 1.63$ for the guiding layer and $n_c = 1.55$ for the cladding layers.

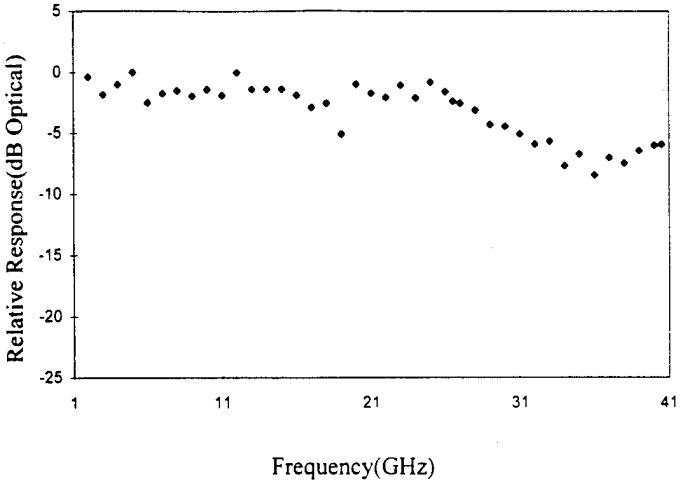

Fig. 2. The measured frequency response curve of the stable polymer electrooptic phase modulator. External microwave mixers were used to down convert the signal at frequencies higher than 22 GHz.

etched area. For the high-frequency measurements, 0.6-μm etching depth and 8–10-μm waveguide width were chosen to compromise the mode quality and waveguide loss. Single-mode operation was achieved with proper launching, yielding good modulation depth. Such dimensions typically have about 13 dB optical insertion loss with a pair of 20× microscope objectives, and on-off ratio better than 13 dB. Similar analysis was also applied to 1.064 μm, indicating that there exist two vertical modes. This could lead to lower modulation depth and unstable launching that were observed in our experiments.

We have used 30-mW input optical power to test the device durability for 24 hours, which is equivalent to an optical power density of about 10^5 W/cm^2 inside the waveguide, and no half-wave voltage change was observable within our experiment error. Optical power levels from 10 to 20 mW have frequently been used for system alignment that may last for hours, and up to 40–50 mW for short time in other measurements where high signal-to-noise ratios are desired. We have devices that are made of films poled over 18 months ago and have been under test for over 12 months in ambient conditions. No change in half-wave voltage was observed for these devices. Damage was observed, however, when 1.064 μm source was used at >30 mW. The difference between 1.064 μm and 1.3 μm is attributed to stronger two photon processes and greater absorption of the generated second harmonic signal at shorter wavelengths. Further experimentation is under way to study the value and the mechanism of damage threshold to our devices.

The microwave circuit design of a polymer traveling wave EO modulator depends upon the poling technique used. The general consideration is to apply the modulation field along the direction of largest EO component, r_{33}. Our NLO polymer film was prepared by corona poling, so that r_{33} is in vertical direction. This makes a microstrip line structure, primarily featured by the ratio of the line width to the electrode separation, a natural choice. Smaller electrode separation is needed to keep the driving voltage low while wider line widths are preferred for good microwave transmission. In our design, a separation of 15 μm was chosen to meet this compromise. The circuit layout was obtained from a commercial design software. Microwave packaging is also an important issue for the circuit design. Available microwave coaxial to microstrip line connectors can go as high as 65 GHz (Wiltron V series, for instance), but the contact glass beads launchers are hundreds of micrometers in diameter. Simple microstrip line design would lead to rather big size mismatch at the contact, limiting the device performance. In our circuit, two contact pads of 60-μm wide and 300-μm long with a 100-μm long linear transition taper were used to match the size of the contact glass beads of two Wiltron V launchers. The microwave transmission, S_{21}, was measured on an HP 8510B network analyzer and compared with the simulation results. The tested S parameters are consistent with simulations under 19 GHz, with slightly higher loss due to the surface roughness, while resonances appear at higher frequencies mainly caused by the contact mismatch. It was demonstrated that using a tapered quasicoplanar contact, the contact problem was solved up to 40 GHz in a thermoplastic NLO polymer modulator [2]. For higher frequencies, coplanar structures, which need in plane poling, may be used to reduce the metal losses that limit the performance of our microstrip lines.

Time-domain measurements of S_{11}, the microwave reflection, were performed in order to determine the microwave effective dielectric constant of the microstrip line circuit with polymer substrate. From the time delay between the two consecutive reflected pulses from the contact pads, the effective dielectric constant was determined to be 1.50. The frequency-length product limitation of such a device was then estimated to be over 100 GHz · cm. The microwave dielectric constant of polyurethane was derived to be about 2.15, somewhat lower than expected. This is believed due to the nonrectangular shape of the microstrip line.

A Lightwave Electronics diode pumped Nd:YAG single-mode laser at 1.319 μm was used as the light source for the device characterization. The device was in polarization modulator configuration [1]. To test the device frequency response, an HP8350A sweep oscillator in combination with an HP8349B power amplifier were used to drive the device from 2 GHz to 20 GHz. Two traveling wave tubes driven by an HP8350B sweep oscillator, covering K band (18–26.5

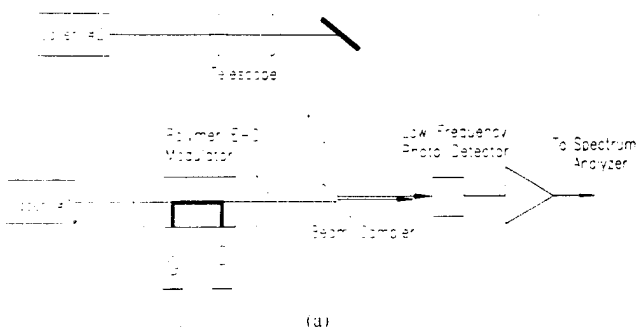

(a)

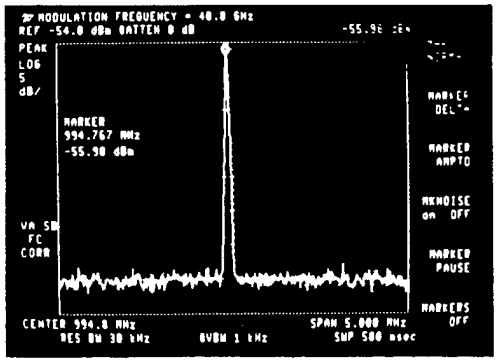

(b)

Fig. 3. The optical-heterodyne detection of the phase modulation. (a) The experiment set up. (b) The 1-GHz heterodyne signal displayed on the spectrum analyzer. The modulation frequency was 40.0 GHz and the lasers were detuned at about 39 GHz.

GHz) and Ka band (26.5–40 GHz), respectively, were used to drive the device in each frequency band. The modulated optical signal was first directly observed on an HP8592A spectrum analyzer with preamplifiers up to 22 GHz, the limit of the spectrum analyzer. Higher frequency signals up to 40 GHz were down converted by a Miteq mixer with maximum conversion loss of 12.4 dB. An HP 8350A sweep oscillator was used as the local oscillator. The mixed down signal was sent through pre-amplifiers, and observed on the spectrum analyzer. The measured response curve was obtained after calibrating the system and is shown in Fig. 2. The device response, flat up to 26 GHz, had a resonance at 19 GHz and tapered down at higher frequencies with more resonances, consistent within the accuracy of our electrical measurement. These measurements were limited by our microwave sources as well as the photodetector and the microwave mixer.

In order to improve our detection system, we recently explored optical-heterodyne detection of the modulated optical signal [12]. The second diode pumped Nd : YAG laser, detuned from the first laser at about the modulation frequency, was used as the local oscillator. The phase modulated light signal from the modulator was sent colinearly with the second laser to a low-frequency detector and observed on a spectrum analyzer (Fig. 3(a))]. The photodetector no longer needs to match the modulation frequency, and the second laser can significantly boost up the signal-to-noise ratio (Fig. 3(b)). In addition, direct observation of the phase modulation from our device can fully use the electrooptic material's nonlinearity. The measured frequency response was consistent with that from the microwave mixer measurement. Current efforts are to extend this measurement method to 60 GHz. Further investigation of novel broad-band microwave circuit designs are also under way to fully take advantage of the good velocity match of these polymer materials.

In conclusion, we have tested high-frequency traveling wave electrooptical modulators made of PUR-DR19 polymer using 1.319-μm light source. The modal properties and bandwidth-length product were calculated based on measured data. The cross-linked polymer demonstrated good temporal stability and durability at high-optical power densities. High-power single-mode operation was obtained, yielding significantly improved signal-to-noise ratios. High-frequency modulation was directly observed to 40 GHz with external microwave mixers. Optical-heterodyne detection was also introduced to observe the phase modulation with improved signal-to-noise ratios.

ACKNOWLEDGMENT

The authors would like to thank Prof. C. Joshi, M. Espiau, and M. Christianson from the Center of High Frequency Electronics at UCLA for supplying required facilities. The authors would also like to thank Prof. L. Yu at University of Chicago who contributed part of the PUR-DR19 polymer.

REFERENCES

[1] W. Wang, D. Chen, H. R. Fetterman, Y. Shi, W. H. Steier, and L. R. Dalton, "Traveling wave electro-optic phase modulator using cross-linked nonlinear optical polymer," *Appl. Phys. Lett.*, vol. 65, no. 8, pp. 929–931, 1994.

[2] C. C. Teng, "Traveling-wave polymeric optical intensity modulator with more than 40 GHz of 3-dB electrical bandwidth," *Appl. Phys. Lett.*, vol. 60, no. 13, pp. 1538–1540, 1992.

[3] D. G. Girton, S. L. Kwiatkowski, G. F. Lipscomb, and R. S. Lytel, "20 GHz electro-optic polymer Mach–Zenhder modulator," *Appl. Phys. Lett.*, vol. 58, pp. 1730–1732, 1991.

[4] R. S. Moshrefzadeh, K. M. White, C. V. Francis, M. W. Kleinschmit, S. K. Mohapatra, G. T. Boyd, R. C. Williams, K. H. Hahn, and D. W. Dolfi, "High speed optical intensity modulator in a novel polymeric material," in *Organic Thin Films for Photon. Applicat. Tech. Dig. 1993*, (Opt. Soci. Amer.), Washington, DC, vol. 17, 1993, p. 325.

[5] G. K. Gopalakrishnan, C. H. Bulmer, W. K. Burns, R. W. McElhanon, and A. S. Greenblatt, "40 GHz, low half-wave voltage Ti : $LiNbO_3$ intensity modulator," *Electron. Lett.*, vol. 28, pp. 826–827, 1992.

[6] K. Noguchi, O. Mitomi, K. Kawano, and M. Yanagibashi, "Highly efficient 40-GHz bandwidth Ti : $LiNbO_3$ optical modulator employing ridge structure," *IEEE Photon. Technol. Lett.*, vol. 5, pp. 52–54, 1993.

[7] S. Y. Wang and S. H. Lin, "High-speed III–V electrooptic waveguide modulators at $\lambda = 1.3\,\mu$m," *J. Lightwave Technol.*, vol. 6, pp. 758–771, 1988.

[8] R. G. Walker, "High-speed III–V semiconductor intensity modulators," *IEEE J. Quantum Electron.*, vol. 27, pp. 654–667, 1991.

[9] F. Kappe, G. G. Mekonnen, C. Bornholdt, F. W. Reier, and D. Hoffman, "35 GHz bandwidth photonic space switch with traveling wave electrodes on InP," *Electron. Lett.*, vol. 30, pp. 1048–1049, 1994.

[10] A. Yariv, *Quantum Electronics*, 3rd ed. New York: John Wiley, 1989, p. 322.

[11] Y. Shi, W. H. Steier, M. Chen, L. P. Yu, and L. R. Dalton, "Thermosetting nonlinear optical polymer: Polyurethane with disperse red 19 side groups," *Appl. Phys. Lett.*, vol. 60, pp. 2577–2579, 1992.

[12] T. S. Tan, R. L. Jungerman, and S. S. Elliott, "Optical receiver and modulator frequency response measurement with a Nd : YAG ring laser heterodyne technique," *IEEE Trans. Microwave Theory Tech.*, vol. 37, no. 8, pp. 1217–1222, 1989.

OPTICALLY-CONTROLLED SERIALLY-FED PHASED ARRAY SENSOR

Harold Fetterman, Yian Chang, *UCLA EE Department*
A. F. J. Tony Levi, David Cohen, *USC EE Department*
Irwin Newberg, *Hughes Aircraft Co.*

Abstract A new sensor suitable for phased array radar and imaging is proposed and demonstrated. This sensor is based on the time dependent nature of modern RF sensor systems and uses a novel optical serial feed which has all the advantages of real time delay and yet only requires one tunable laser, one optical modulator and one fiber optic grating delay. Initial results are presented to establish the viability of this approach. The results have shown true time delay for a 2-element array from 7GHz through 12GHz.

1. INTRODUCTION

We propose a new sensor, suitable for phased array radar, microwave imaging and related applications. This sensor uses a serial feed concept that represents a new departure, in these systems, that will yield a major simplification in both optical and microwave components. Unlike many of the systems currently under investigation, which use a parallel approach, our system with both phase and true time delay requires but a single tunable laser, modulator and time delay element. In addition to discussing this new architecture, we also present initial experiments establishing the viability of this approach and defining possible extensions.

The approach proposed is predicated upon using the pulsed nature of microwave radar systems in a similar manner to the clock system used in digital configurations. In this case precise timing control is used to distribute RF pulses with phase and time delay information to each element in an operating array. Specifically, the transmit function can be best described in terms of a timing unit and a distribution network as shown is Fig. 1. The desired delays for a given RF beam direction are generated sequentially by the timing unit and then demultiplexed into concurrent signals to feed the radiators by the distribution network.

The timing portion uses an electrically tuned DBR laser which is amplitude modulated with the desired microwave pulses using an optical modulator. After the modulator the laser light is directed through an optical circulator to a fiber optic grating. A typical laser light reflection spectrum from the grating is shown in Fig. 2. The grating reflects light back at different positions along the fiber depending upon the optical wavelength. Thus a wavelength-selective delay can be imposed onto each RF modulated optical pulse. In the basic system, discussed here, each serially fed optical pulse has a unique wavelength and therefore a unique time delay, relative to the RF pulse gate, which has been chosen to produce a given pointing direction. The number of pulses in the fully loaded line corresponds to the number of radiating elements in the array or subarray.

Returned light from the third port of the circulator enters the distribution network formed by the tapped optical delay line. It is important to note that this tapped optical delay line is used to demultiplex serial signals into parallel ones, and does not generate the delays for beam

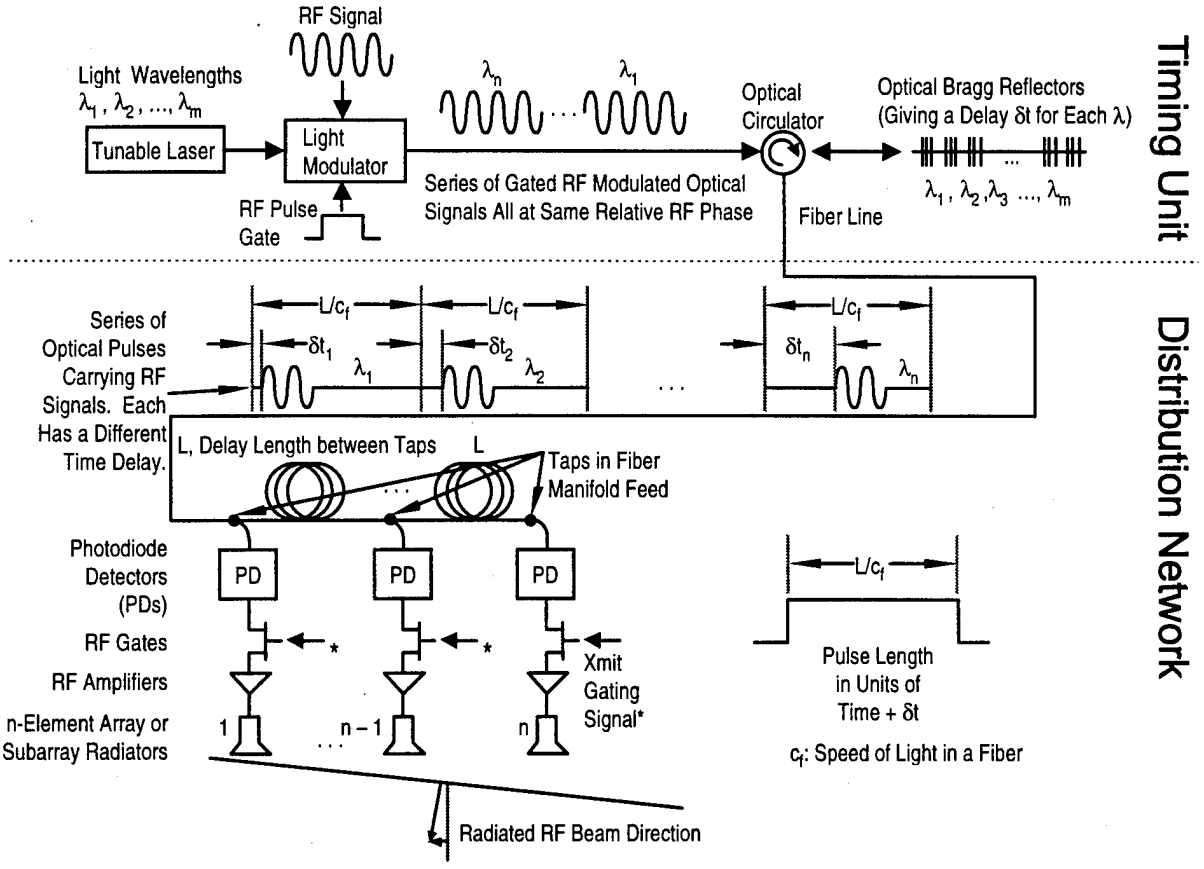

Fig. 1 Basic XMIT Mode Implementation for Array of n Elements.

steering. Once the series of optical pulses arrive at the correct delay line taps for each antenna element, the microwave modulation is obtained using photodetectors. The microwave signals from these detectors are simultaneously gated on with microwave switches (Xmit gates) when the tapped line is fully loaded. Each element's microwave pulse has the correct time delay set by the fiber grating to form a radiating beam in the desired direction. After the signal is radiated the switches are turned off and the line is reloaded. The number of radiating directions is limited only by the number of available laser wavelengths and Bragg reflectors. Although our initial efforts use a two-wavelength laser system and a fiber grating with discrete wavelength selectivity, the system will ultimately use a continuously tunable DBR laser with a continuously chirped grating to provide continuous scanning.

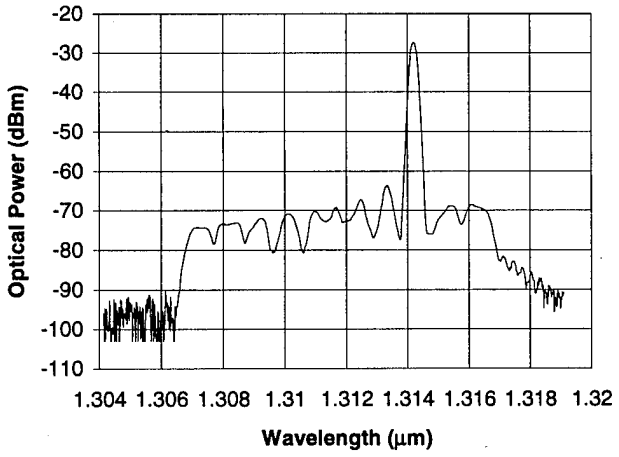

Fig. 2 Typical reflection spectrum of laser light from the fiber grating. It also shows the spontaneous emission background level resulting from reflection of the other reflectors.

2. DEMONSTRATION

To establish the viability of this approach, we have built a two-element transmitter with two optical wavelengths. The two wavelengths ($\lambda_1 = 1.307\mu m$, $\lambda_2 = 1.309\mu m$) were generated by two fixed wavelength laser diodes. By switching the diodes on and off alternately, we emulated a tunable laser. The RF signals feeding the array were monitored on a digital sampling oscilloscope. By correctly gating the signals coming out from the photodetectors, CH1 received the second pulse and CH2 received the first pulse. The pulse width was 6ns at a repetition rate of ≈25MHz which corresponded to the delay length L≈2m. The true time delay measured from the two channels of the oscilloscope was about 35ps from 7GHz through 12GHz. This agrees with the design of the fiber grating and Fig. 3 shows the monitored signals at

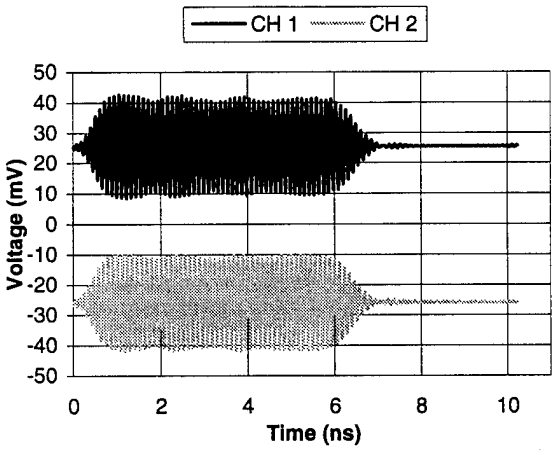

Fig. 3 λ_1 generated before λ_2. CH1 carried by λ_2 and CH2 carried by λ_1. The pulse width was 6ns with 700ps rise time. The 35ps time delay was too small to be seen in this scale.

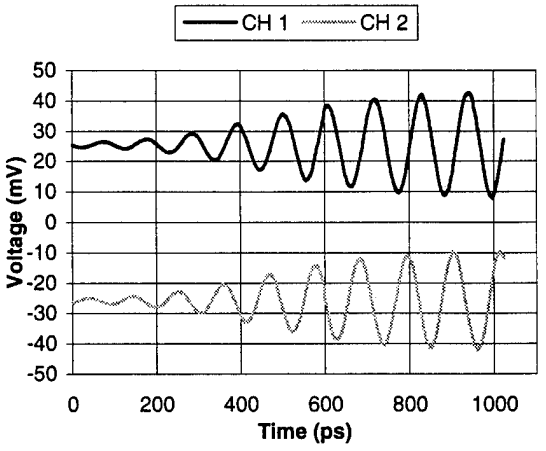

Fig. 4 This shows the leading edge of the pulses in Fig.3. λ_1 pulse (CH2) was leading λ_2 pulse (CH1) by 35ps. The RF frequency was 9.040GHz.

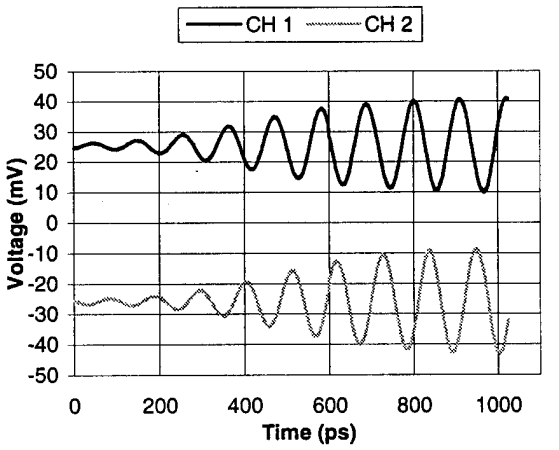

Fig. 5 λ_1 generated after λ_2. CH1 was leading CH2 in this case, a reverse of Fig. 4. This shows the RF beam was directed to the opposite side of boresight direction.

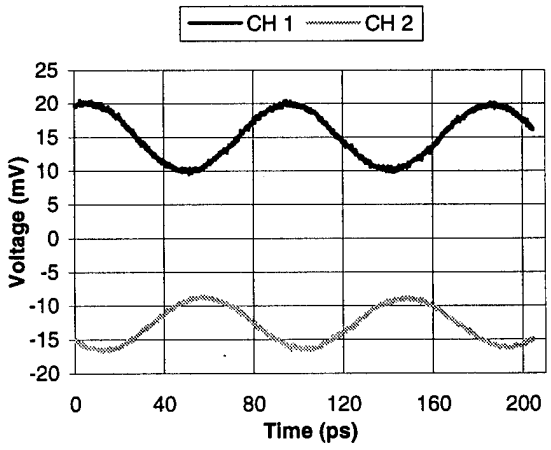

Fig. 6 The middle portion of pulses at 11.325GHz. λ_1 generated before λ_2. It shows the same amount of delay (35ps) as seen is Fig. 4.

9.040GHz. These two pulses were carried by two different wavelengths, CH1 was carried by λ_2 and CH2 was by λ_1. λ_1 pulse was generated before λ_2 pulse in the timing unit and it was delayed to match up with λ_2 pulse in the distribution network by the delay length L. The Xmit gating ensures that only the correct pulse reaches each element.

Fig. 4 shows the leading edge of the monitored pulses. A 35ps time delay can be seen between the signals. When we reversed the order of wavelength generation to λ_2 pulse before λ_1 pulse, the time delay was also reversed as shown in Fig. 5. This reverse in time delay directed the RF beam to the opposite side of boresight direction. To show the delay between the two channels was true time delay, we measured it at different RF frequencies ranging from 7GHz to 12GHz. Fig. 6 shows the measurement at 11.325GHz. The time delay was 35ps, equals that at 9.040GHz. The middle portion of pulses were chosen for higher accuracy because best fitting could be applied using sine functions. The leading edges were similar to those in Fig. 4 and 5 at all frequencies.

3. CONCLUSIONS

A new serially-fed true time delay system has been proposed and the basic concept has been experimentally verified. It uses only one tunable laser, one optical modulator and one delay element to achieve beam steering. The system is quite versatile and can be used to control both one and two dimensional arrays. Furthermore, a natural extension to the receive mode can also be implemented for passive imaging. Essentially, by using the natural timing of our pulsed radar we are able to greatly simplify and to increase the flexibility of optically controlled systems.

The system we have presented is the simplest unit based upon the concept of a serial feed. It is possible to greatly enhance this system in several areas. For example, the concept of using multiple frequencies at the optical modulator input. Splitting losses for large systems may require optical amplifiers or the use of a modified corporate feed with appropriate delays rather than a single tapped line delay. However the system is extremely flexible and can be extended to meet specific requirements such as range gating and higher resolution performance.

This work has been supported by the National Center for Integrated Photonic Technology under ARPA contract #MDA972-94-1-0001 and by the Air Force Office of Scientific Research.

Yian Chang: PhD. Student at University of California, Los Angeles, CA90095. Voice: (310) 825-2734 Fax: (310) 206-9497 E-mail: ychang@ee.ucla.edu.
David Cohen: PhD. Student at University of Southern California, Los Angeles, CA90089-1112. Voice: (213) 740-5583 Fax: (213) 740-9280 E-mail: davidcoh@usc.edu.
Harold R. Fetterman: Professor of Electrical Engineering Department at University of California, Los Angeles, CA90095. Voice: (310) 825-3431 Fax: (310) 206-9497 E-mail: fetter@ee.ucla.edu.
A. F. J. Tony Levi: Professor of Electrical Engineering Department at University of Southern California, Los Angeles, CA90089-1112. Voice: (213) 740-7318 Fax: (213) 740-8158 E-mail: alevi@alnitak.usc.edu.
Irwin L. Newberg: Project Manager of Radar & Communications Systems, Hughes Aircraft Co., PO Box 92426, Los Angeles, CA90009-2426. Voice: (310) 334-6834 Fax: (310) 607-5699 E-mail: inewberg@msmail4.hac.com.

PHOTONICS TECHNOLOGY LETTERS

Optically-Controlled Serially-Fed Phased Array Sensor

David Cohen*, Yian Chang†
A. F. J. Levi*, Harold Fetterman†
Irwin Newberg‡

Abstract

A new type of RF-photonic sensor system design suitable for radar and communication phased arrays is proposed which uses an optical serial feed. This system has all the advantages of true time delay and yet only requires one tunable laser and one fiber optic grating delay. In addition to discussing the capabilities and simplicity of this configuration, we also present initial experiments establishing the viability of the basic approach.

* Department of Electrical Engineering, University of Southern California, Los Angeles, CA 90089-1112
† Department of Electrical Engineering, University of California at Los Angeles, Los Angeles, CA 90095
‡ Radar and Communication Systems, Hughes Aircraft Company, Los Angeles, CA 90009-2426

I. INTRODUCTION

We propose a new photonic sensor system suitable for RF phased array sensors. This system uses a serial feed concept that represents a major simplification in both optical and microwave components compared with conventional parallel systems[1]-[6]. Our system provides both phase and true time delay for beam steering and it requires a single tunable laser, optical modulator, and time delay element[7]. We present initial experiments establishing the viability of our approach in which the use of fiber optic techniques, such as long and low-loss delay lines, are intrinsic to the operation of the system.

Our design exploits the pulsed nature of most microwave sensors in a manner similar to clocked systems used in digital configurations. Precise timing control of photonic signals is used to distribute RF pulses with time/phase delay information to each element in a radiating/receiving array. In order to describe the proposed mechanism of operation, we divide the transmit function into two parts; the first part is the timing unit, shown in figure 1a. The most technology intensive component, the fast and broad-band tunable laser shown on the left, can tune rapidly over at least 20 nanometers by proper current adjustment.[8] A typical laser of this type can be electronically tuned in less than a nanosecond. Using an optical modulator, the light from the laser is amplitude modulated at the desired microwave operating frequency and is gated at the radiated pulse width. After leaving the modulator the light is passed through an optical circulator and

then into a fiber grating. The reflected light from the grating returns to the circulator and is directed onto a tapped optical delay line as shown in figure 1b.

In our system the timing information is obtained via the fiber grating which yields a wavelength-selective propagation delay for each gated pulse. Although our initial efforts use a grating with discrete wavelength selectivity, the system may alternately incorporate a continuously chirped grating. Since the wavelength of the laser can be tuned continuously over a 20 nm range, and the fiber grating reflectors have a 0.3 nm FWHM (corresponding to an 53 GHz bandwidth), the system can access at least 60 different time delays. Each serially-fed optical pulse has a unique time delay, relative to the RF gate timing. It is these delays that will ultimately produce the given pointing direction of our phased array. The number of pulses in the fully loaded line corresponds to the number of radiating elements in the array (or subarray).

The tapped delay line consists of a fiber having equally spaced taps. The optical propagation time between these taps corresponds to the length of the longest radiated pulse. It is important to note that the RF gate frequency in this approach must be equal to (or an integral multiple of) the inter-tap delay time. From the circulator, each gated pulse will arrive with the additional delay imposed by the fiber grating at the intended tap on the delay line at the same time.

The microwave signal from the optical detector, located at each tap, is gated on with a microwave switch when the tapped delay line is fully loaded. Each antenna

element's microwave pulse therefore has the correct time delay, as set by the fiber's Bragg grating reflector, to form a radiating beam in a desired direction. There is complete freedom in choosing this direction limited only by the number of available laser wavelengths and associated Bragg grating reflectors. After the signal is radiated the switches are turned off and the line is reloaded. In a higher duty cycle system (~100%) a modification can be used in which the line can be continuous loaded.

II. EXPERIMENTAL

Instead of using a tunable laser, it is possible to use arrays of lasers, including VCSELs, that are switched on and off to obtain a large set of precise optical wavelengths. To evaluate the basic concept of switching wavelengths to rapidly switch time delays in our serially fed system, we have set up a prototype experiment using two 1.3 μm lasers and a ten grating reflector fiber. These lasers are alternately switched on and off and are tuned to different grating reflectors on a fiber optic line separated by 1.7 mm corresponding to 17.5 psec round trip. The lasers are alternately switched on and off as shown in figure 2a. As indicated, the pulse widths in this particular experiment, are on the order of 6 ns with the complete switching time occupying less than 1 ns. There is no fundamental limit to the length of the pulses used in this experiment; 6 ns was only chosen for convenience. In figure 2b we show the optical signal, with a 10 GHz microwave modulation, reflected from the grating. The typical -35dB side-mode suppression in the DBF laser is enhanced by a few dB after passing through the fiber

grating. This is due to the fact that the reflection wavelength of the neighboring line does not overlap with the DFB's natural subsidiary maxima. Therefore we obtain about -40dB (-80dB electrical) optical purity which can be directly converted to the maximum obtainable signal to noise performance of the system.

Measurements have been made at 3, 10 and 18 GHz to examine the precision and switching dynamics of the microwave phase change. In figure 3a we show the reflected light, modulated at 3 GHz, detected and displayed upon a digital sampling oscilloscope. The scope is triggered with the same synthesizer which drives the modulator. Note that the results at 10 GHz (3b) is also switched, with a phase shift corresponding to 17.5 ps (63°) by changing the laser wavelength. This experiment was also repeated at 18 GHz and yielded a phase shift of 110° as shown in figure 3c. Finally, by switching to another grating reflector on the fiber corresponding to a delay of 54.9 ps, a phase shift of 200° at 10 GHz was obtained as shown in figure 3d.

These measurements demonstrate that wavelength switching speeds and the reproducibility required for the laser can be obtained using commercially available components. These results also establish that current fiber grating delay lines offer sufficiently high contrast ratios to limit the background scattered light level in the system. Note that obtained phase noise ratio of better than 80 dB is outstanding for such a system and was limited by the RIN noise, and spectral purity, of the lasers used.

III. RECEIVER MODE

Although only the basic transmit mode is presented here, the same system can be utilized in the receive mode and is shown in figure 4. Since there is no optical or microwave pulse gating only the carrier phase is required at each antenna element for a given direction of observation. As indicated in the figure each wavelength is distributed to a given receiver mixer and provides an LO shifted in phase the exact reverse as was used in steering the beam in XMIT. This reverse phase (or conjugate) can be generated using the grating delay in reverse.

Essentially, the compatible receiver we propose utilizes the reversed phase delays to yield the equivalent of a configurable matched filter. Thus the signals from the XMIT photodiodes are fed to a mixer which homodynes this optically generated microwave local oscillator with the received microwave signal. The signals from each antenna element are then added coherently in a simple summer signal processor to form the received antenna beam signal. In actual practice an electronic switch could be used between XMIT and receive functions in a full RF array design to allow the same signal/timing unit and optical feed to be used to generate RF signals with steering phases for XMIT and receive. A low frequency laser can be used, as shown in figure 4, to transmit the composite summed signal to a remote site for further processing and display.

It is important to note that these delayed RF signals, generated by laser tuning and grating delay, have a RF phase characteristic of a true time delay system. This yields a

wide tuning frequency bandwidth capability for constant pointing. The technique is relatively simple and capable of steering the receive beam through all the angles as in the transmit mode. Because of the receiving technique used, the proposed system can meet the RF performance specifications of a large subset of potential users. By using parallel delay lines the duty cycle can be increased to virtually 100% and it can be used in passive imaging systems.

IV. Conclusion

A novel serially-fed true time delay system has been proposed and the basic concept has been experimentally verified. The system we have presented is the simplest implementation based upon a serial feed. It uses only one tunable laser, modulator and delay element to achieve completely addressable time/phase. The system is versatile and could be used to control both one and two dimensional arrays as well as multibeam systems. Because the amplitude and time delay for each radiating element is programmable, arbitrary beam forming is possible. Essentially, by using the natural timing of pulsed RF systems we are able to greatly simplify, to reduce the cost, and to increase the flexibility of optically controlled radar, communication and electronic warfare applications.

ACKNOWLEDGMENT

This work has been supported by the National Center for Integrated Photonic Technology under ARPA contract #MDA972-94-1-0001 and by the Air Force Office of Scientific Research.

REFERENCES

[1] D. Dolfi, M. Labeyrie, P. Joffre and J. P. Huignard, "Liquid crystal microwave phase shifter," *Elect. Lett.*, vol. 29, no. 10, pp. 926-928, 1993.

[2] H. R. Fetterman, Y. Chang, D. C. Scott, S. R. Forrest, et al., "Optically controlled phased array radar receiver using SLM switched real time delays," *IEEE Microwave and Guided Wave Lett.*, vol. 5, no. 11, pp. 414-416, 1995.

[3] L. Xu, R. Taylor and S. R. Forrest, "True time-delay phased-array antenna feed system based on optical heterodyne techniques," *IEEE Photon. Technol. Lett.*, vol. 8, no. 1, pp. 160-162, 1996.

[4] R. D. Esman, M. Y. Frankel, J. L. Dexter, L. Goldberg, et al., "Fiber-optic prism true time-delay antenna feed," *IEEE Photon. Technol. Lett.*, vol. 5, no. 11, pp. 1347-1349, 1993.

[5] L. J. Lembo, T. Holcomb, M. Wickham, P. Wisseman and J. C. Brock, "Low-loss fiber optic time-delay element for phased-array antennas," *Proceedings of the SPIE - The International Society for Optical Engineering*, vol. 2155, pp. 13-23, 1994.

[6] A. Molony, C. Edge and I. Bennion, "Fibre grating time delay element for phased array antennas," *Elect. Lett.*, vol. 31, no. 17, pp. 1485-1486, 1995.

[7] G. A. Ball, W. H. Glenn and W. W. Morey, "Programmable fiber optic delay line," *IEEE Photon. Technol. Lett.*, vol. 6, no. 6, pp. 741-743, 1994.

[8] M. Schilling, W. Idler, E. Kuhn, G. Laube, et al., "Integrated interferometric injection laser: novel fast and broad-band tunable monolithic light source," *IEEE J. of Quantum Elect.*, vol. 27, no. 6, pp. 1616-1624, 1991.

ILLUSTRATION CAPTIONS

Figure 1 (a) Basic XMIT mode implementation for array of n elements. It shows only one laser, one optical modulator and one delay element are needed.

(b) Tapped optical delay line used as the distribution network to demultiplex serial pulses into parallel ones.

Figure 2a Laser 1 and Laser 2 are alternately switched on and off with pulse widths about 6 ns and switching time less than 1 ns.

Figure 2b The optical spectrum of λ_1 after reflection from the fiber grating for the case of 10 GHz modulation, and 167 MHz wavelength switching. This shows the spontaneous emission background level resulting from reflection of the other grating reflectors.

Figure 3a True time delay (TTD) @ 3 GHz. The switching of the wavelengths was done at 167 MHz. The separation was about 17.5 ps, or about 18°. The signal is inverted due to the RF amplifier.

Figure 3b TTD @ 10 GHz. This demonstrates a 17.5 ps time delay resulting in a phase shift of 63°.

Figure 3c TTD @ 18 GHz. This demonstrates a 17.5 ps time delay resulting in a phase shift of 110°.

Figure 3d TTD @ 10 GHz. A different grating reflector was used here. It shows a larger time delay (54.9 ps) resulting in a phase shift of 200°.

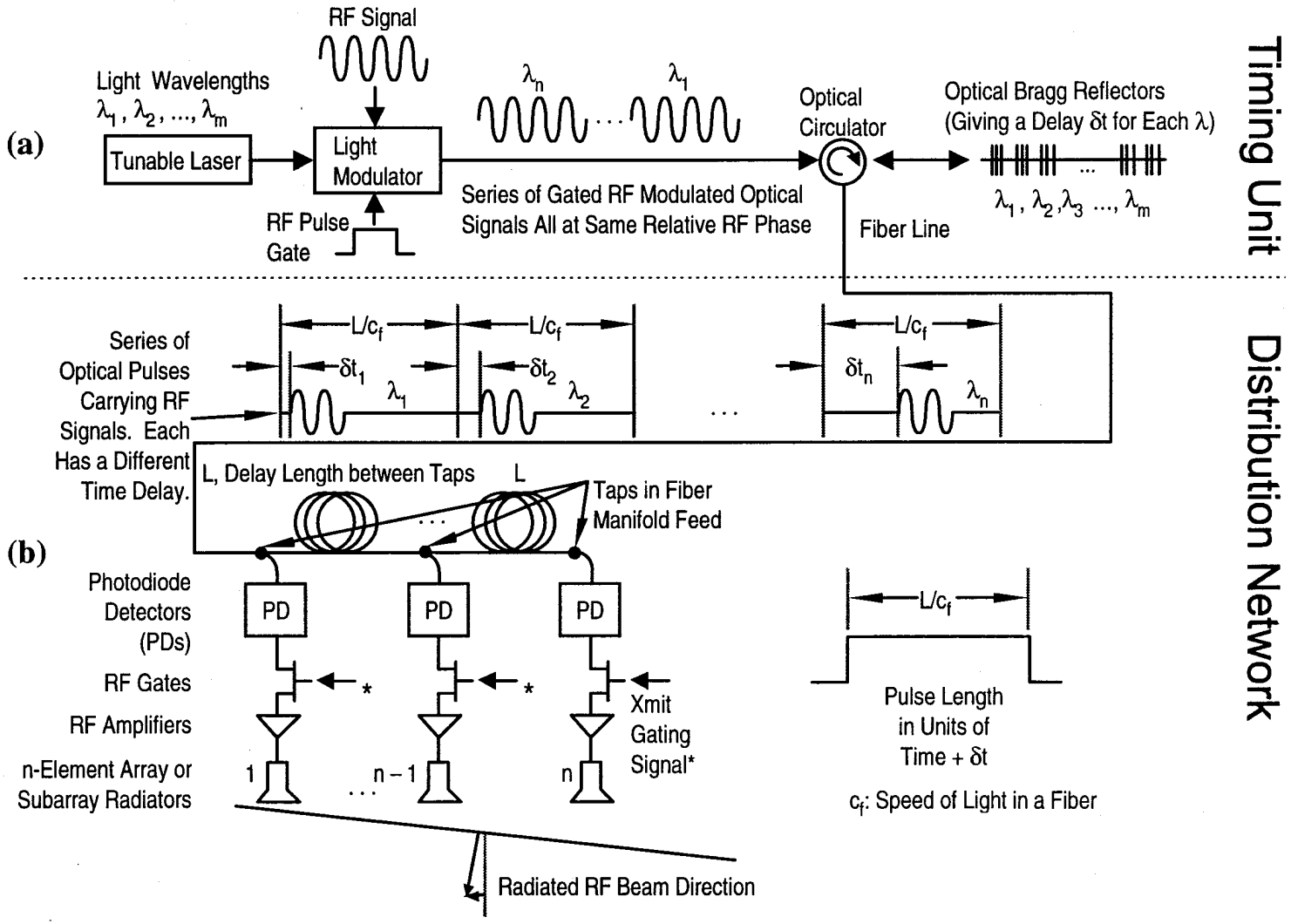
Timing Unit
Distribution Network
(a)
RF Signal
Light Wavelengths
$\lambda_1, \lambda_2, \ldots, \lambda_m$
Tunable Laser
Light Modulator
RF Pulse Gate
$\lambda_n \cdots \lambda_1$
Series of Gated RF Modulated Optical Signals All at Same Relative RF Phase
Optical Circulator
Optical Bragg Reflectors (Giving a Delay δt for Each λ)
$\lambda_1, \lambda_2, \lambda_3 \ldots, \lambda_m$
Fiber Line
(b)
Series of Optical Pulses Carrying RF Signals. Each Has a Different Time Delay.
L/c_f
δt_1
λ_1
δt_2
λ_2
δt_n
λ_n
L, Delay Length between Taps
L
Taps in Fiber Manifold Feed
Photodiode Detectors (PDs)
PD
RF Gates
RF Amplifiers
n-Element Array or Subarray Radiators
1
n – 1
n
Xmit Gating Signal*
Pulse Length in Units of Time + δt
c_f: Speed of Light in a Fiber
Radiated RF Beam Direction

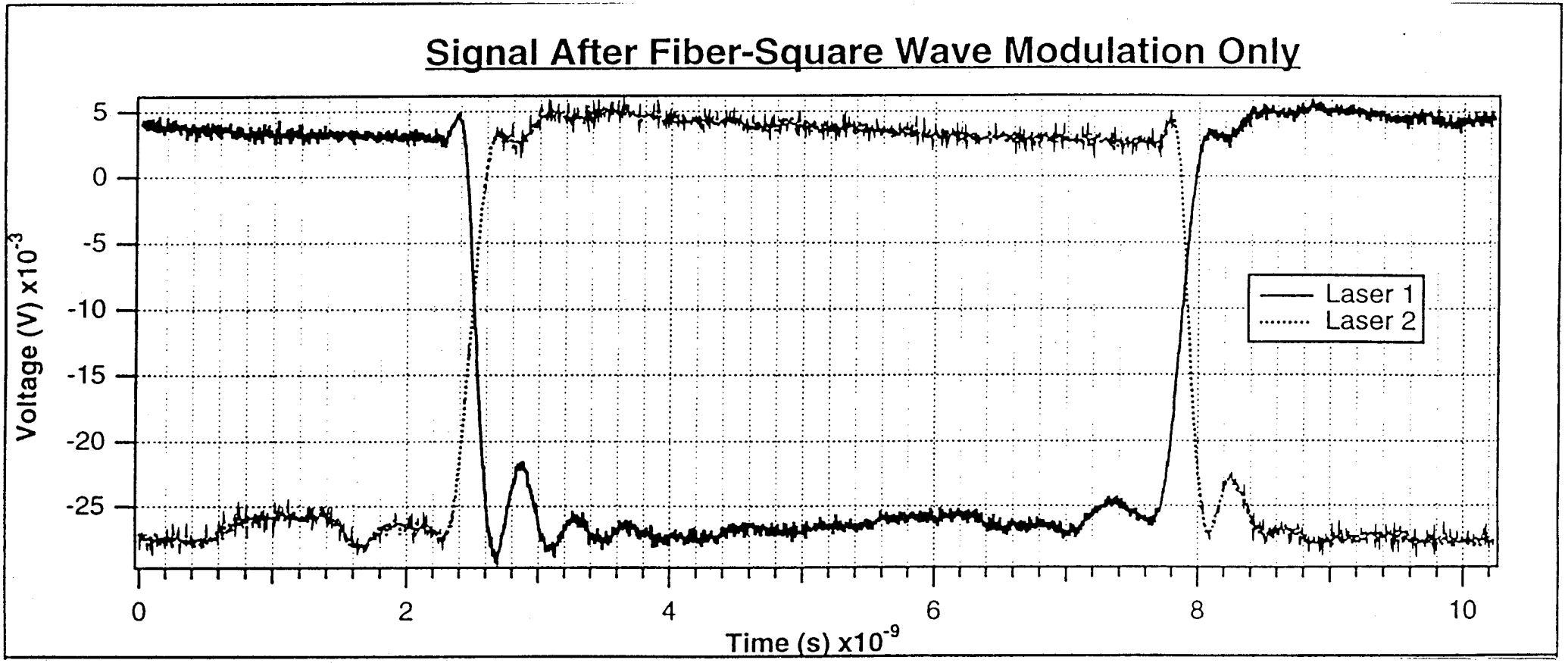
Signal After Fiber-Square Wave Modulation Only
Voltage (V) x10^-3
5
0
-5
-10
-15
-20
-25
0
2
4
6
8
10
Time (s) x10^-9
Laser 1
Laser 2

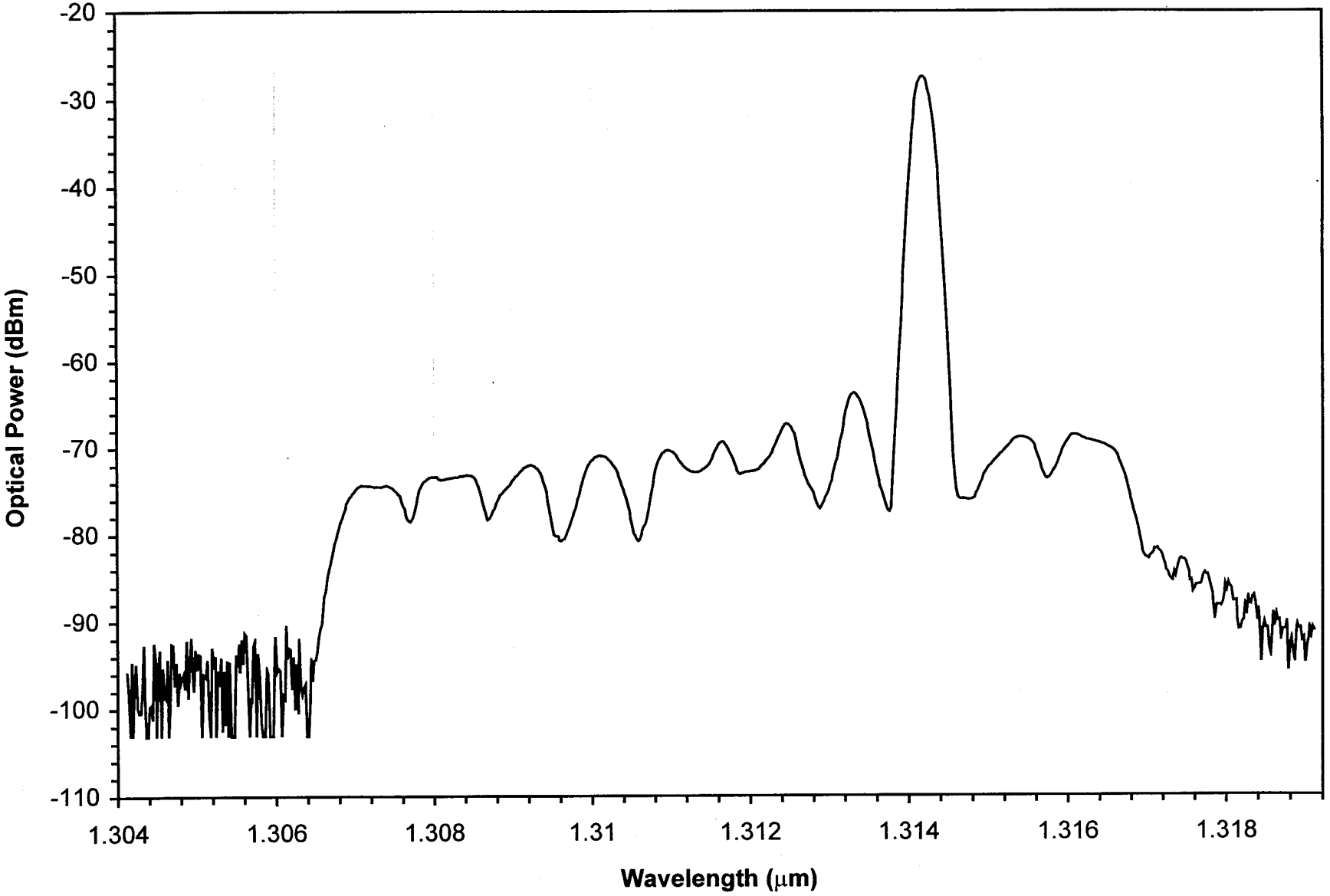
-20
-30
-40
-50
-60
-70
-80
-90
-100
-110
Optical Power (dBm)
1.304
1.306
1.308
1.31
1.312
1.314
1.316
1.318
Wavelength (μm)

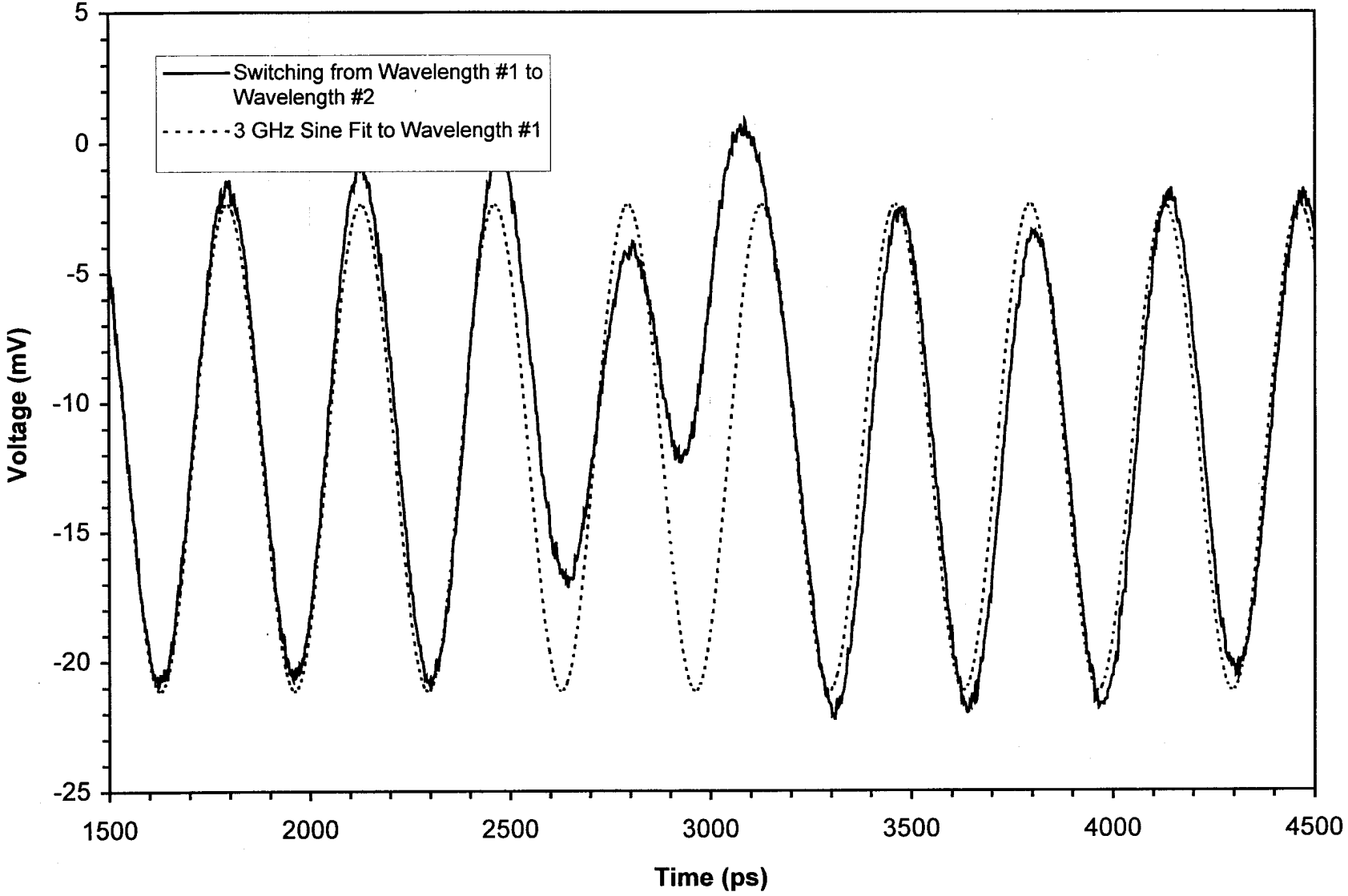
Switching from Wavelength #1 to Wavelength #2
3 GHz Sine Fit to Wavelength #1
Voltage (mV)
5
0
-5
-10
-15
-20
-25
1500
2000
2500
3000
3500
4000
4500
Time (ps)

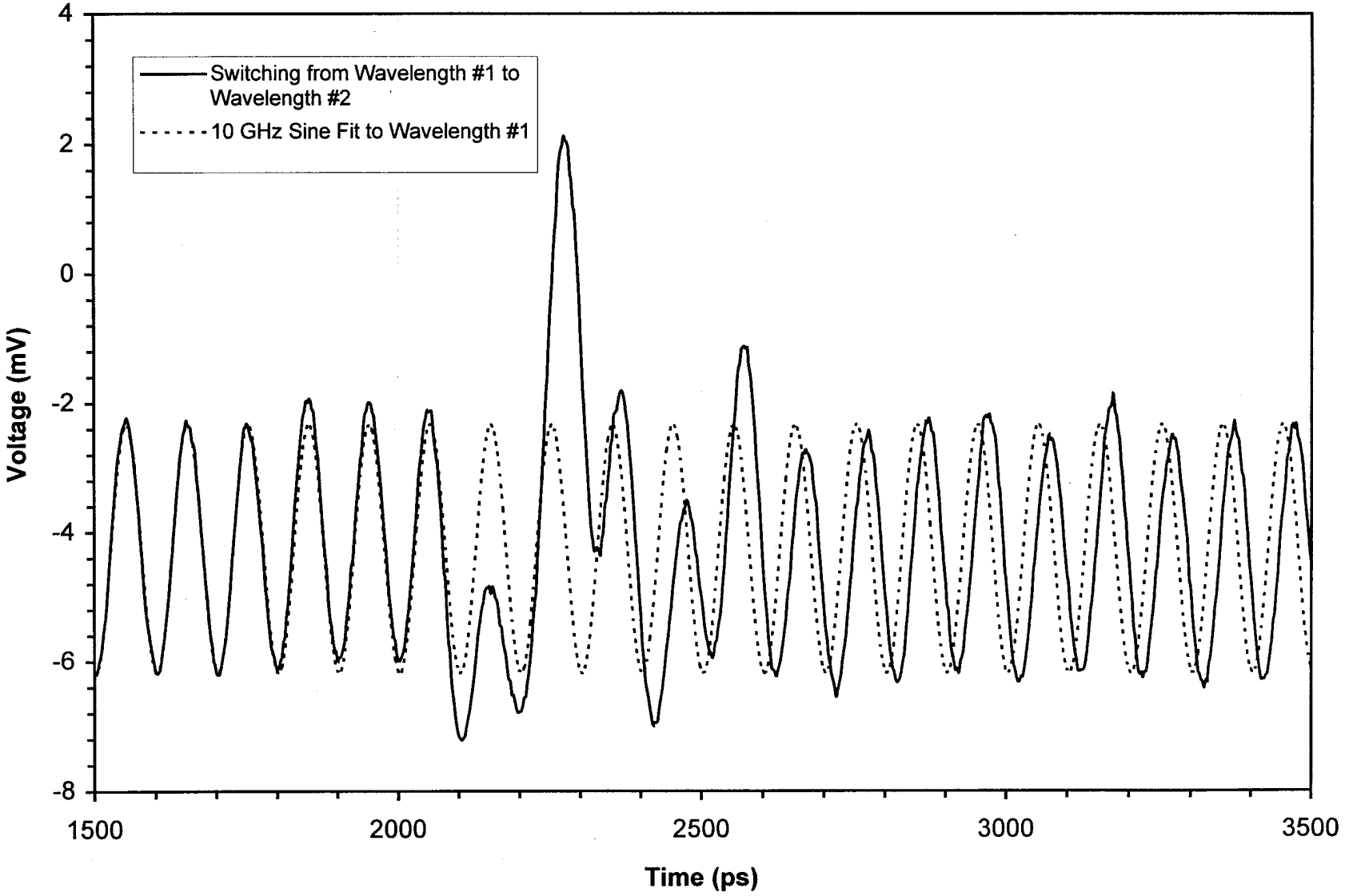
Switching from Wavelength #1 to Wavelength #2
10 GHz Sine Fit to Wavelength #1
Voltage (mV)
4
2
0
-2
-4
-6
-8
1500
2000
2500
3000
3500
Time (ps)

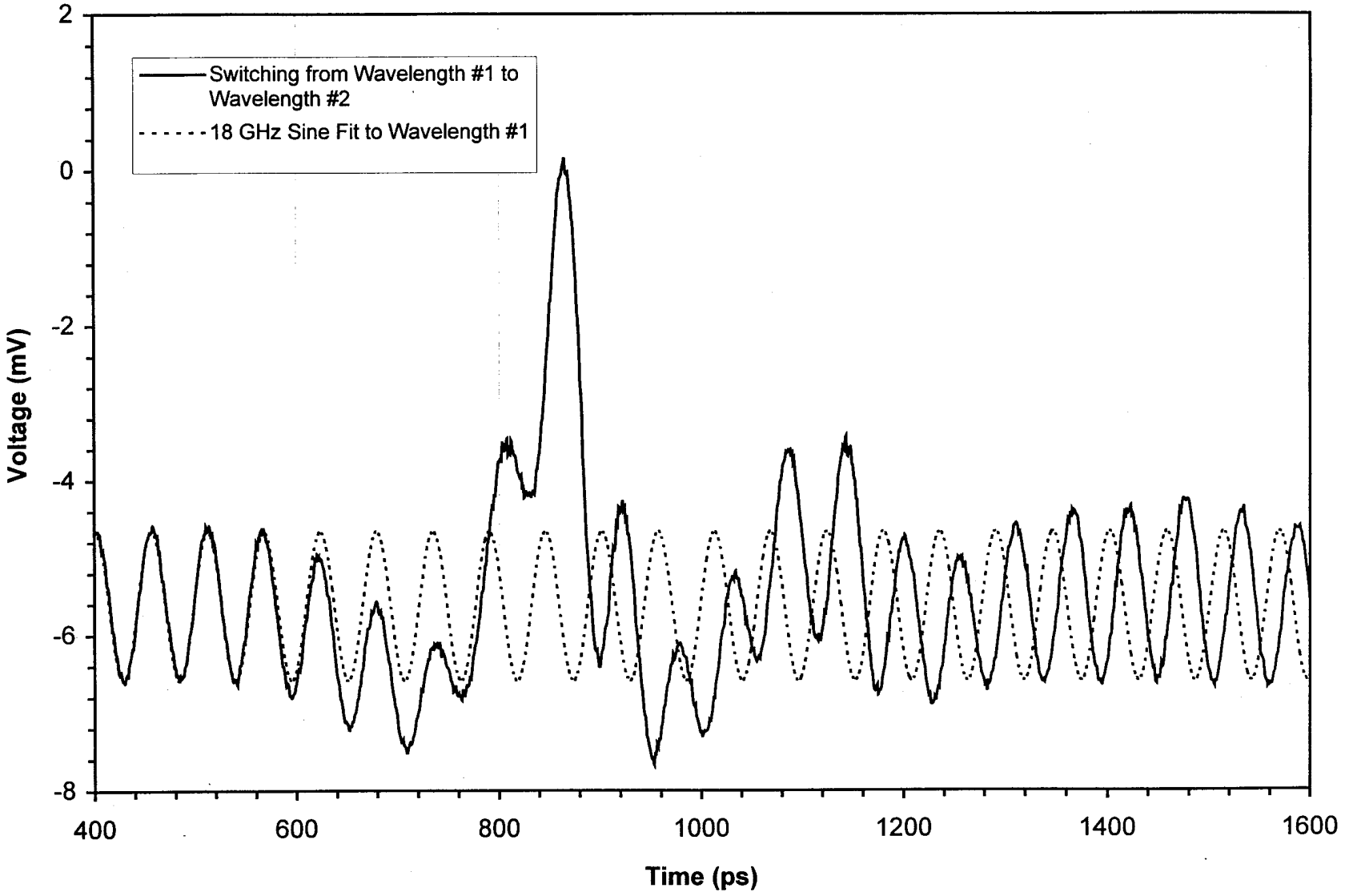
Switching from Wavelength #1 to Wavelength #2
18 GHz Sine Fit to Wavelength #1
Voltage (mV)
2
0
-2
-4
-6
-8
400
600
800
1000
1200
1400
1600
Time (ps)

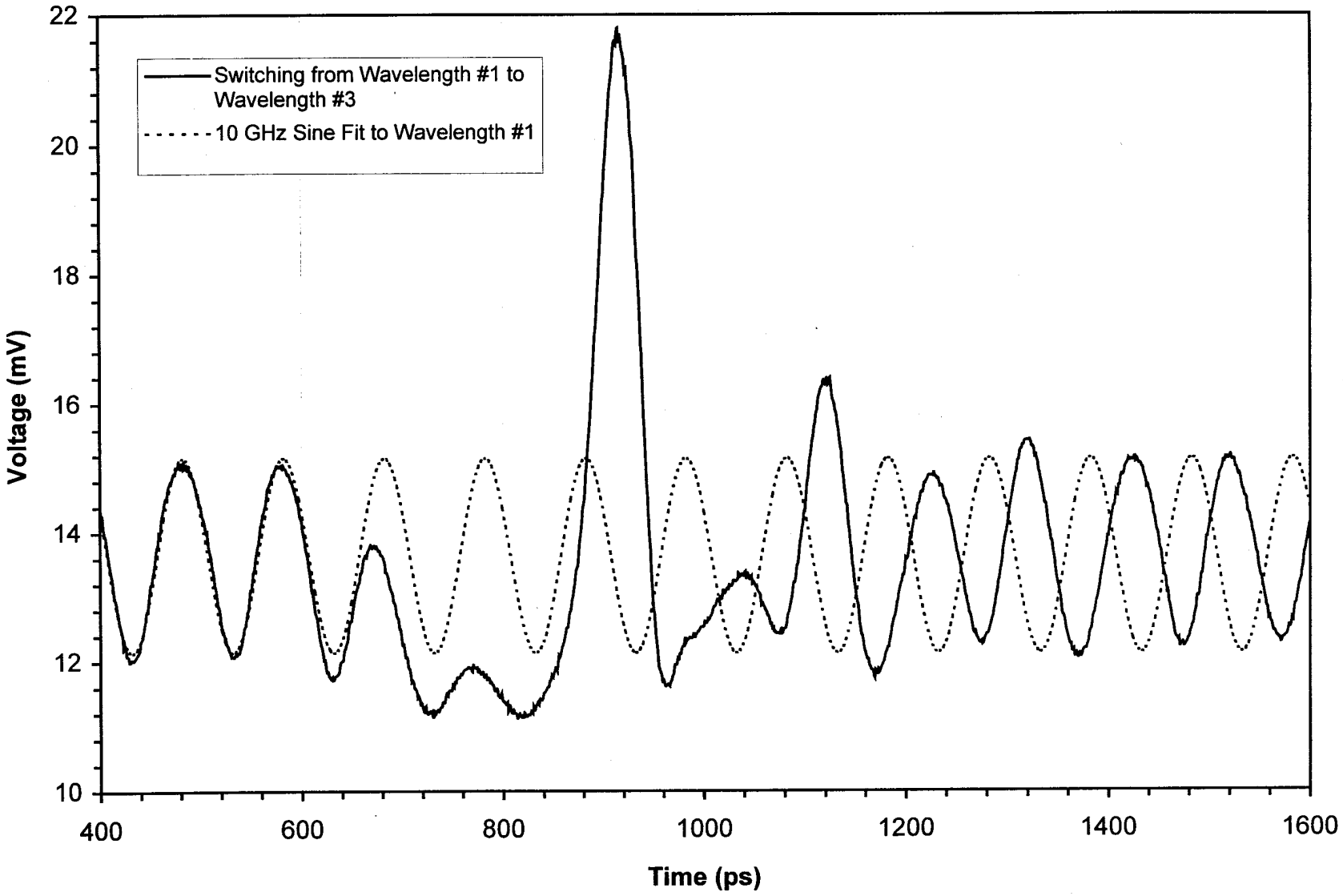
Switching from Wavelength #1 to Wavelength #3
10 GHz Sine Fit to Wavelength #1
Voltage (mV)
22
20
18
16
14
12
10
400
600
800
1000
1200
1400
1600
Time (ps)

Optically Controlled Phased Array Radar Receiver Using SLM Switched Real Time Delays

H. R. Fetterman, *Fellow, IEEE*, Y. Chang, D. C. Scott, S. R. Forrest, F. M. Espiau, M. Wu, *Member, IEEE*, D. V. Plant, *Member, IEEE*, J. R. Kelly, A. Mather, W. H. Steier, *Fellow, IEEE*, R. M. Osgood, Jr., *Fellow, IEEE*, H. A. Haus, *Life Fellow, IEEE* and G. J. Simonis

Reprinted from
IEEE MICROWAVE AND GUIDED WAVE LETTERS
Vol. 5, No. 11, November 1995

Optically Controlled Phased Array Radar Receiver Using SLM Switched Real Time Delays

H. R. Fetterman, *Fellow, IEEE*, Y. Chang, D. C. Scott, S. R. Forrest, F. M. Espiau, M. Wu, *Member, IEEE*, D. V. Plant, *Member, IEEE*, J. R. Kelly, A. Mather, W. H. Steier, *Fellow, IEEE*, R. M. Osgood, Jr., *Fellow, IEEE*, H. A. Haus, *Life Fellow, IEEE*, and G. J. Simonis

Abstract—**We report the results of a demonstration of a real time delay, optically controlled phased array radar receiver. This implementation employed a free space configuration based upon an optical switching network using liquid crystal spatial light modulators (SLM's). A three-delay unit, two-antenna array receiver was implemented at an optical wavelength of 1.3 μm and demonstrated "squint-free" operation over the entire X-band (8–12 GHz) with an angular accuracy of 1.4°. Finally, a novel configuration for the two-antenna element SLM architecture was proposed and demonstrated equivalent system performance with a reduction in the number of components.**

INTRODUCTION

RECENTLY, there has been considerable interest in employing optical true time delays as a means for optically controlling phased array antennas. Several methods have been proposed to accomplish this task including the use of fiber loops in conjunction with bias switched detector arrays [1], optical heterodyne techniques for generating and sorting delays [2], and bulk optical delay lines using spatial light modulators (SLM's) [3], [4]. In the experiments presented here, we demonstrate an optically controlled phased array radar receiver using the SLM/bulk optics approach. This is the first demonstration using the SLM/bulk optics architecture at an optical wavelength of 1.3 μm that exhibits "squint free" operation over the entire X-band (8–12 GHz). In addition, the use of computer processing techniques on the data collected has resulted in an angular accuracy of 1.4° using only two antenna array elements and three SLM optical delay units. Finally, a novel configuration for the SLM receiver architecture is proposed and demonstrated that can increase the digital resolution from 15 sampled points to 64, improving the angular accuracy of the radar receiver without increasing the number of components.

Fig. 1 displays the configuration of our optically controlled phased array radar receiver that is based on the spatial light modulator (SLM) architecture previously proposed by Dolfi *et al.* [3]. An X-band horn radiates into the two-element antenna array at an unknown angle, θ. The plane waves emanating from the horn will couple to the antennas at different times, thereby generating a phase difference between the signals at the output of the antennas. This phase difference is given mathematically by $\Delta\varphi_m = (2\pi d/\lambda_m)\sin(\theta)$ where d is the spacing between the antennas, λ_m is the wavelength of the microwave signal from the horn, and θ is the angle of the horn measured with respect to broadside of the antenna array [1]. In our system, we determine the microwave phase difference, $\Delta\varphi_m$, by optical processing techniques and then determine the angle of the horn through this equation.

The antenna array consists of two exponentially tapered coplanar double-strip antennas with constant impedance of 175 Ω over a 5–20 GHz band. The spacing between the antennas was $d = 20$ mm. The signals acquired by the antennas drive two $LiNbO_3$ Mach–Zehnder optical modulators (3 dB RF modulation bandwidths of 10 GHz) which intensity modulates the output from two 1.3 μm distributed feedback (DFB) laser diodes. The DFB lasers were temperature and current stabilized with average output optical powers of 10 mW and linewidths of 10 MHz.

The microwave phase information is now encoded onto the two light beams that traverse through the optical processing network, which consists of three delay units. Each delay unit contains a polarization rotating SLM and polarization beam splitting cubes as shown in Fig. 1. The liquid crystal SLM's can rotate the 1.3 μm optical polarization by 90°, when 16 V are applied, with an extinction ratio of 32 dB. The first delay unit can delay the optical signals by Δt, the second by $2\Delta t$, and the third by $4\Delta t$ units of time. By employing this methodology, one can obtain $2^{(n+1)} - 1$ distinct optical delay combinations where n is the number of delay units. Thus, in our two-antenna, three-delay unit system, we obtain 15 distinct delays.

The optical delay network adds a suitable phase difference, $\Delta\varphi_{\text{delay}}$, between the two microwave signals. The two microwave signals are then extracted from the light beams by two

Manuscript received June 8, 1995. This work was supported by the National Center for Integrated Photonics Technology and the Air Force Office of Scientific Research under the direction of H. R. Schlossberg.

H. R. Fetterman, Y. Chang, D. C. Scott, F. M. Espiau, and M. Wu are with the Department of Electrical Engineering, University of California at Los Angeles, Los Angeles, CA 90024 USA.

S. R. Forrest is with the Advanced Technology Center for Photonics and Optoelectronic Materials, Princeton University, Princeton, NJ 08544 USA.

D. V. Plant is with the Department of Electrical Engineering, McGill University, Montreal, Canada H3A 2A7.

J. R. Kelly is with the Liquid Crystal Institute, Kent State University, Kent, OH 44242 USA.

A. Mather and W. H. Steier are with the Department of Electrical Engineering, University of Southern California, Los Angeles, CA 90089-0483 USA.

R. M. Osgood, Jr. is with the Department of Electrical Engineering and Applied Physics, Columbia University, New York, NY 10027 USA.

H. A. Haus is with the Department of Electrical Engineering and Computer Science, Massachusetts Institute of Technology, Cambridge, MA 02139-4307 USA.

G. J. Simonis is with the Army Research Laboratory, Adelphi, MD 20783 USA.

IEEE Log Number 9414635.

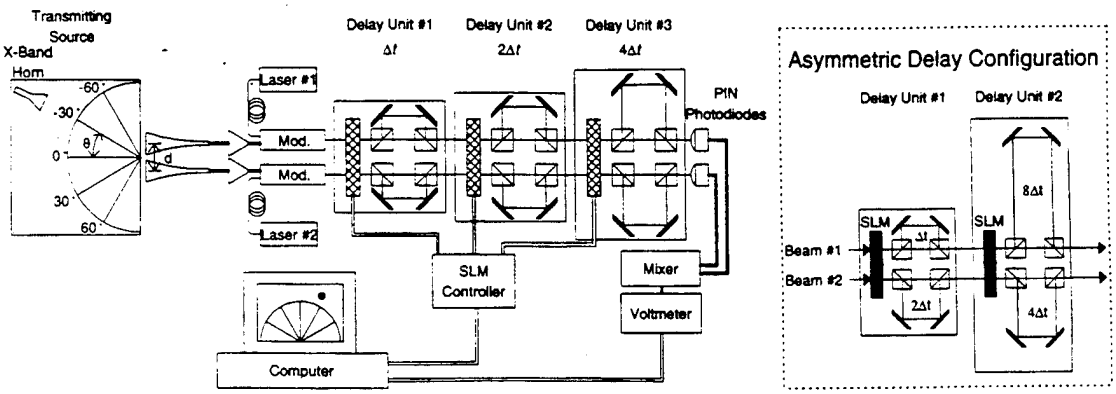

Fig. 1. (a) Schematic of the three-unit optically controlled true time delay phased array radar receiver. Polarization beam splitters and liquid crystal SLM's are used to switch the beams through different optical delay paths. (b) The asymmetric configuration used to increase the angular resolution.

InGaAs/InP p-i-n photodiodes that have 30 GHz bandwidths [5]. The microwave outputs of the two photodiodes are then homodyne mixed in a conventional microwave mixer. From homodyne mixing theory, the output of the mixer contains a dc component given by

$$V_{DC} = A + B\cos[\underbrace{2\pi f_m(p\Delta t)}_{\Delta\varphi_{\text{delay}}} + \Delta\varphi_m]$$

where A and B are constants, f_m is the microwave frequency, and p is an integer in the range $-7 \le p \le 7$ for our three delay unit system [6]. From this equation, we find that as we switch through the different optical delay paths the homodyne mixing voltage, V_{DC}, follows a cosine of frequency f_m and phase $\Delta\varphi_m$. Extraction of the phase $\Delta\varphi_m$ from this cosine function then uniquely determines the angle of the source.

We observe that the measured dc voltage from the homodyne mixing will be a maximum when $\Delta\varphi_{\text{delay}} = -\Delta\varphi_m$ and since $\Delta\varphi_{\text{delay}}$ is a known parameter, we can determine the sought after microwave phase difference that was originally incident on the two antennas and thus calculate the angle at which the X-band horn is located. Since $\Delta\varphi_{\text{delay}}$ is discrete our resulting real-space angular accuracy, θ_{res}, is determined by $\theta_{\text{res}} = \arcsin(c\Delta t/d)$ [1]. Given $\Delta t = 5.5$ ps and $d = 20$ mm, we obtain an angular accuracy of $\theta_{\text{res}} \cong 5°$ for our system. We significantly improved the angular accuracy of our system by determining $\Delta\varphi_m$ using a least squares fit to the discrete set of data [7]. A least squares fit for this data is obtained by minimizing the function $\Pi = \sum_{i=1}^{15} |V_{DCi} - [A + B\cos(\omega_m\tau + \Delta\varphi_m)]|^2$ where A, B, and $\Delta\varphi_m$ are the adjustable parameters. Fig. 2 displays a least squares curve fitting to the 15 sampled points with the horn at a real-space angle of $-25°$ and a microwave frequency of 10.5 GHz. From the least squares fit, we obtain $\Delta\varphi_m = -1.89$ radians, which corresponds to a calculated real-space angle of $-25.98°$.

To determine the angular accuracy of this technique, we calculate the "standard error of the mean" of the data shown in Fig. 2. $\sigma_M = (\sigma/\sqrt{N-1})$ where σ_M is the standard error of the mean, σ is the standard deviation, and N is the number of measurements taken (15 for our system) [8]. The standard error of the mean was calculated to be 0.097 radians, which corresponds to a real-space angular uncertainty of 1.4°. Thus,

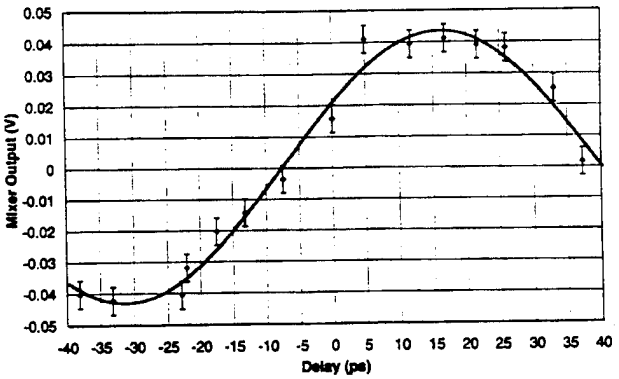

Fig. 2. Homodyne mixing output voltage versus optical delay time at 10.5 GHz with the X-band horn at $-25°$. The least squares fit to the measured data determines the microwave phase delay, $\Delta\varphi_m$, with improved accuracy.

the angular accuracy of our radar receiver has improved from 5 to 1.4°. The angular accuracy can be increased at the rate of $1/\sqrt{N-1}$ by increasing the number of delay units thereby increasing the number of sampled points.

As was mentioned, one of the primary motivations for using a true time delay processing system for a phased array radar receiver is that it exhibits "squint free" behavior, resulting in wide instantaneous bandwidths [1]. If one were to use conventional microwave phase shifters in place of our optical true time delay network, the determination of the angle of the incoming radar signal from the target would be $\theta = \arcsin[c \cdot \Delta\varphi_{\text{phase}}/(2\pi d \cdot f_m)]$ and is a function of frequency [1]. Thus, as the frequency of the radar changes, the target angle appears to shift. This undesirable "beam squint" behavior can be eliminated by replacing the microwave phase shifters with the optical true time delay network of Fig. 1. When using a true time delay system the target angle is given by $\theta = \arcsin(c \cdot \tau/d)$ and is independent of frequency [1].

In making our measurements over a broad range of frequencies, deviations of several degrees attributed to mutual coupling [9] were observed at some frequencies and angles. Our data is corrected for these effects, using a digital sampling oscilloscope for calibration, and plotted as a function of frequency in Fig. 3. Squint free operation is shown over a 8–12 GHz band which is a ±20% bandwidth around the center

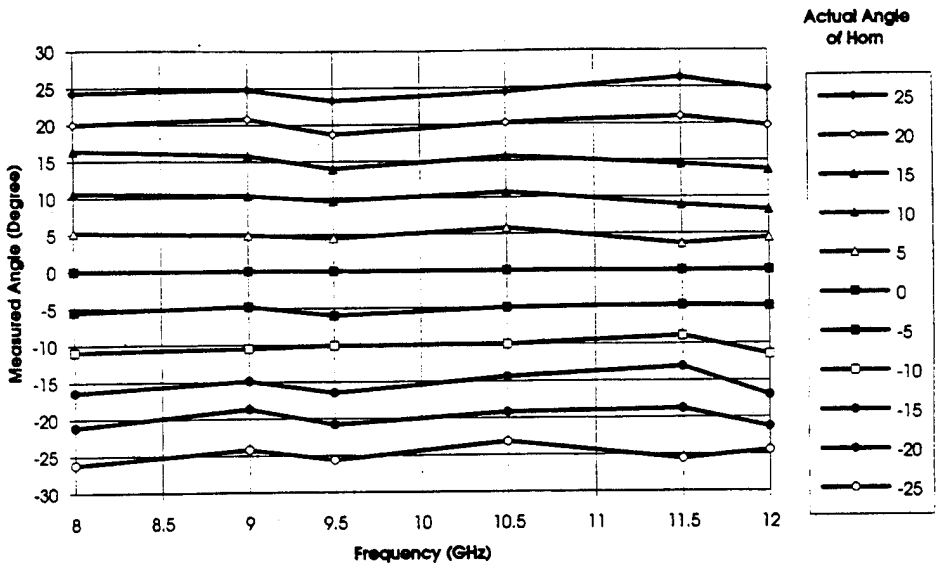

Fig. 3. Measured angle from −25–25° over an 8–12 GHz band exhibiting "squint free" operation measured in the symmetric configuration. Deviations of the measurements from the actual angle of the horn are attributed to random phase shifts in the cables, amplifiers, and mixers. Comparable data was achieved using the asymmetric system.

frequency of 10.5 GHz. The standard deviation of the angular error is <1.1° at all frequencies, which is within our specified angular accuracy. The maximum deviations from the actual angle are approximately 2° and are attributed to random phase shifts in the cables, amplifiers, and mixers.

The angular accuracy of the system can be improved by increasing the number of delay units. The angular accuracy of this system can also be significantly increased without increasing the number of delay units by noticing that the use of symmetric delays for both light beams as shown in Fig. 1 is an inefficient configuration for obtaining different combinations of optical delay. For example, we found that the three delay unit system in Fig. 1 could provide 15 different combinations of optical delay given by the formula $2^{(n+1)}-1$ where $n = 3$ delay units. There are, however, 49 other possible combinations in the three-unit system that are degenerate in that they reproduce one of the aforementioned 15 optical delays. If one could design the optical delay network such that this degeneracy were removed, one could obtain 2^{2n} distinct optical delay combinations.

We demonstrate this concept using the asymmetric two-delay unit system shown in the inset of Fig. 1, which gives 16 optical delay combinations yielding approximately the same angular accuracy as the previously presented symmetric three-delay unit configuration. The standard deviation of the angular error for this configuration was measured to be 1.2° at 10.5 GHz displaying the same angular accuracy of the symmetric three-delay unit system. This concept can be extended to higher number of antenna elements by joining the two element subarrays in combinations to form large phased array apertures [1].

In summary, the first demonstration of an optically controlled true time delay phased array radar receiver using the SLM/bulk optics approach at an optical wavelength of 1.3 μm has been described and a real-space angular accuracy of 1.4° was obtained. The system operated with "squint free" behavior over the entire X-band (8–12 GHz) demonstrating a wide instantaneous bandwidth. Furthermore, a new SLM-based architecture was proposed and demonstrated a large angular accuracy with a reduced number of system components. The simplicity and high performance of this system suggests its applicability to realistic phased array radar applications.

ACKNOWLEDGMENT

The authors would like to acknowledge helpful discussions with I. Newberg from the Hughes Aircraft Corporation.

REFERENCES

[1] W. Ng, A. A. Walston, G. L. Tangonan, J. J. Lee, I. L. Newberg, and N. Bernstein, "The first demonstration of an optically steered microwave phased array antenna using true-time-delay," *J. Lightwave Technol.*, vol. 9, no. 9, pp. 1124–1131, 1991.

[2] P. M. Freitag and S. R. Forrest, "A coherent optically controlled phased array antenna system," *IEEE Microwave and Guided Wave Lett.*, vol. 3, no. 9, pp. 293–295, 1993.

[3] D. Dolfi, M. Labeyrie, P. Joffre, and J. P. Huignard, "Liquid crystal microwave phase shifter," *Electron. Lett.*, vol. 29, pp. 926–928, 1993.

[4] N. A. Riza, "Liquid crystal-based optical delay units for phased array antennas," *J. Lightwave Technol.*, vol. 12, no. 8, pp. 1440–1447.

[5] Y. Liu, S. R. Forrest, G. L. Tangonan, R. A. Jullens, R. Y. Loo, V. L. Jones, D. Persechini, J. L. Pikulski, and M. M. Johnson, "Very-high-bandwidth InGaAs p-i-n detector arrays," *IEEE Photon. Technol. Lett.*, vol. 3, no. 10, pp. 931–933, 1991.

[6] G. P. Agrawal, *Fiber-Optic Communication Systems*. New York: Wiley, 1992.

[7] R. W. Hornbeck, *Numerical Methods*. Englewood Cliffs, NJ: Prentice-Hall, 1975.

[8] W. Lichten, *Data and Error Analysis in the Introductory Physics Laboratory*. MA: Allym and Bacon, 1988.

[9] M. Skolnik, *Radar Handbook*, 2nd ed. New York: McGraw-Hill, 1990.

Optical Mixing in Epitaxial Lift-Off Pseudomorphic HEMT's

D. Bhattacharya, *Student Member, IEEE*, P. S. Bal, H. R. Fetterman, *Fellow, IEEE*, and D. Streit, *Senior Member, IEEE*

Abstract—**In this letter, we present optical mixing in epitaxial lift-off (ELO) pseudomorphic HEMT's (PHEMT's) at difference frequencies in the microwave regime up to 22 GHz. The 3 μm gate length AlGaAs–InGaAs PHEMT's were lifted off their host GaAs substrates and subsequently attached to quartz slides. It was observed that the ELO devices consistently resulted in stronger signals (~7 dB) than the non-ELO devices under frontside and backside illumination. This is attributed to improved optical coupling efficiency, a decrease in substrate leakage, and an illumination-induced back gating effect for the ELO films.**

I. Introduction

RECENTLY, there has been much investigation into employing the epitaxial lift-off process (ELO) in applications in the area of optoelectronics. By proving itself as a viable method to integrate devices of dissimilar material systems, ELO has quickly become one of the most promising methods to address the technological problems associated with integration of optoelectronic integrated circuits (OEIC's) [1], [2]. ELO affords the designer of OEIC's the capability to choose different materials which are optimized for specific functions. The various devices, each made on optimal material systems, can be integrated into a single OEIC. In the ELO process, epitaxially grown thin films are lifted off their original substrates and "glued" onto a more suitable substrate.

The high electron mobility transistor (HEMT) has shown great promise as a device in photonic systems. The optical control of HEMT's has been investigated by numerous researchers [3], [4]. Optical mixing at difference frequencies up to 94 GHz have been achieved in integrated HEMT/slot antenna structures [5]. While the HEMT has shown great promise as a high-frequency device, the strength of the signals at high frequencies has been disappointing. One method to improve the signal strength involves the use of the epitaxial lift-off technique. By lifting a device off of its original opaque substrate and reattaching it to another transparent substrate, the optical coupling efficiency into the device can be improved.

In this letter, we demonstrate optical mixing in 3-μm AlGaAs–InGaAs ELO PHEMT's on quartz substrates at microwave frequencies to 22 GHz. Our study includes quantitative comparisons of optical mixing signals on ELO devices before and after liftoff, under frontside and backside illumination. Our results highlight the improvement in optical coupling efficiency for the lifted off devices. These experiments also confirm the fact that ELO PHEMT's can be employed in many roles including the optical mixing, detection, and generation of microwave signals.

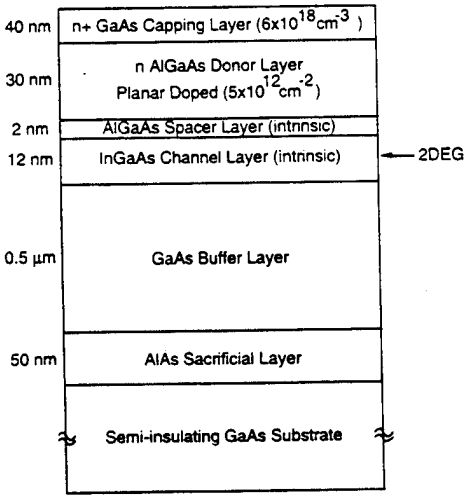

Fig. 1. Cross section of pseudomorphic epitaxial lift-off high electron mobility transistor, detailing layer structure.

II. Device Parameters and Fabrication

The layer structure of our pseudomorphic HEMT's are shown in Fig. 1. The layers of the wafer were grown on a semi-insulating GaAs substrate using molecular beam epitaxy (MBE). Hall mobility measurements on the samples yielded mobilities of 4760 cm^2/V-s and 58 000 cm^2/V-s at 300 K and 77 K, respectively. The 40 nm GaAs capping layer was heavily doped with Si at 6.0 $\times$ 10^{18} cm^{-3}. The 30 nm $Al_{0.2}Ga_{0.8}As$ donor layer was planar doped with Si at a level of 5.0 $\times$ 10^{12} cm^{-2}. A 2-nm undoped AlGaAs spacer layer was included to further separate the 2 DEG channel electrons from coulombic interactions with the ionized dopant atoms in the donor layer. A 12-nm undoped $In_{0.2}Ga_{0.8}As$ pseudomorphic layer was used as the 2 DEG channel. Finally, a 50-nm AlAs layer was included to facilitate the lift-off process. The devices had gate lengths of 3 μm, gate widths of 50 μm, and a source to drain spacings of 9 μm.

The ELO process consisted of two steps: first, detaching the epitaxial film from the growth substrate and second, reattaching the film to a quartz substrate. The detaching process is based on the extremely selective etching rate of AlAs in HF solution. The sample was initially covered with

Manuscript received December 28, 1994; revised June 20, 1995. This work was supported by the Air Force Office of Scientific Research under the direction of H. R. Schlossberg and by the National Center for Integrated Photonics Technology.

D. Bhattacharya, P. S. Bal, and H. R. Fetterman are with the Department of Electrical Engineering, University of California, Los Angeles, Los Angeles, CA 90024 USA.

D. Streit is with TRW Electronic Systems and Technology Division, Electronic Systems Group, Redondo Beach, CA 90278 USA.

IEEE Log Number 9414259.

Apiezon W wax dissolved in tricholoroethylene (TCE). This serves to give the film mechanical support, to slightly bow the film during etching to allow reaction products to escape, and to protect the top layers of the device from the HF etchant. The sample was then immersed in 10% electronic grade HF overnight for etching of the sacrificial layer. The released film was approximately 0.5-μm thick. The film was then placed on a quartz substrate while wet and left to dry for about 48 hours under weight. In the drying process, attractive forces between the substrate and the semiconductor squeeze out the water. As the water escapes, the separation between the lifted film and the new substrate decreases until short-range, attractive Van der Waals forces can hold the two together [6].

III. Experimental Results and Discussion

The optical mixing process can be described as follows: If we assume two electromagnetic light plane waves of frequency ω_1 and ω_2 and amplitudes E_1 and E_2 are incident upon a detector, then the resultant amplitude of the waves can be written as [7]

$$E_t = E_1 \cos \omega_1 t + E_2 \cos \omega_2 t. \tag{1}$$

The detector measures the intensity, which is the square of (1) and can be written

$$E_t^2 = \frac{E_1^2}{2} + \frac{E_2^2}{2} + E_1 E_2 \cos(\omega_1 - \omega_2)t. \tag{2}$$

The high-frequency term has been disregarded in (2). The vector amplitudes of the two waves have been added, giving rise to a single modulated wave at the difference or beat frequency. The change in the photocurrent, $\Delta I_p(t)$, due to optical illumination is related to the optical power incident on the device, P_{inc}, by the relation

$$\Delta I_p(t) = \frac{q\eta}{h\upsilon} \cdot \frac{E_t^2 A}{Z_0} = \frac{q}{h\upsilon} \cdot \eta \cdot P_{\text{inc}} \tag{3}$$

where q is the electron charge, h is Planck's constant, υ is the frequency of the incident light, and η is the quantum efficiency of the device. The quantum efficiency is related to the responsivity, R, by $\eta = (h\upsilon/q)R = (h\upsilon/q)(\Delta I_p(t)/P_{\text{inc}})$.

The experimental setup of our optical measurements on the ELO PHEMT's is shown in Fig. 2. A single frequency, temperature stabilized HeNe and a continuous wave ring dye laser, optically pumped by an Argon ion laser were used as the local oscillator and signal fields. The dye laser was operated with Kiton Red 620 dye (600–640 nm) to ensure GHz tunability around the wavelength of HeNe (632.991 nm). External feedback to a temperature controlled Fabry–Perot reference cavity ensured stability of the dye laser radiation. The wavelength of the dye laser was monitored with a optical wavemeter that has 0.001 nm resolution. The HeNe was operated at 0.5 mW and the dye laser was operated at 100 mW. The linewidth and stability of both lasers were typically less than one MHz. The collinear optical beams were focused onto the gate of our devices with a 5× lens objective. A RF probe station was used to mount and test the various devices from the front and back side. Coplanar RF probes were used to make electrical contact to the devices.

Under illumination, dc measurements showed an large increase in quantum efficiency and responsivity for ELO devices versus non-ELO devices. The devices were biased at $V_{\text{ds}} = 2.0$ V and $V_{\text{gs}} = -1.0$ V, at the threshold of pinchoff. For the non-ELO devices, the responsivity and the quantum efficiency were measured to be 1.4 A/W and 275%, respectively. For the ELO devices under frontside and backside illumination, the responsivity and quantum efficiency increased to 4.6 A/W and 900%, and 4.9 A/W and 960%, respectively.

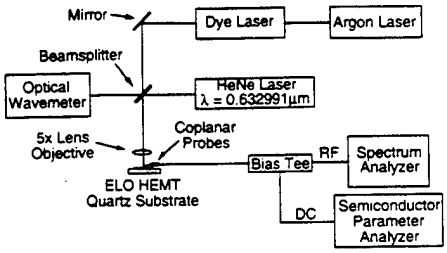

Fig. 2. Experimental setup of optical heterodyne measurements.

The microwave optical response of the devices was measured from 11–22 GHz. The measurements were made on non-ELO devices, on ELO devices under frontside illumination, and on ELO devices under backside illumination. The results of these measurements are shown in Fig. 3(a). In Fig. 3(b), the mixed signal at 22 GHz is shown for the ELO device under backside illumination. From Fig. 3(a), it can be seen that the optical frequency response of the devices are excellent. There is very little roll-off in the optical mixing signal up to 22 GHz. The differences in the frequency response for the various configurations are within the experimental error of the measurement and are not due to any intrinisic behavior of the devices. Surprisingly, the maximum RF extrinsic transconductance g_m was measured to be 3.5 mS for the lifted devices even though the electrical frequency response of these large devices yielded poor results. An improvement in signal-noise ratio of about 7 dB was observed for the ELO devices versus the non-ELO devices throughout the frequency range. Only a nominal gain in signal strength (~2 dB) was observed for the ELO devices when illuminated from the backside versus the frontside.

The improvement in optical responsivity and quantum efficiency for ELO devices under frontside and backside illumination has been studied previously [8]. This study indicated that the larger optical response is a result of a double pass through the active region of the device caused by reflections from the contact metallization under backside illumination. However, our measurements indicate that there is very little difference between illuminating from the backside versus frontside and a double pass would at most only account for a 3 dB improvement in signal. In our measurements under frontside illumination, a reflecting stage was used. Thus, the improvement in signal realized for backside illumination due to a double pass through the active region is also realized for frontside illumination in our case. In addition, the amount of signal injected into the active region depends in large part on the planar geometry of the metallization. The differences from the observations in [8] is largely due to differences in metal geometry. The slightly larger signal (~2 dB) in the case of backside illumination can be explained by the shadowing effect of the contact metallization.

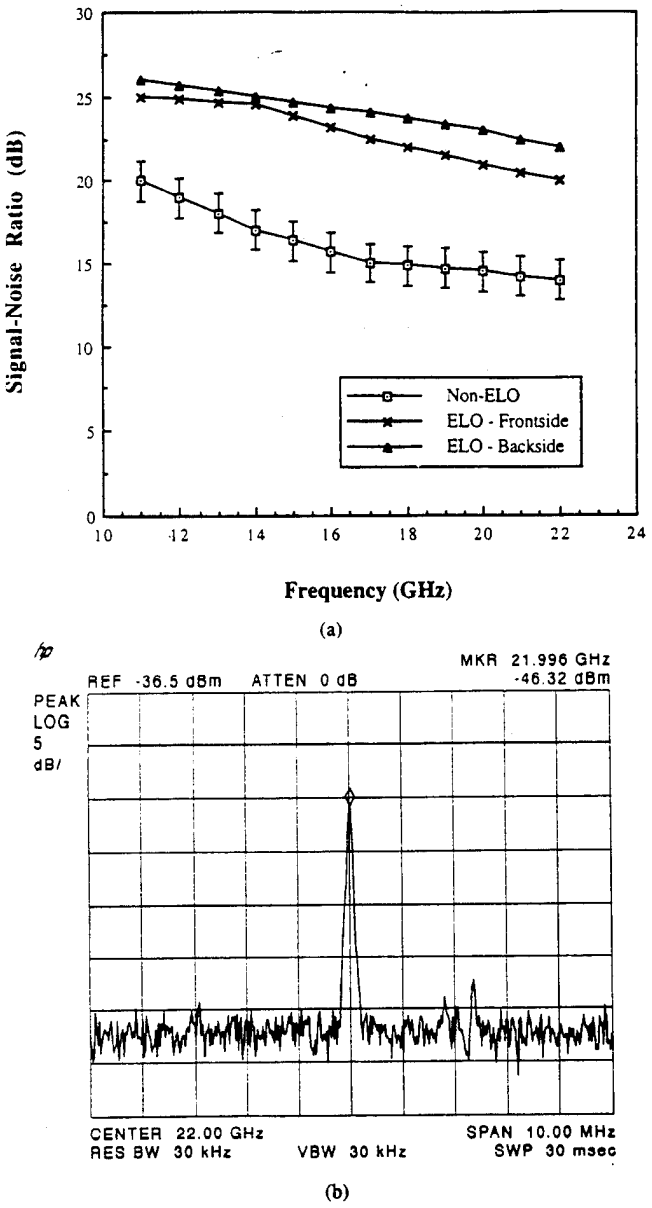

Fig. 3. (a) Measured optical mixing response curves in non-ELO devices, ELO devices under frontside illumination, and ELO devices under backside illumination, and (b) optical mixing signal of ELO device under backside illumination at 22 GHz on the spectrum analyzer.

A substrate leakage/back gating argument is one possible explanation for our results. For the non-ELO devices, any light that is not absorbed in the active region proceeds through the buffer layer and into the substrate. Carriers that are generated in the buffer layer have only a small possibility of falling into the 2 DEG channel. Many of these carriers will be lost due to recombination in the buffer layer and to substrate leakage. For the ELO devices, it has been shown that a back gating effect, caused by charge buildup at the ELO film/host substrate, can raise the Fermi level in the GaAs buffer layer and the 2 DEG channel [9]. Now, carriers which are generated in the buffer layer have a larger possibility of falling into the 2 DEG channel due to the back gate potential, thereby increasing the number of carriers available for conduction. Also, carrier confinement is improved. This back gating effect accounts for larger signals in the ELO devices under backside or frontside illumination.

Most likely, the improvement in our signal in the ELO devices is due to a combination of all the factors mentioned above, including improved optical coupling efficiency, back gating, and a reduction in substrate leakage.

IV. Conclusion

In conclusion, we have successfully demonstrated optical mixing in pseudomorphic epitaxial lift-off HEMT's at microwave frequencies. It has been observed that the signals are stronger by approximately 7 dB throughout the frequency range for the ELO devices. This is attributed to improved coupling efficiency, a decrease in substrate leakage, and an illumination-induced back gating effect for the ELO films. Only a minor difference in signal strength is observed for ELO HEMT's that were illuminated from the backside versus the frontside, which can be attributed to a shadowing effect of the contact metallization for frontside illumination. The excellent frequency response and signal-to-noise ratios obtained from these devices indicate that they can be major additions to new optoelectronic integrated systems. Current efforts in this area includes extending the mixed signal frequency to millimeter waves and testing at 1.3 μm for applications in communication systems.

Acknowledgment

The authors would like to thank E. Yablonovitch for technical assistance in the lift-off process, A. C. Han for growing the samples, and M. Espiau of the Center for High Frequency Electronics for technical assistance in setting up the probe station.

References

[1] W. K. Chan, A. Yi-Yan, and T. Gmitter, "Grafted semiconductor optoelectronics," *IEEE J. Quantum Electron.*, vol. 27, no. 3, pp. 717–725, 1991.

[2] A. Ersen, I. Schnitzer, E. Yablonovitch, and T. Gmitter, "Direct bonding of GaAs films on silicon circuits by epitaxial liftoff," *Solid-State Electron.*, vol. 36, pp. 1731–1739, Dec. 1993.

[3] A. J. Seeds and A. A. A. DeSalles, "Optical control of microwave semiconductor devices," *IEEE Trans. Microwave Theory Tech.*, vol. 38, no. 5, pp. 577–585, 1990.

[4] R. N. Simons and K. B. Bhasin, "Analysis of optically controlled microwave/millimeter-wave device structures," *IEEE Trans. Microwave Theory Tech.*, vol. 34, no. 12, pp. 1349–1355, 1986.

[5] H. R. Fetterman, D. P. Prakash, D. C. Scott, and W. Wang, "Integrated optically driven millimeter wave sources and receivers," in *1994 IEEE MTT-S Int. Microwave Symp. Dig.*, vol. 3, pp. 1493–1496, May 1994.

[6] E. Yablonovitch, D. M. Hwang, T. J. Gmitter, L. T. Florez, and J. P. Harbison, "Van der Waals bonding of GaAs epitaxial films onto arbitrary substrates," *Appl. Phys. Lett.*, vol. 56, pp. 2419–2421, June 1990.

[7] A. T. Forrester, R. A. Gudmundsen, and P. O. Johnson, "Photoelectric mixing of incoherent light," *Phys. Rev.*, vol. 99, pp. 1691–1700, Sept. 1955.

[8] P. G. Young, R. N. Simons, S. A. Alterovitz, R. R. Romanofsky, and E. D. Smith, "RF control of epitaxial lift-off PHEMT's under backside illumination," *IEEE J. Quantum Electron.*, vol. 30, no. 8, pp. 1782–1786, 1994.

[9] R. A. Mena, S. E. Schacham, P. G. Young, E. J. Haugland, and S. A. Alterovitz, "Transport properties of epitaxial lift-off films," *J. Appl. Phys.*, vol. 74, pp. 3970–3976, Sept. 1993.

Laser-Fabricated Delay Lines in GaAs for Optically Steered Phased-Array Radar

Louay Eldada, *Member, IEEE*, Robert Scarmozzino, Richard M. Osgood Jr., *Fellow, IEEE*, David C. Scott, Yian Chang, and Harold R. Fetterman

Abstract—**We have used laser direct fabrication techniques to implement optical delay lines on an epitaxial GaAs/AlGaAs substrate. These integrated photonic circuits, which are important for optically-controlled phased-array radar, include asymmetric splitters with various splitting ratios, smoothly curved 90° bends, as well as linear waveguides. The delay lines were tested and found to have the desired delay and a power-output uniformity of ±2–4%.**

I. Introduction

SINGLE-MODE optical fiber networks have been proposed for signal distribution and beam forming in compact, light-weight phased-array radar antennas and receivers [1]–[3]. More recently, the use of integrated optical circuitry has been suggested [4]. Aside from compactness, such a monolithic time-delay network offers more precision for the microwave phase than fiber delay lines because the lengths of the waveguides on substrates such as SiO_2 or GaAs can be fabricated to micrometer-scale accuracy, i.e. much less than the corresponding microwave wavelength. In addition, the integration of detectors to the optical waveguides offers greater mechanical rigidity than the various fiber-device interfaces between the delay lines and the necessary optoelectronic devices.

In this paper, the necessary elements of the design of optical delay lines, which are suited for implementation with our laser etching technology, are first discussed. The optimization of the various components that form these circuits is then presented. Finally, the fabrication steps for the delay line and the characterization results for the completed delay-line circuits are discussed.

II. Design

The chief issues when designing a delay line is to obtain a low-on-chip-loss structure and to achieve even power distribution and the desired time delays in each of the output ports. For a device working on real-time delay, the phase difference between the modulation received at the output of two elements is given by

$$\Delta\phi = \frac{2\pi n f \Delta l}{c} \tag{1}$$

where

n = the refractive index of the transmission medium

f = the reference microwave frequency

Δl = the optical path length difference between the elements

c = the velocity of light in vacuum.

In our case, the objective was to produce a prototype at microwave frequency using integrated optical structures. Our design frequency was 10.24 GHz [5], and the desired $\Delta\phi$ was 12.5°, which for a GaAs waveguide implies a path-length difference of 300 μm.

Our optical delay lines were designed with a main optical bus out of which asymmetric splitters with different splitting ratios divided off a specific fraction of the light and guided it into 90° smooth bends terminated by linear waveguides for cleaving, as shown in Fig. 1(a). The splitters are repeated at set space intervals to yield the desired optical-path delay which, in the case of the structure shown in Fig. 1(a), is 300 μm. The splitting ratios are designed so that the total power is equally split among all the outputs.

The design procedure was first to design the asymmetric splitters and the 90° smooth bends separately by computer simulation and then the optimized designs were prototyped for confirmation. Subsequently, these splitters and bends were included in the delay-line structure which was also simulated and prototyped.

The delay lines were designed in our laboratories using an in-house software package that simulates 2D or 3D beam propagation in waveguiding structures [6]. It uses implicit finite difference beam propagation techniques along with transparent boundary conditions. Furthermore, Padé approximations of various orders are used to accurately deal with wide-angle propagation. This software allows general waveguiding structures to be defined, simulated, and analyzed in terms of coupling, interference, power loss, etc. The use of these beam propagation simulation capabilities enabled us to study various designs for such circuits, and minimize experimental iterations.

The 90° smoothly-curved bends were simulated to find the acceptable trench separation [see inset of Fig. 1(b)]. In these computer simulations, the effective index in the waveguide

Manuscript received September 23, 1994; revised April 21, 1995. This work was supported by the National Center for Integrated Photonic Technology, the Defense Advanced Research Projects Agency, the Air Force Office of Scientific Research, and the Army Research Office.

L. Eldada was with Microelectronics Sciences Laboratories, Columbia University, New York, NY 10027 USA. He is now with AlliedSignal Inc., Morristown, NJ 07962 USA.

R. Scarmozzino and R. M. Osgood, Jr. are with Microelectronics Sciences Laboratories, Columbia University, New York, NY 10027 USA.

D. C. Scott, Y. Chang, and H. R. Fetterman are with the Department of Electrical Engineering, University of California, Los Angeles, CA 90024 USA.

IEEE Log Number 9414408.

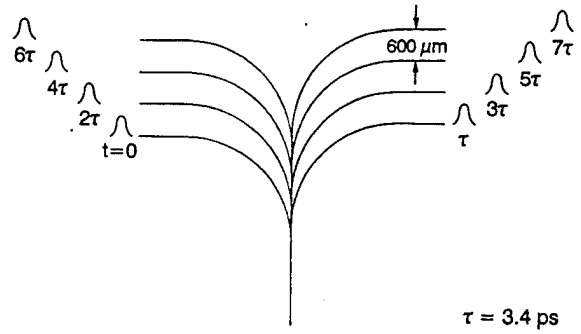

(a)

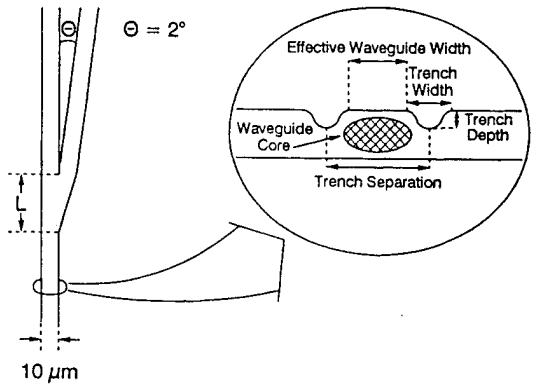

(b)

Fig. 1. Schematic diagrams showing (a) the design of a two-sided eight-output optical delay-line circuit and (b) the design of an asymmetric splitter showing the interaction length L in the splitting region. This parametric dimension allows variation of the switching percentage. The inset in (b) shows the cross-sectional profile of the waveguides.

region was chosen as $n = 3.3848$, and the lateral-effective-index difference between the guide area and the trench area was $\Delta n = 0.0152$. The results of these simulations are presented in Fig. 2. In these simulations, the bend radius of curvature was set at 2 mm (for reasons that will be clear below), while the trench separation was varied from single-mode to multimode dimensions. As the single-mode regime was examined at increasing trench separations (from 5 μm to 7 μm), the loss was found to decrease at higher widths, a result which is an expected trend with improved confinement. However, as the trench separation was increased from 7 μm to 20 μm in the multimode range, the loss was found to increase, mostly due to a larger transition loss at the beginning of the bends. Although trench separations resulting in single-mode structures were achievable, a slightly larger trench separation of 10 μm that resulted in multimode behavior was selected as a compromise between efficient coupling to optical fibers and low loss in the bends. Note that the 10-μm guides have an effective width—defined as the flat portion of the rib top—of 6 μm, a value used in most subsequent computer simulations.

Computer simulations were also carried out for 90° bends with different radii of curvature. The simulations assumed the same parameters as the above bend calculations for the effective index and the lateral effective index difference, and the guide width was set at 6 μm. In the first stage of these

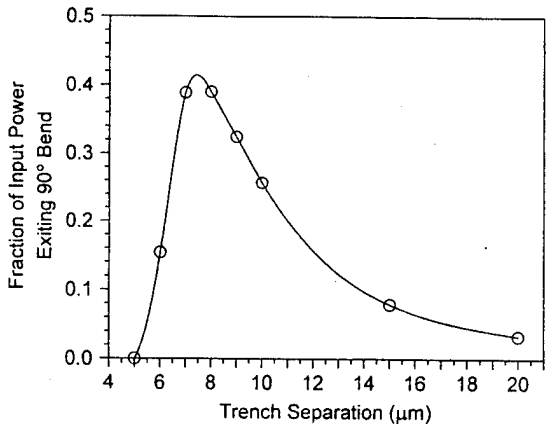

Fig. 2. Computer simulation of the fraction of the input power exiting 90° bends with different trench separations. The radius of curvature is 2 mm.

simulations, the radiation loss was monitored as a function of the radius of curvature, and it was found to exhibit the expected exponential decrease with the radius. However, the large radii of curvature cause large structures with high linear losses (i.e., material losses which are the sum of the scattering loss due to surface roughness at the air/GaAs interface, and the absorption losses which include band edge and free carrier absorptions). Therefore, when the total losses (i.e., linear losses and radiation loss) were monitored as a function of the radius of curvature, they were found to first decrease with increasing radii of curvature and then increase. Quantitatively, bends with 1, 2, and 4-mm radii of curvature (having, respectively, 1.57, 3.14, and 6.28-mm total length) exhibited, respectively, 4.15, 0.24, and 0.11-dB radiation loss, and 4.31, 0.55, and 0.74-dB total loss; thus the radius of curvature of choice, where the total loss was at a minimum, was 2 mm.

In our design for the asymmetric splitters, the splitting ratio was varied by changing the interaction length L in the splitting region [see Fig. 1(b)]. The branching angle was set at 2° because it was known from previous work [7] that this is the largest angle for low-loss branches in our waveguide technology. These devices were simulated to obtain the theoretical percentage of switched power from the optical bus into the bent arm as a function of interaction length. The simulations assumed the same parameters as the calculations for 90° bends with different radii of curvature, i.e. the same effective index, lateral effective index difference, and waveguide width. A simulation for the case of $L = 200$ μm is shown in Fig. 3(a). In that simulation, light is launched into a 200-μm-long straight waveguide leading into a 200-μm-long interaction region, which is followed by a 600-μm-long 2° branch. Since the waveguide is multimode, the propagating beam has a nonstationary "shape." A theoretical plot of the percentage of power switched versus interaction length obtained from such simulations is shown by the solid curve in Fig. 3(b) (the experimental data points in that figure will be discussed later). As in a directional coupler, the percentage of power coupled into the bent arm varies with interaction length; only the first half-cycle of such a variation is plotted in Fig. 3(b) since it is sufficient to give the needed range of splitting ratios.

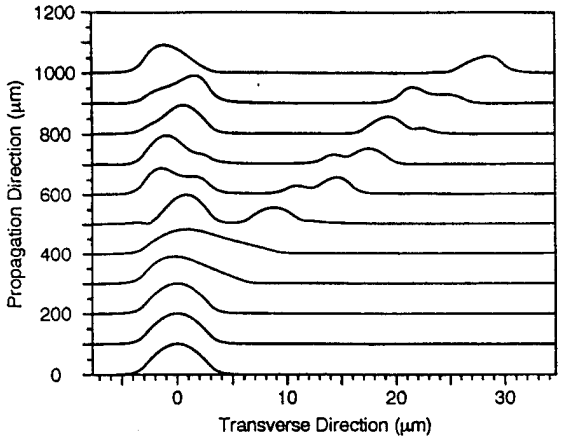

Fig. 3. (a) Computer simulation of wave propagation in an asymmetric splitter for the case of $L = 200$ μm. The results of several such simulations for different values of L are shown in (b) where the percentage of power coupled into the bent guides of asymmetric splitters is plotted as a function of interaction length (solid line). Also included in (b) are the experimental operational characteristics of splitter prototypes.

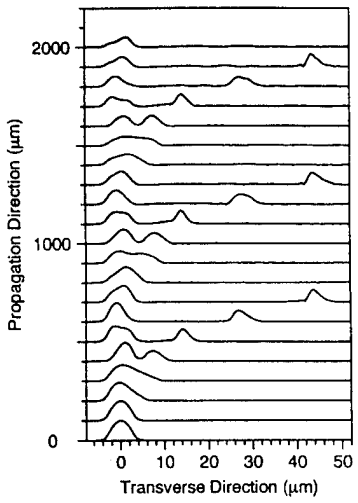

Fig. 4. Computer simulation of wave propagation in a one-sided four-output optical delay line.

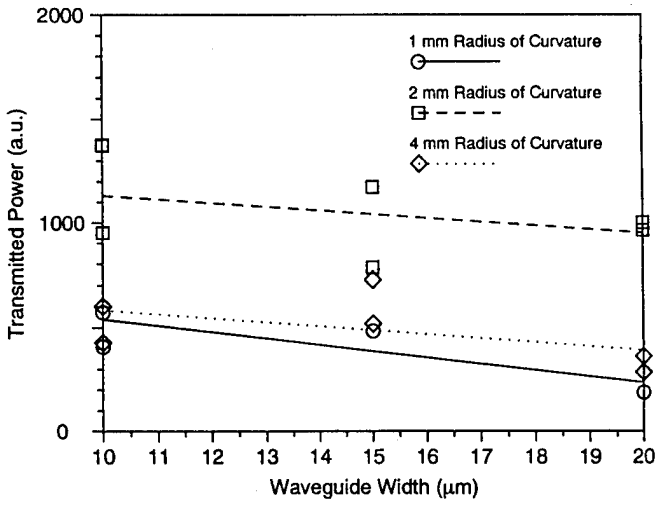

Fig. 5. Transmission of bends of different radii of curvature (1, 2, and 4 mm) and different widths (10, 15, and 20 μm).

The plot indicates that up to 50% of switched power to the bent arm is achievable within a 300-μm length. This result is important since, in our delay-line design, the maximum available distance between successive splitters is limited to 300 μm and switching values of up to 50% must be achieved within that length.

Two different designs were considered for the overall circuit. The first design was that of a single-sided four-output optical delay line, which is essentially the right half of the final desired structure shown in Fig. 1(a). The path difference between two consecutive outputs was 600 μm which, in GaAs, corresponds to a time delay of 6.8 ps. In order to allow the total power to be equally split among all the outputs, there were three asymmetric splitters along the device with 25, 33.3, and 50% splitting percentage, respectively, where in an x% splitter x% of the power goes through the curved bend and the balance remains in the optical bus. Note that the first section of each quarter-circle bend (from the point where its tangent is parallel to the optical bus to the point where its tangent is at 2° to the bus) was replaced by a 2°-off-axis straight guide to reduce evanescent coupling between the bend and the bus. Fig. 4 shows a computer simulation for this structure using our beam-propagation software. This simulation shows that while the structure is multimode, the beam still maintains a generally Gaussian shape in the bends, and that shape is comparable from bend to bend. Furthermore, this simulation demonstrates that the power distribution is uniform among the output ports, indicating that the same splitting ratio obtained in discrete splitters is observed in the complete delay-line circuit; this confirms that the design of the delay line minimizes coupling of power between the bend and the optical bus.

The second design was for the two-sided eight-output optical delay line, which was our goal structure shown in Fig. 1(a). The path difference between two consecutive outputs (one on the left and one on the right) was 300 μm, which corresponds to a time delay of 3.4 ps in GaAs. Again, in order to allow the total power to be equally split among all the outputs, there were 7 asymmetric splitters along the device and they were 12.5, 14.3, 16.7, 20, 25, 33.3, and 50% splitters.

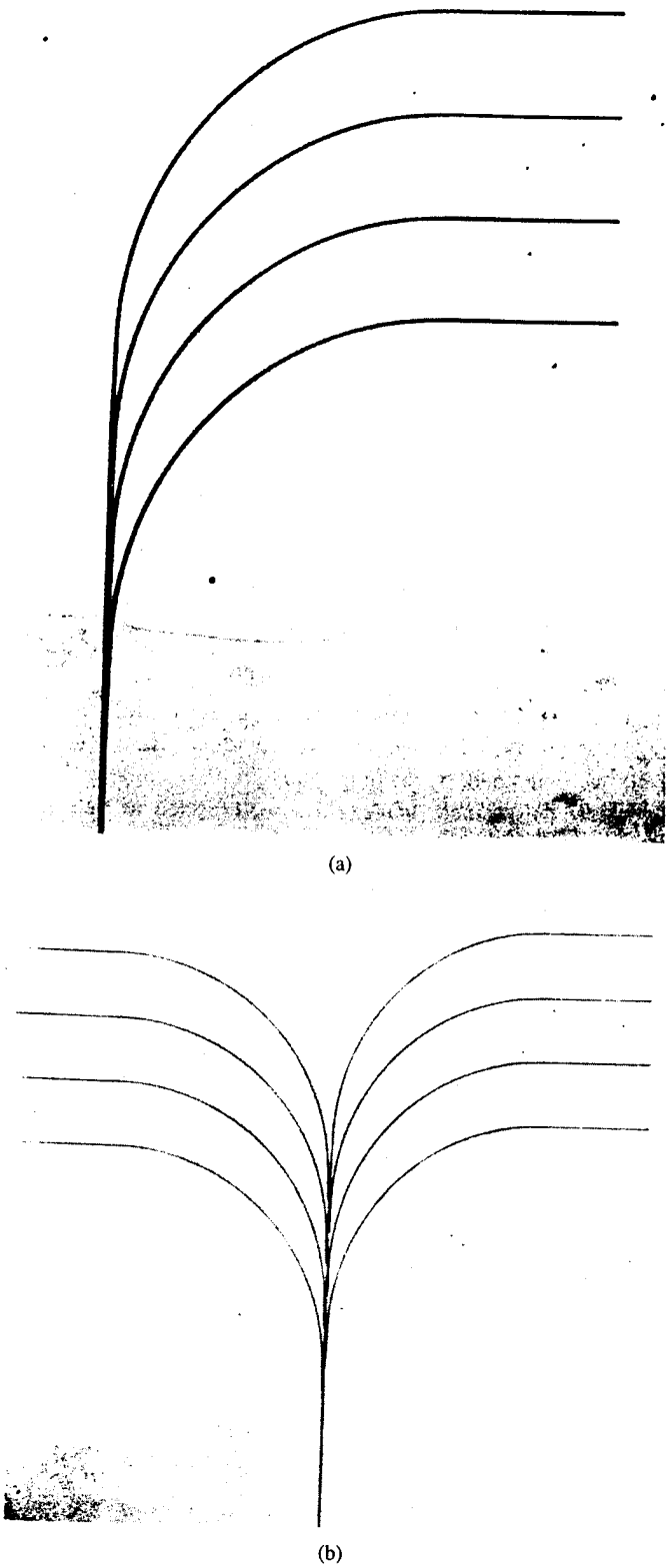

Fig. 6. Optical micrographs of (a) a one-sided four-output delay line and (b) a two-sided eight-output delay line.

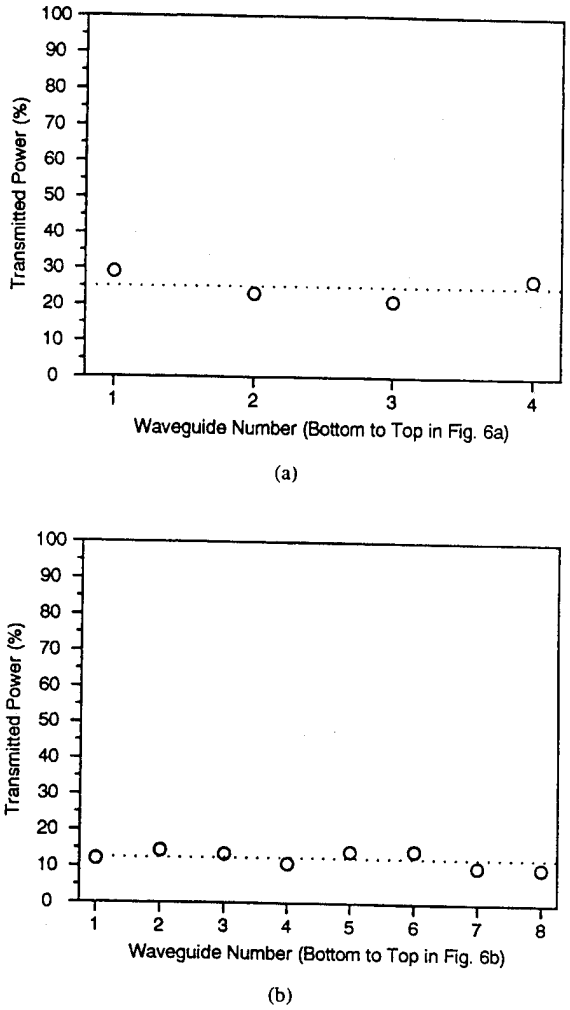

Fig. 7. Percentage of power transmitted out of each arm for (a) a one-sided four-output delay line where the outputs are within 4% of 25% and (b) a two-sided eight-output delay line where the outputs are within 2% of 12.5%.

III. Fabrication and Characterization

Before fabricating the entire circuit, the design parameters of its individual components were optimized. In order to obtain results that would reflect the operational characteristics of the individual components in the final circuit, the optimization was done experimentally by developing prototypes based on the computer simulation results. Those components included 90° smooth bends and asymmetric splitters. The fabrication process was based on a technique recently developed for direct-writing of optical waveguide devices in semiconductor surfaces [7]–[10]. The process uses a focused laser beam to etch micrometer-scale grooves photoelectrochemically in GaAs/AlGaAs heterostructures, thereby patterning rib-like optical waveguide structures [see inset of Fig. 1(b)]. The laser wavelength used in etching was 275 nm; the laser spot size was about 2 μm (full width at $1/e$ intensity); the etchant was $HCl:HNO_3:H_2O::4:1:50$; and the substrate was a vertically single-mode waveguide structure consisting of a 1.3-μm layer of n-GaAs on a 2.7-μm layer of n-$Al_{0.1}Ga_{0.9}As$.

For all characterization experiments, the wavelength used was 1.3 μm, at which wavelength $n_{GaAs} = 3.4049$ and $n_{AlGaAs} = 3.3566$, and light was launched in the waveguiding structures by butt-coupling a fiber to the cleaved input facet of the sample. In the GaAs/AlGaAs heterostructure, IR light is confined vertically within the higher-refractive-index GaAs layer. Since the two etched grooves extend partway through the

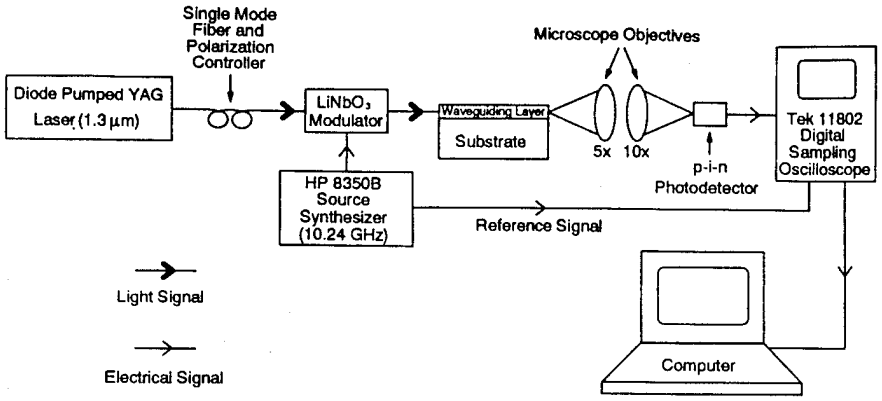

Fig. 8. Schematic diagram of the setup used in measuring the delay.

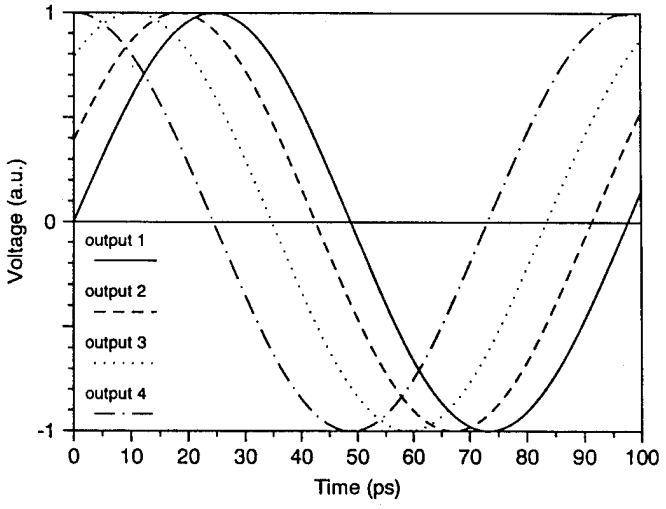

Fig. 9. 10.24-GHz signals measured at the four outputs of a one-sided delay line after subtraction of the reference signal. The phase shift between these waveforms gives the delay in each arm.

GaAs layer, light is confined in the region between the grooves by virtue of the greater effective index in the unetched region compared to the etched region [7]–[10] as in a conventional rib or ridge waveguide. The etching can be done in a single step because the technique is maskless; thus, in conjunction with computer-controlled scanning of the optical beam, this technique can be used as a prototyping tool for developing and testing new integrated optical circuits. Furthermore, the writing rates are sufficiently high, i.e. between 50 and 100 μm/s, that the technique is capable of patterning low-density features with long lineal dimensions over comparatively large planar areas.

Earlier work demonstrated that basic waveguiding structures can be written using this approach. This work included the writing of low-loss (0.5–1.0 dB/cm) single-mode linear waveguides [7] and high quality "building-block" passive components such as bends, Y-branches, and directional couplers [7], [11]; more recently, other active devices were demonstrated as well [12].

The fabrication of smoothly-curved 90° bends demanded precise control of both the x and the y translation stages of the etching apparatus. The software controlling the stages was refined so as to execute spatially varying adjustments in the speed and acceleration in both the x and the y directions. These changes ensured that the curve drawn followed the coordinates of the data file with fidelity (to within $\pm$ 0.1μm); the procedure also produces a constant tangential speed and thus a constant etch depth. With this computer control, bends of different radii of curvature (1, 2, and 4 mm) and widths (10, 15, and 20 μm) were defined by etching pairs of 0.5-μm-deep 2-μm-wide trenches. Linear waveguides were added to both ends of the bends so as to allow more convenient cleaving and subsequent optical testing. The fiber-to-waveguide coupling loss in these structures which have asymmetric cross-sections ranged between 5 and 10 dB, depending on the waveguide width. The transmission of these bends was measured and the results are shown in Fig. 5. As can be seen in that figure, bends with a 2-mm radius of curvature had the lowest loss. This result agrees with our computer simulation of 90° bends with different radii of curvature, and can be understood by the fact that bends with a 1-mm radius of curvature incurred excessive radiation loss, whereas those with a 4-mm radius of curvature incurred excessive linear loss. In addition, the results of Fig. 5 show that the bends with the closer trenches (10 μm) were less lossy, a result that was expected from our computer simulation of 90° bends with different trench separations in the multimode regime (see Fig. 2). Thus, the operational characteristics of the fabricated 90° bends agreed with the simulations in all regards; namely, 10 μm and 2 mm were the optimal values for the trench separation and the radius of curvature, respectively. These values were selected for use in the delay-line circuit.

Asymmetric splitters with various splitting ratios were also prototyped. As mentioned above, the splitting ratio was varied by changing the interaction length L in the splitting region [shown in Fig. 1(b)]. These devices were characterized and a plot of the percentage of power switching out of the optical bus and into the bent arm vs. interaction length is shown in Fig. 3(b) with the theoretical plot. Notice that the experimental data points follow the theoretical curve quite well. Using the experimental data, the interaction length was selected to yield the desired splitting ratio for the various splitters.

After the design parameters of the individual components of the delay lines were separately optimized, these components were fabricated into complete delay lines. The computer-controlled fabrication sequence involved simply merging the separate data files. First, one-sided four-output delay lines were fabricated as shown in Fig. 6(a). The structures were characterized in terms of the percentage of power transmitted out of each arm. As shown in Fig. 7(a), all the outputs are within 4% of 25%. The total on-chip losses (i.e., excluding the facet losses) incurred by such structures were measured to be 2.05 dB for the whole structure, i.e., when the sum of the four outputs is compared with the light coupled into the input waveguide. Of these losses, 1.81 dB are due to linear losses in the 1.81-cm total waveguide length (the linear losses of 1 dB/cm consist of 0.4 dB/cm absorption loss and 0.6 dB/cm scattering loss); the remaining 0.24 dB is due to the curvature in the 90° bends, which agrees with the value predicted earlier in the simulation of these bends; this loss is comparable to some of the best reported in the literature [4], [13]. Two-sided eight-output delay lines were also fabricated, and one such structure is shown in Fig. 6(b). As demonstrated in Fig. 7(b), the measured power in each output arm is within 2% of 12.5%.

A measurement of the time delays between successive outputs was carried out on the four-output circuit. The setup used in this test is shown in Fig. 8. Light modulated at 10.24 GHz was launched into the input waveguide and, with the use of a high-frequency digital sampling oscilloscope and curve-fitting software, the phase shift between the microwave signals at each of the outputs and a reference signal was measured; a comparison of these phase shifts yielded the time delay between different outputs due to the path difference. A plot showing the four waveforms measured relative to the reference signal is shown in Fig. 9. These measurements yielded, for each path difference of 600 μm, a delay of 8 $\pm$ 2 ps, which includes the expected value of 6.8 ps.

IV. Conclusion

In summary, the technique of laser-induced photoelectrochemical etching, in conjunction with advanced computer simulations, was used to fabricate photonic-integrated optical-delay circuits for phased-array radar. The fabrication process is rapid; for example, the eight-output delay lines with $\sim$ 2 cm total length of waveguiding structures were etched in under 15 minutes. The computer simulations, combined with rapid prototyping abilities, allowed the design and optimization of the delay lines prior to fabrication. These structures were tested and found to exhibit good splitting ratios and appropriate delays. These results show that high-quality large-area all-optical circuits can be fabricated efficiently. Finally, the techniques discussed in this paper appear promising for prototyping of other large-scale photonic integrated circuits including switching arrays and wavelength demultiplexers.

References

[1] W. Ng, A. A. Walston, G. L. Tangonan, J. J. Lee, I. L. Newberg, and N. Bernstein, "The first demonstration of an optically steered microwave phased array antenna using true-time-delay," *J. Lightwave Technol.*, vol. 9, pp. 1124–1131, 1991.

[2] K. Y. Lau, "Optoelectronic technologies for optically controlled phased array radar," in *MTT Conf. Tech. Dig.*, 1992, pp. 365–368.

[3] A.Seeds, "Optical beamforming techniques for phased-array antennas," *Microwave J.*, pp. 74–83, 1992.

[4] W. Ng, D. Yap, A. Narayanan, R. Hayes, and A. Walston, "A detector-switched GaAs monolithic time-delay network for microwave phased arrays at L and X band," in *Integrated Photon. Res. Topical Meet. Tech. Dig.*, 1993, Palm Springs, CA, vol. 10, pp. 418–421.

[5] H. R. Fetterman, Y. Chang, D. C. Scott, S. R. Forrest, F. M. Espiau, M. Wu, D. V. Plant, J. R. Kelly, A. Mather, W. H. Steier, R. M. Osgood Jr., H. A. Haus, and G. J. Simonis, "Optically controlled phased array radar receiver using SLM switched real time delays," to appear in *IEEE Photon. Technol. Lett.*

[6] R. Scarmozzino and R. M. Osgood Jr., "Comparison of finite-difference and Fourier-transform solutions of the parabolic wave equation with emphasis on integrated-optic applications," *J. Opt. Soc. Amer.*, vol. A8, pp. 724–731, 1991. For application of beam propagation techniques to complex integrated-optic problems, see I. Ilic, R. Scarmozzino, R. M. Osgood Jr., J. T. Yardley, K. W. Beeson, and M. J. McFarland, "Modeling multimode-input star couplers in polymers," *J. Lightwave Technol.*, vol. 12, pp. 996–1003, 1994.

[7] L. Eldada, M. N. Ruberto, R. Scarmozzino, M. Levy, and R. M. Osgood Jr., "Laser-fabricated low-loss single-mode waveguiding devices in GaAs," *J. Lightwave Technol.*, vol. 10, pp. 1610–1616, 1992.

[8] A. E. Willner, M. N. Ruberto, D. J. Blumenthal, D. V. Podlesnik, and R. M. Osgood Jr., "Laser fabricated GaAs waveguiding structures," *Appl. Phys. Lett.*, vol. 54, pp. 1839–1841, 1989.

[9] M. N. Ruberto, R. Scarmozzino, A. E. Willner, D. V. Podlesnik, and R. M. Osgood Jr., "Graded-effective-index waveguiding structures fabricated with laser processing," *SPIE Proc.*, vol. 1215, pp. 538–557, 1990.

[10] M. N. Ruberto, X. Zhang, R. Scarmozzino, A. E. Willner, D. V. Podlesnik, and R. M. Osgood Jr., "The laser-controlled micrometer-scale photoelectrochemical etching of III-V semiconductors," *J. Electrochem. Soc.*, vol. 138, pp. 1174–1185, 1991.

[11] L. Eldada, M. Levy, R. Scarmozzino, and R. M. Osgood Jr., "Laser rapid prototyping of photonic integrated circuits," *SPIE Proc.*, vol. 2213, pp. 36–47, 1994.

[12] L. Eldada, N. Zhu, M. N. Ruberto, M. Levy, R. Scarmozzino, and R. M. Osgood Jr., "Rapid direct fabrication of active electro-optic modulators in GaAs," *J. Lightwave Technol.*, vol. 12, pp. 1588–1596, 1994.

[13] R. J. Deri and E. Kapon, "Low-Loss III-V semiconductor optical waveguides," *IEEE J. Quantum Electron.*, vol. 27, pp. 626–640, 1991.

Louay Eldada (M'88) was born in Beirut, Lebanon, on October 3, 1966. He received the B.S. and M.S. degrees from the Columbia University School of Engineering and Applied Science in 1989 and 1991, and the M.Phil. and Ph.D. degrees from the Columbia University Graduate School of Arts and Sciences in 1993 and 1994, all in electrical engineering.

In 1990, he worked as a Research Assistant at the IBM East Fishkill laser laboratory. His work involved setting up laser systems for the study of interaction of light with matter. In 1991, he engaged in research at the Columbia University Microelectronics Sciences Laboratories in a variety of topics related to laser-induced processing of electronic materials, especially III-V compound semiconductors. These topics included materials deposition, patterning, and etching as well as integrated optical devices and photonic integrated circuits modeling, fabrication, and characterization. Since 1994, he has been conducting research in optical polymers at AlliedSignal in Morristown, NJ. His work involves the design, fabrication, and characterization of high-performance optical interconnect devices and circuits in polymeric materials.

Dr. Eldada is a member of the Lasers and Electro-Optics Society and the Optical Society of America.

Robert Scarmozzino was born in New York, NY, on July 12, 1961. He received the B. S. and M. S. degrees from the Columbia University School of Engineering and Applied Science in 1982 and 1983, and the Ph.D. degree from the Columbia University Graduate School of Arts and Sciences in 1987, all in applied physics. His graduate research was in the area of plasma physics, and primarily consisted of an experimental and theoretical study of collisionless trapped particle instabilities.

Since 1987, he has been engaged in research at the Columbia University Microelectronics Sciences Laboratory in a variety of applied physics topics related to laser-induced semiconductor processing. These include experiments with, and modeling of, materials deposition and etching, and process diagnostics. More recently, his work has been concentrated in the areas of integrated optics and optoelectronics, and has involved both simulation and fabrication of novel photonic devices and circuits. He is currently a Research Scientist at the Columbia University Microelectronics Sciences Laboratory.

Dr. Scarmozzino has been a member of the American Physical Society, the Materials Research Society, the Electrochemical Society, the International Society for Optical Engineering, and the Sigma Xi Society.

Richard M. Osgood Jr. (SM'82-F'87) received the B. S. degree in engineering at the U.S. Military Academy, the M. S. Degree in physics at Ohio State University, and the Ph.D. in physics at the Massachusetts Institute of Technology.

He is Professor of applied physics and electrical engineering at Columbia University in the City of New York. Prior to this appointment, he served on the scientific staff of M.I.T., Lincoln Laboratory (Solid State Physics Division), the U.S.A.F. Avionics Laboratory, and the U.S.A.F. Materials Laboratory. Throughout his professional career he has performed research in many areas of Electrical Engineering, Physical Chemistry, and Optical Physics. His most extensive research has been in the development of new infrared and ultraviolet lasers, the application of laser-induced chemistry to materials preparation, and optical surface physics and chemistry.

Dr. Osgood is a member of the ACS, OSA, MRS, and Fellow of the OSA. He is Co-Editor of *Applied Physics*. Along with Dr. Steven Brueck, he organized the first MRS symposium on Laser Diagnostics and Photochemical Processing. He has served as a consultant to numerous government and industrial organizations, including the DARPA Materials Research Council, DOE Basic Energy Sciences Advisory Board and the Los Alamos National Laboratory Chemistry Advisory Board. In Oct. of 1983, he was elected to a 3-year term as councillor of the Materials Research Society. In 1986, he was selected to be an IEEE-CLEOS Distinguished Traveling Lecturer. He was also appointed Distinguished Traveling Lecturer of the APS for 1991–1993. In 1991, he received the R.W. Wood Prize from the Optical Society of America. He was formerly the Co-Director of the Columbia Radiation Laboratory and Director of the Microelectronics Sciences Laboratories. During the academic year 1994-1995, he was Visiting Professor of Electrical Engineering at the Massachusetts Institute of Technology.

David C. Scott received the B. S. degree in electrical engineering from the University of California at Los Angeles in 1990 and the M. S. degree in electrical engineering in 1992. He is currently working toward his Ph.D. degree at UCLA specializing in the optical control of HBT's and applications toward optoelectronic systems.

Yian Chang received the B.S. degree in physics from the National Tsing-Hua University in Taiwan in 1988 and the M.S. degree in physics from the University of California at Los Angeles in 1991. He is currently working toward his Ph.D. degree at UCLA specializing in the microwave and millimeter wave phase conjugation.

Harold R. Fetterman (F'90) received the Ph.D. degree from Cornell University in 1967.

He is currently a Professor in the Department of Electrical Engineering at the University of California at Los Angeles. He joined UCLA after 14 years at the MIT Lincoln Laboratory, where he was active in submillimeter-wave/millimeter-wave detectors and source programs. He successfully developed heterodyne receivers and solid-state sources with applications in plasma diagnostics, remote sensing, and radar modeling. Since coming to UCLA, he has concentrated on millimeter-wave GaAs and InP devices and the optical control and testing of high frequency systems.

Dr. Fetterman is a Fellow of OSA.

Microwave Phase Conjugation using Arrays of Nonlinear Optically Pumped Devices

Y. Chang, D. C. Scott and H. R. Fetterman
Electrical Engineering Department
University of California at Los Angeles
Los Angeles, CA 90095, USA

Abstract

Phase conjugation is a technique for reversing both the direction of propagation and the overall phase factor of an incoming wave. Up to date, most of the development has been concentrated on the optical regime due to the nonlinearity and power density restriction. Extension of phase conjugation techniques to microwave frequencies has been explored using arrays of mixing elements with antennas to form nonlinear surfaces.[1] In this work, we report the use of optical signals as carriers of the microwave pump signal. This optical injection technique is the key to making simple, viable, low cost microwave phase conjugation element arrays.

1. INTRODUCTION

In general, phase conjugation technique utilizes the nonlinearity of a medium to reverse the phase factor of an incoming wave. The properties of phase conjugate waves are useful in applications requiring automatic pointing and tracking, phase aberration corrections, phase conjugate resonators, and many other applications. Various nonlinear optical effects can be utilized to conjugate the phase of an optical beam in real time.[2] Among these effects, three wave mixing (TWM) utilizes the second-order nonlinearity. With a crystal as the nonlinear material, the induced nonlinear polarization can be written as:

$$P_{NL} = \chi^{(2)} E^2 \tag{1}$$

Of all possible second-order terms that arise from E^2, we are interested only in terms which satisfy the frequency and momentum relation:

$$\omega_1 - \omega_2 = \omega_3,\ \mathbf{k}_1 + \mathbf{k}_2 = \mathbf{k}_3 \tag{2}$$

where subscript 1 is for the pump beam, 2 is for the incoming wave, 3 is for the phase conjugate wave and $\omega_1 = 2\omega, \omega_2 = \omega_3 = \omega$. Equation 2 sets up a very strong restriction on TWM in crystals: all three waves must be close to collinear. However, if the nonlinearity is strong enough such that the phase conjugate wave can be generated on a surface, the momentum relation is relaxed from equation 2 and thus TWM can be effective even the waves are not close to collinear. The restriction of small angular field of view of the input wave can also be removed if degenerate four wave mixing (DFWM) technique is used. In a conventional DFWM experiment, the useful nonlinear polarization induced can be written as:

$$P_{NL} = \chi^{(3)} E^3 \tag{3}$$

The phase conjugate wave arises from the terms satisfy:

$$\omega_1 + \omega_2 = \omega_3 + \omega_4,\ \mathbf{k}_1 + \mathbf{k}_2 = \mathbf{k}_3 + \mathbf{k}_4 \tag{4}$$

where subscripts 1 and 2 are for the pump beams, 3 is for the phase conjugate wave, 4 is for the incoming wave and $\omega_1 = \omega_2 = \omega_3 = \omega_4 = \omega$.

Efforts to extend optical phase conjugation techniques to longer wavelengths have encountered severe difficulties due to the small nonlinear susceptibility of crystals and the low power density in this regime. In the search for alternative materials suitable for the use in microwave and millimeter wave nonlinear optics, artificial media were found to have much larger nonlinearity than in the case of crystals. Using shaped microparticle suspensions as the nonlinear medium, microwave phase conjugation has been demonstrated in a waveguide environment utilizing DFWM.[3].

In this paper, we demonstrate two concepts: 1. optical injection of the microwave TWM pump signal into the nonlinear devices. 2. using an array of optically injected elements to generate phase conjugate waves.

2. EXPERIMENT

To demonstrate the concept of using microwave devices in TWM to generate conjugate phase, a triple balanced mixer can be used as the nonlinear element. The mixer output signal can be written as:

$$V_{IF} = a(V_{LO} + V_{RF})^2 \tag{5}$$

The conjugate phase arises from the term with the difference frequency: $\omega_{LO} - \omega_{RF}$. The incoming signal sending into the RF port of the mixer carries a phase factor $\omega t + \varphi$. It is mixed with $2\omega t$ (LO) to generate the conjugate phase: $\omega t - \varphi$ (IF). The other second-order terms can be filtered out by a bandpass filter.

The initial efforts to demonstrate optical injection used fiber optics feeds and eliminated the need of a frequency doubling amplifier for generating the pump signal (2ω), as shown in Fig. 1.

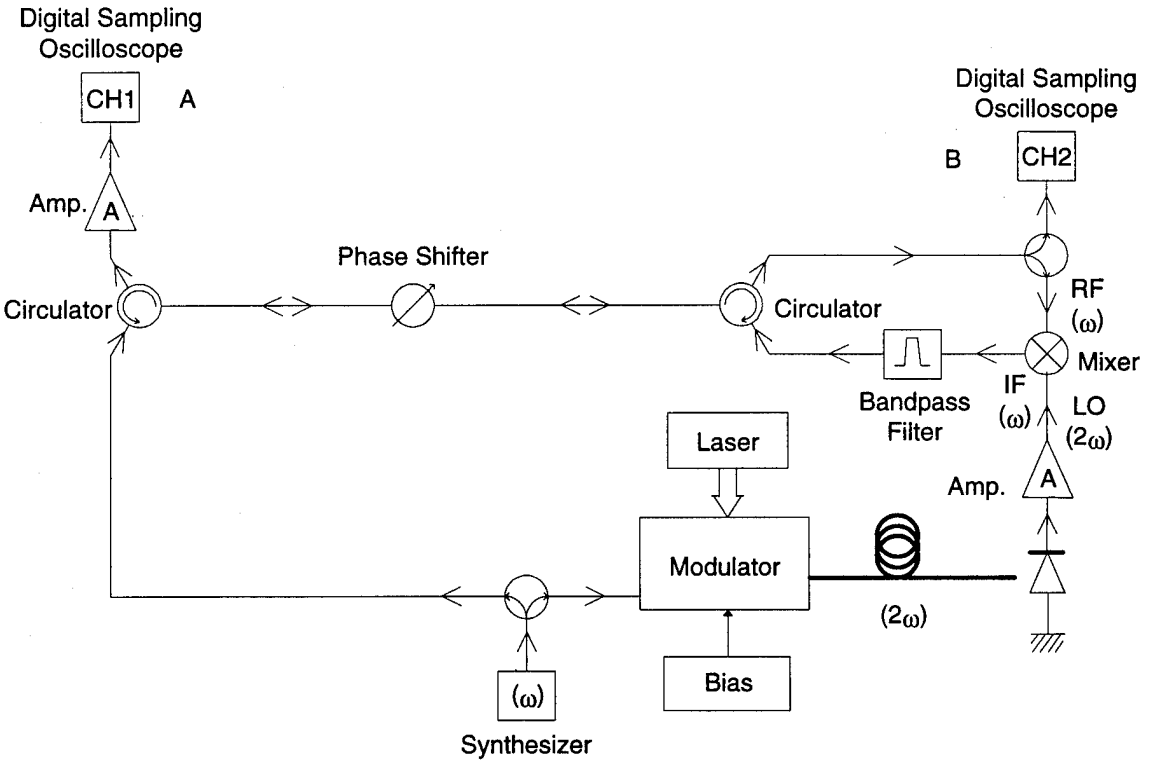

Fig. 1. Initial experimental setup of optically injected conjugate phase generation.

A $LiNbO_3$ electro-optical modulator was biased at its transfer function extremum, therefore producing modulation at 2ω (20GHz) of the 1.3μm laser beam. After this the light was routed via optical fibers to a PIN diode[4] and the microwave pump signal 2ω was extracted. The 2ω signal was then amplified and sent to the mixer to generate phase conjugate signal. The results are shown in Fig. 2. To prove the signal received at A in Fig. 1 is the phase conjugate signal of the input signal, a phase shifter was inserted in the microwave path. After the incoming signal passed through the phase shifter, it carried a phase shift $+\varphi$. TWM reversed this phase shift to $-\varphi$ and then sent the signal back. As this $-\varphi$ phase-shifted signal passed through the phase shifter, it picked up an additional phase shift $+\varphi$. Therefore at A the overall phase shift caused by the phase shifter was zero: $-\varphi + \varphi = 0$. It is clearly shown in Fig. 2 that the conjugate signal was virtually unchanged while the incoming signal was shifted due to the phase shifter change. This setup used only one element therefore it was an one dimensional experiment and could not be applied to reversing the wavefront. In order to extend to three dimensional phase conjugation, a two dimensional planar array must be used. This issue will be addressed later in the paper.

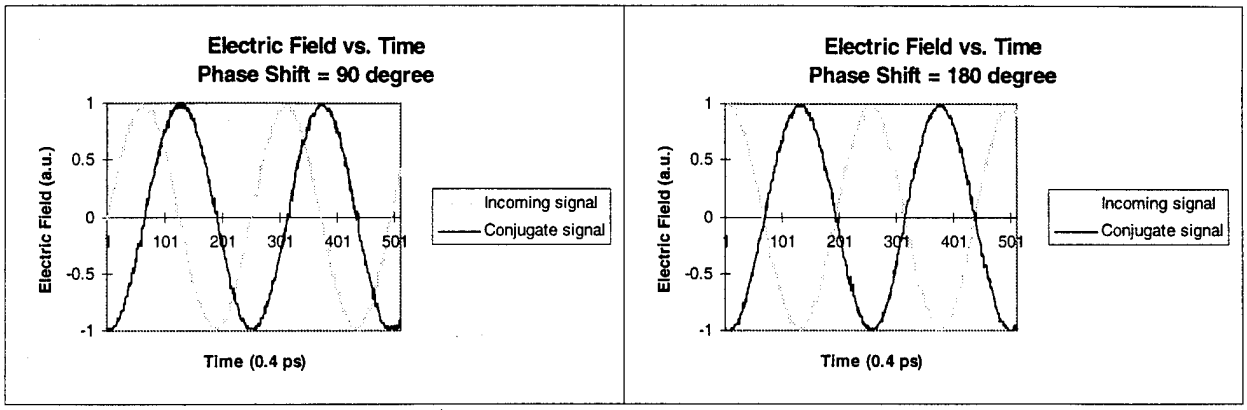

Fig. 2. Incoming and conjugate signals of optically injected phase conjugation generation, monitored on the digital sampling oscilloscope. The incoming signals were recorded at B in Fig. 1 and the conjugate signals were recorded at A in Fig. 1.

In a microwave feed system, the field distribution can pose a significant design challenge. Optical injection of the pump signal can eliminate such problems. Another advantage of optical injection is that it relieves the need of a high power, high frequency (2ω) microwave source. Currently our study of this optical injection concentrates on using a single HBT[5] as the phototransistor and the mixing device. Instead of using a balanced mixer to separate the input signals and the mixed signals, a two-stage mixing is being studied. The incoming signal $\omega t+\varphi$ is first mixed with Ωt to obtain the phase factor $(\Omega-\omega)t-\varphi$. All the other frequency components including the incoming signals are filtered out by a bandpass filter. It is then mixed in the second stage with $(2\omega-\Omega)t$ to acquire the needed phase factor $\omega t-\varphi$. Again a bandpass filter is used to block other frequencies. This two-stage TWM configuration is shown in Fig. 3.

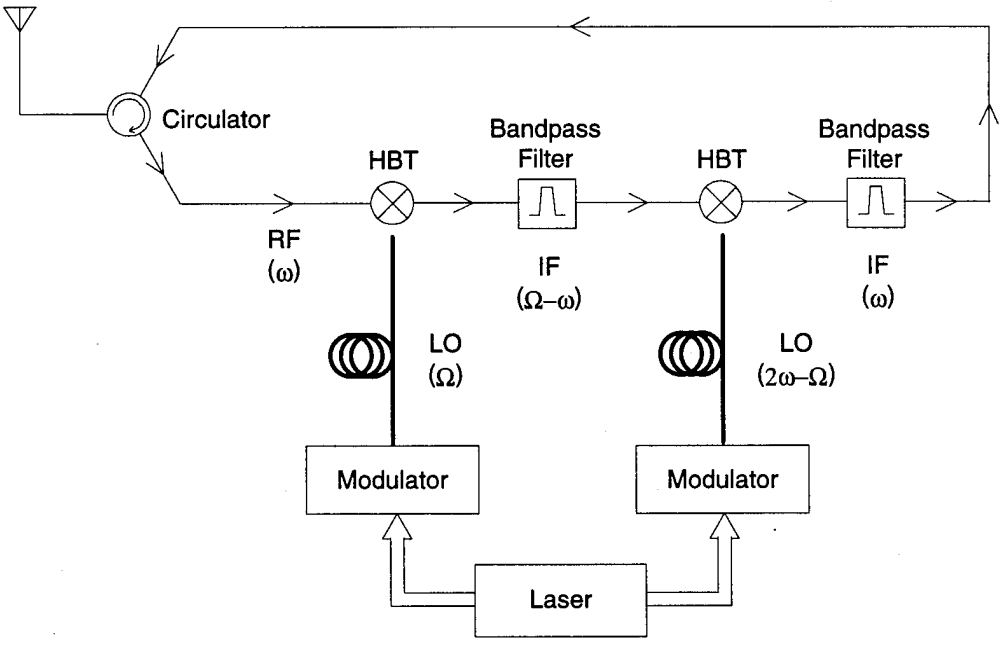

Fig. 3. Schematic of the two-stage three wave mixing experiment. It can be thought as a four wave mixing with two pump beams at Ω and $2\omega-\Omega$.

Up to this point, our discussion concentrated on generating phase conjugate signal at a single element. These one dimensional demonstrations would have little practical use if one could not extend this phase conjugate generation technique to higher dimensions. It can be proven that if the generated phase factor is conjugate to that of the incoming wave on a plane, it will be conjugate everywhere. Therefore an array of conjugate generation elements can provide the ability of generating phase conjugate waves. To demonstrate this concept, a two-element system was

built to show the directivity originated from phase conjugation. The setup is shown in Fig. 4. Both the transmitting horn and the receiving horn are mounted on rotational stages. The receiving horn is slightly higher and behind the transmitting one. After setting up the transmitting horn at an arbitrary angle, the receiving horn was moved around until the received signal was maximized on the sampling oscilloscope. The receiving horn was always able to follow the transmitting horn. To prove this directivity was caused by phase conjugation instead of reflection, the pump signal was turned off at one element and the directivity disappeared. A dielectric material was also inserted into the microwave path and the received signal showed no phase shift. By moving the receiving horn around, we also found the FWHM width of the conjugate beam was approximately 60°. This agreed with the theoretical value calculated by two-element interference.

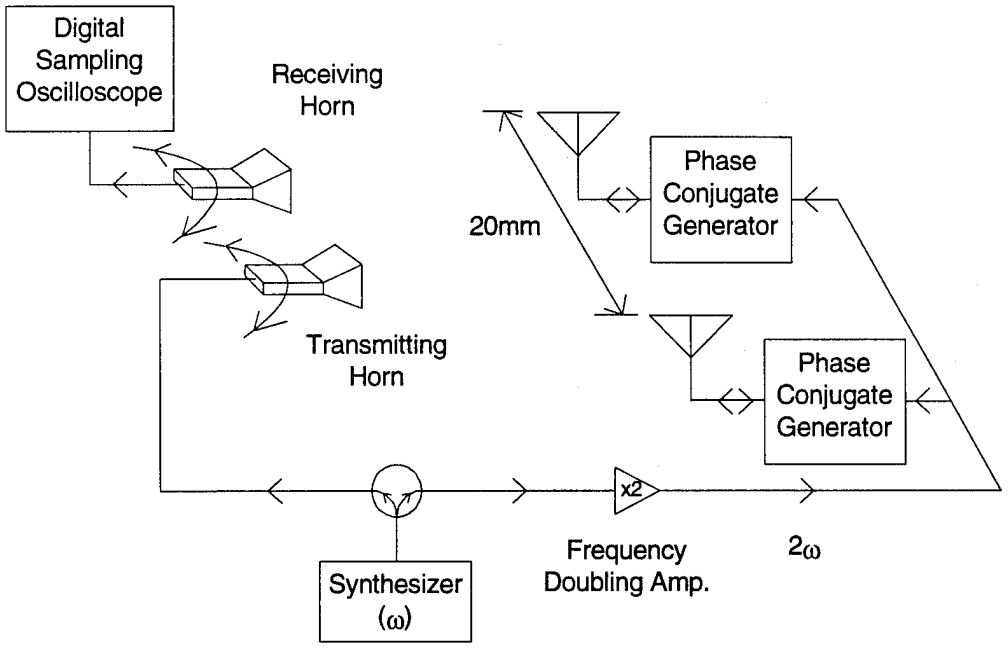

Fig. 4. Experimental setup of the two-element array phase conjugation system. The phase conjugate generators shown in the drawing are similar to the mixer circuit in Fig. 1.

The next generation edge coupled HBTs are being fabricated with an optical waveguide in the base collector depletion regions. The passive waveguide is designed to maximize input light coupling while the HBT is independently optimized for high speed mixing operation. These HBTs can then be integrated to form microwaves nonlinear optically pumped surfaces (MNOPS) as shown in Fig. 5. These surfaces can be thought as an artificial nonlinear material which can operate at tens of GHz .

3. CONCLUSION

We have demonstrated that optically injected microwave devices in conjunction with antennas can be used to generate free space phase conjugate waves in the microwave and millimeter wave regime. By using HBTs with integrated optical waveguides, this technique can be simplified and more efficient. The directivity and wavefront quality of conjugate waves will be improved as the number of conjugate elements increases. Currently, we are constructing a four-element array based on optically pumped TWM.

The authors would like to thank Prof. R. W. Hellwarth for the helpful discussions.

This research is supported in part by AFOSR and NCIPT.

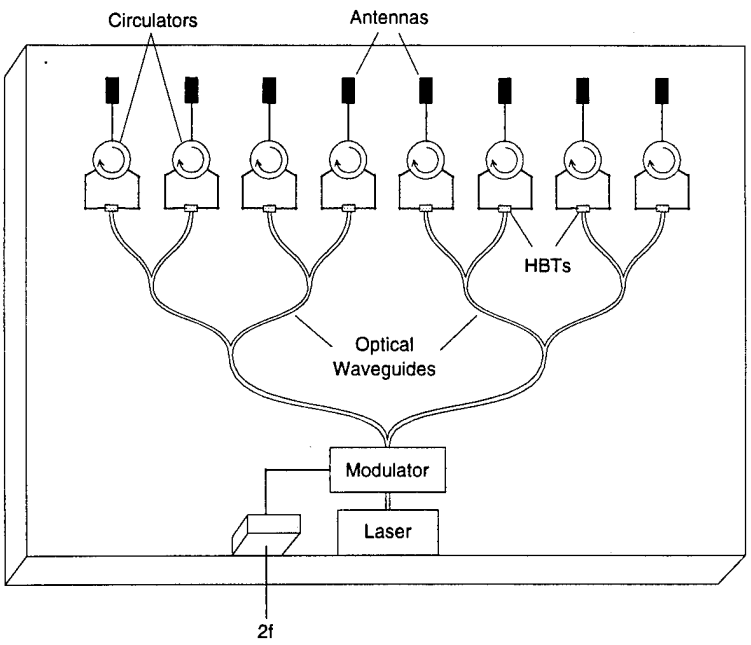

Fig. 5. Microwaves nonlinear optically pumped surface for two dimensional phase conjugation generation.

4. REFERENCES

[1] C. C. Cutler, R. Kompfner and L. C. Tillotson, "A Self-steering Array Repeater," Bell Syst. Tech. J., vol. 42, pp. 2013-2032, Sept. 1963.

[2] M. Gower and D. Proch, Optical Phase Conjugation, Springer-Verlag, New York, 1994.

[3] R. Shih, H. R. Fetterman, W. W. Ho, R. McGraw, D. Rogovin, and B. Bobbs, "Microwave Phase Conjugation in a Liquid Suspension of Elongated Microparticles," Phys. Rev. Lett., vol. 65, pp. 579-582, July 1990.

[4] Y. Liu, S. R. Forrest, G. L. Tangonan, R. A. Jullens, R. Y. Loo, V. L. Jones, D. Persechini, J. L. Pikulski, and M. M. Johnson, "Very-high-bandwidth InGaAs PIN Detector Arrays," IEEE Photon. Technol. Lett., vol. 3, pp. 931-933, Oct. 1991.

[5] D. C. Scott, D. V. Plant and H. R. Fetterman, "60 GHz Sources Using Optically Driven Heterojunction Bipolar Transistors," App. Phys. Lett., vol. 61, pp. 1-3, July 1992.

100 GHz CW GaAs/AlGaAs MULTIQUANTUM WELL IMPATT OSCILLATORS

C. C. Meng and H. R. Fetterman
Department of Electrical Engineering
University of California, Los Angeles
Los Angeles, CA 90024

D. C. Streit, T. R. Block and Y. Saito
TRW
Space & Electronics Group
Redondo Beach, CA 90278

ABSTRACT

Multiquantum well structures can be applied to the high frequency IMPATT oscillators. The first CW operation of GaAs/AlGaAs multiquantum well IMPATT oscillators at 100 GHz is reported here. Preliminary results yielded 6.4 mW CW power at 100.3 GHz in a non-optimized circuit. Significantly higher powers are anticipated with further optimization of the circuit parameters. The modern epitaxial technology opens up a new field for the two terminal high frequency sources.

Utilization of millimeter wave systems demands a high frequency high power semiconductor source. IMPATT (IMPact ionization Avalanche Transit Time) devices are still the most powerful solid state and convenient high frequency sources for the frequency range of 50-100 GHz. For a high frequency operation, an IMPATT device is biased at high electric fields and saturation of ionization rates occurs. The strong reduction of the nonlinearity of the avalanche process at high electric fields results in a wide avalanche injection current pulse in a less localized avalanche region and degrades the device efficiency [1]. The ionization rate saturation limitations can be reduced by replacing the bulk avalanche region by a multiquantum well structure [2]-[4]. Efficiencies of 13% at 100 GHz and 10% at 140 GHz were projected for GaAs/AlGaAs single-drift flat-profile multiquantum well IMPATT devices. Higher efficiency can be expected by using double-drift and (or) Read type structures. Christou et al. made a GaAs/AlGaAs multiquantum well MITATT (MIxed Tunneling Avalanche Transit Time) device and achieved 2% efficiency at 94 GHz under pulsed operation [5]. In this letter, we report the first experimental results of CW operation of GaAs/AlGaAs multiquantum well IMPATT devices at 100 GHz. Although direct comparison with GaAs devices is not possible, because of the different circuit parameters, the successful operation of this quantum well device at high frequency proves the feasibility of using such heterojunction structures.

For a high frequency operation, an IMPATT device must be biased at high electric fields and saturation of the ionization rates occurs. The strong reduction of the nonlinearity of the avalanche process results in a wide avalanche injection current pulse in a less localized avalanche region and degrades the device efficiency. The ionization rate saturation limitations can be reduced by replacing the bulk avalanche region by a GaAs/AlGaAs multiquantum well structure. In a multiquantum well structure, when

an electron (hole) enters the barrier region, it loses some energy to the band discontinuity and encounters a higher ionization threshold energy. Thus, an electron (hole) can gain some energy without impact ionization while traveling through the barrier region if the barrier thickness is less than the energy relaxation length. When the electron (hole) exits the barrier and enters the well, an electron (hole) starts from a non-zero energy to reach the ionization threshold energy. The periodic property of a multiquantum well structure serves as a constant supply for the non-zero starting energy. Thus, the effect of a multiquantum well structure is to reduce the effective ionization threshold energy and correspondingly enhance the ionization rate. Because a higher electric field results in a larger non-zero starting energy and thus a stronger ionization rate enhancement, the ionization rate saturation limitations are reduced in a multiquantum well structure [4].

A single-drift flat-profile was designed and grown on a p^+ ($2 \times 10^{19}/cm^3$, Zn doped) GaAs substrate in an MBE system. Figure 1 illustrates the layer structure of the $GaAs/Al_{0.3}Ga_{0.7}As$ multiquantum well IMPATT device. First, a $5000\mathring{A}$ p^+ ($2\times10^{19}/cm^3$, Be doped) layer was grown on a (100) p^+ GaAs substrate, followed by a $2500\mathring{A}$ n^- active region consisting of five periods of $GaAs/Al_{0.3}Ga_{0.7}As$ quantum wells ($100\mathring{A}$ barrier length and $100\mathring{A}$ well length) for the avalanche region and $1500\mathring{A}$ bulk GaAs for the transit time drift region. The doping densities of GaAs and $Al_{0.3}Ga_{0.7}As$ layers were specified to be $2 \times 10^{17}/cm^3$ and $1.4 \times 10^{17}/cm^3$ respectively to keep the simple growth condition of a constant Si flux. The transit time drift angle (0.75π) at 100 GHz is close to optimal when the electron saturation velocity is 4×10^6cm/sec at 500 K. Finally, a $4000\mathring{A}$ n^+ ($2 \times 10^{18}/cm^3$, Si doped) layer was grown as a cap. The corresponding I-V curve for structure in figure 1 is shown in figure 2. The device shows low leakage current and has the desired hard breakdown voltage at 10 V.

Circular AuGe(900Å)/Ni(150Å)/Au(1μm) metal patterns and mesas were defined on the epitaxial side of the wafer by a conventional photolithography technique. A thick layer of silver (75μm) was electroplated on the epitaxial side of the wafer before the wafer was chemically thinned down from the substrate side to facilitate the handling of this thin wafer for the rest of the fabrication process. After the wafer was chemically thinned down to 10 μm, circular AuGe(900Å)/Ni(150Å)/Au(1μm) metal patterns and mesas were then also defined on the substrate side of this thin wafer. The devices were alloyed on a hot plate. Diodes were separated by dissolving the supporting silver shim.

The diode was then mounted on a diamond heat sink by a thermal compression bonding technique and packaged inside a tiny quartz ring. Inside the package the final device area was adjusted by the trim procedure to have approximate 1 pf at zero bias for r.f. testing.

A W-band (75-110 GHz) reduced height waveguide (10 mil in height) Kurokawa type circuit was used as the oscillator circuit. Three quarter-wavelength reduced height waveguide sections formed a Chebyshev transformer and transformed the reduced height waveguide impedance to the full height waveguide impedance. The oscillator circuit was followed by a simple high frequency measurement set-up. A wavemeter was used to measure the oscillation frequency and r.f. power were obtained from a calibrated thermistor power meter. Figure 3 illustrates the output power and oscillation frequency as a function of the bias current for a diode under test and 6.4 mW CW oscillation at 100.3 GHz has been obtained at 364 mA bias current. Figure 4 shows the spectrum of a CW multiquantum well IMPATT oscillator at 101.3 GHz. Devices tested in a pulsed mode showed oscillation at 94 GHz with power of 127 mW and 2.2% efficiency. All the output powers measured have not been corrected by the circuit loss and thus the real powers from the devices are higher. The device-circuit impedance match-

ing has not been optimized and with further circuit improvement orders of magnitude higher power could be realized from such devices.

In conclusion, the performance of GaAs/$Al_{0.3}Ga_{0.7}As$ multiquantum well IMPATT devices at W-band frequencies was described. Multiquantum well structures have been successfully applied to the high frequency IMPATT devices for the first time to our knowledge. These devices also offer some impressive possibilities for new types of optical control since light can be selectively absorbed in the narrow bandgap well materials. The operation of GaAs/AlGaAs multiquantum well IMPATT devices at frequencies around 100 GHz opens up a new field for the applications of modern epitaxy technologies to two terminal high frequency sources.

ACKNOWLEDGEMENT

This work was supported in part by the Air Force Office of Scientific Research under the direction of Dr. H. R. Schlossberg.

REFERENCES

[1] T. Misawa, Solid-State Electron. **15**, 457, 1972.

[2] D. Lippens, O. Vanbesien and B. Lambert, Journal De Physique, **C5**, 487, 1987.

[3] C. C. Meng and H. R. Fetterman, International Semiconductor Device Research Symposium, 79, 1991.

[4] C. C. Meng and H. R. Fetterman, Solid-State Electron., **36**, 435, 1993.

[5] A. Christou and K. Varmazis, Appl. Phys. Lett. **48**, 1446, 1986.

FIGURE CAPTION

Figure 1. Multiquantum well IMPATT device epitaxial layer structure.

Figure 2. Room temperature I-V curve for the multiquantum well IMPATT structure in figure 1.

Figure 3. Output power and oscillation frequency as a function of the bias current for a CW multiquantum well IMPATT oscillator.

Figure 4. Spectrum of the CW multiquantum well IMPATT diode at 101.3 GHz with 3 MHz resolution bandwidth.

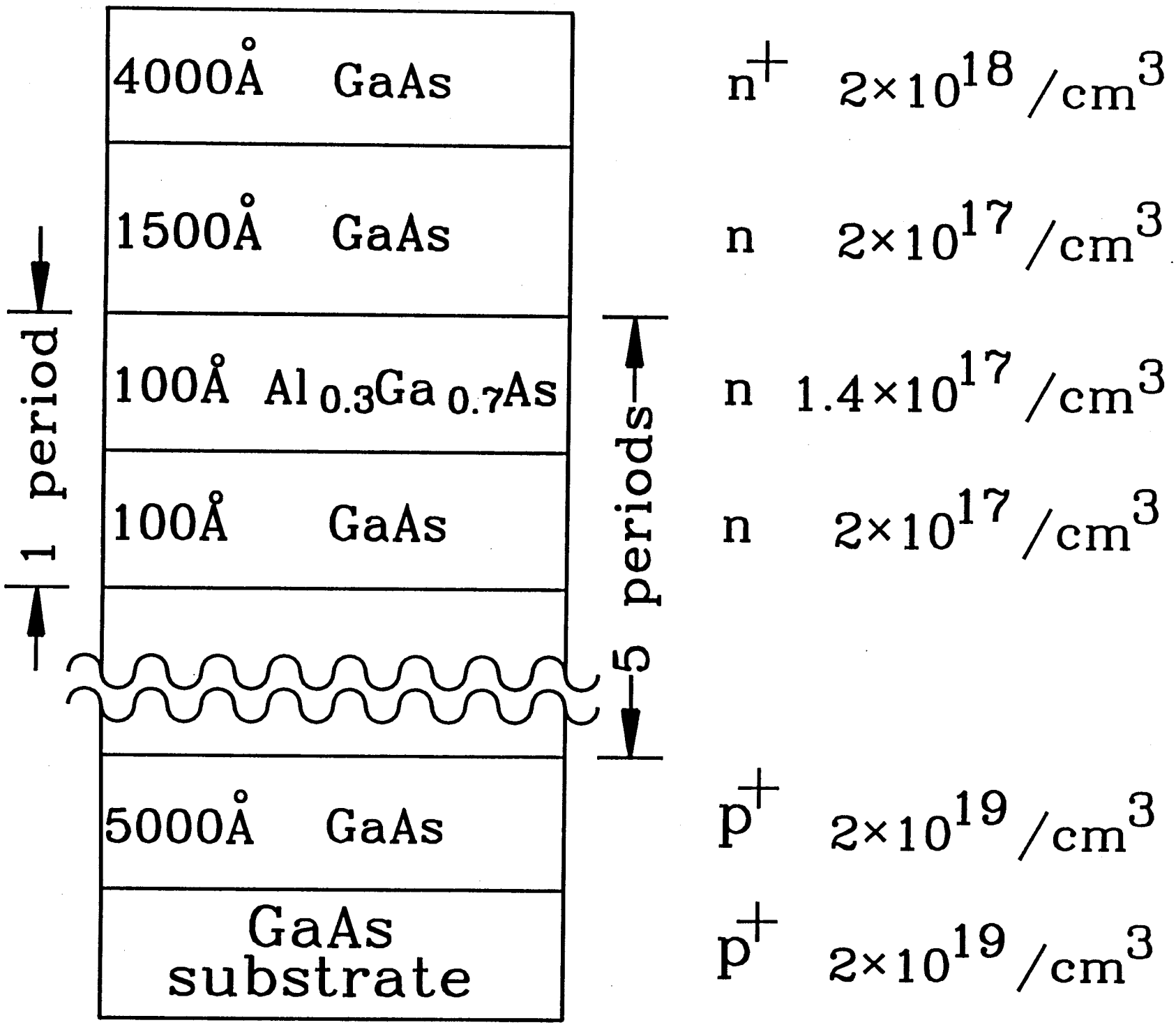
4000Å GaAs
1500Å GaAs
100Å Al0.3Ga0.7As
100Å GaAs
5000Å GaAs
GaAs substrate
1 period
5 periods
n+ 2×10^18 /cm^3
n 2×10^17 /cm^3
n 1.4×10^17 /cm^3
n 2×10^17 /cm^3
p+ 2×10^19 /cm^3
p+ 2×10^19 /cm^3

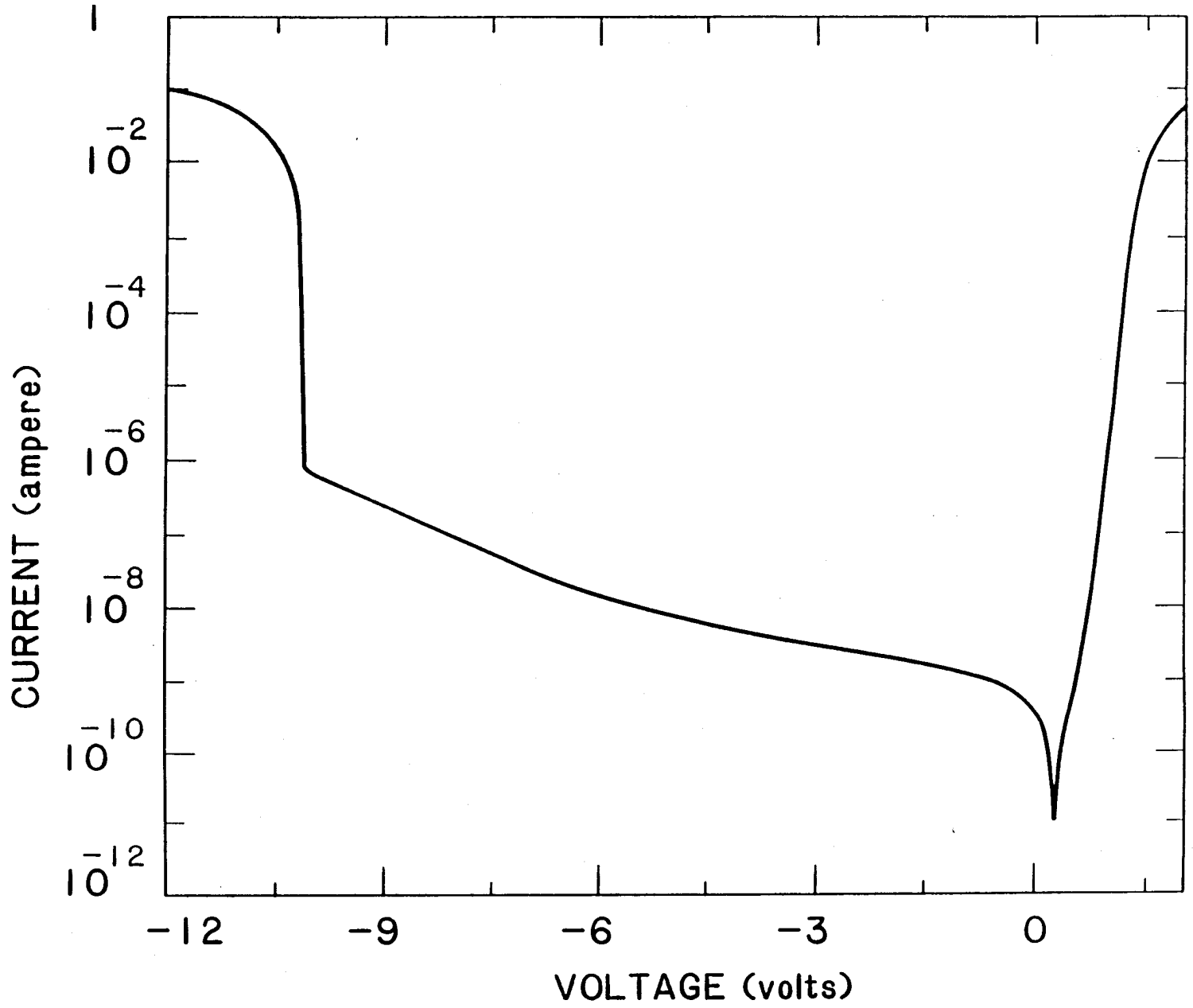
1
10^{-2}
10^{-4}
10^{-6}
10^{-8}
10^{-10}
10^{-12}
CURRENT (ampere)
-12
-9
-6
-3
0
VOLTAGE (volts)

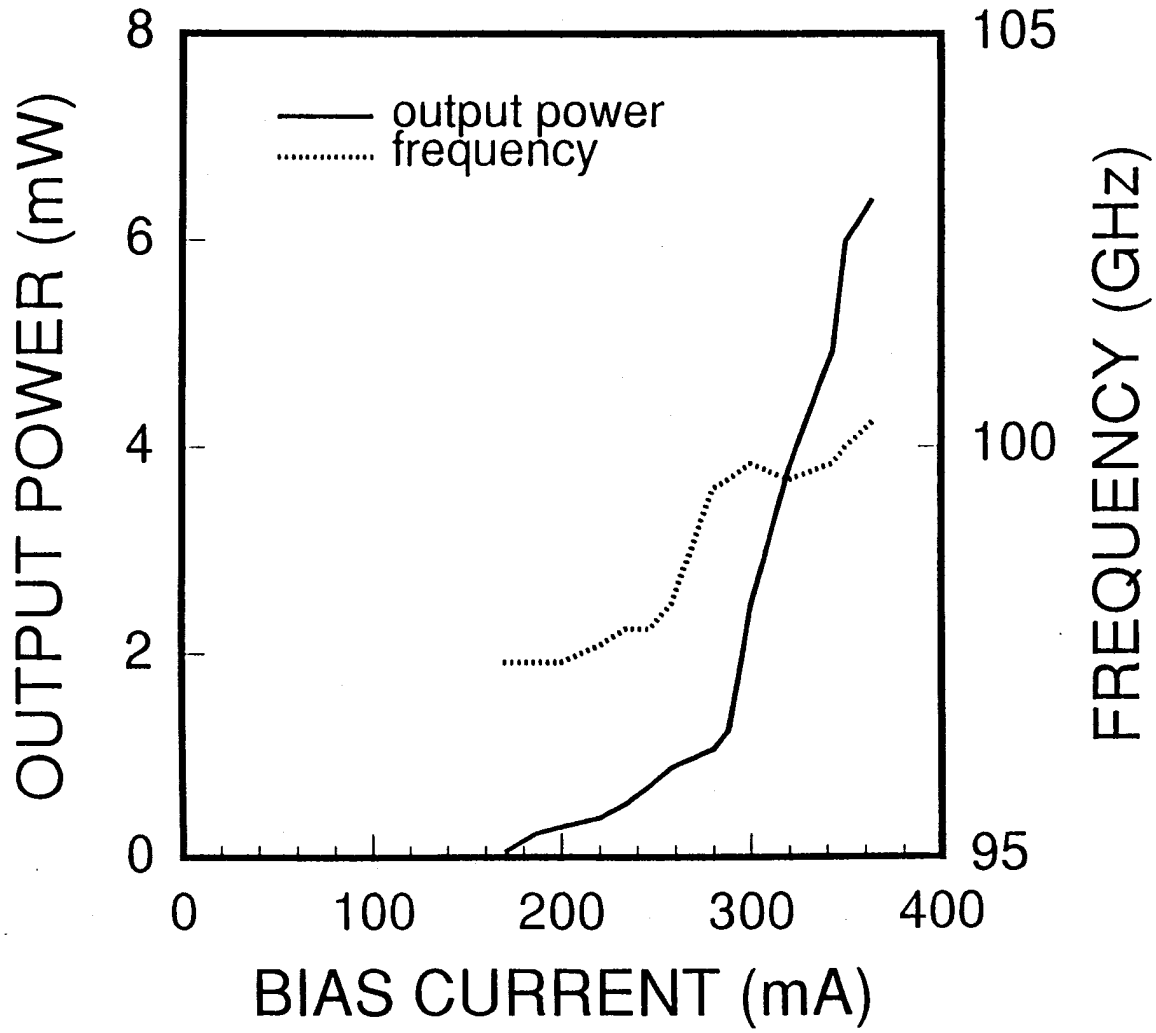
output power
frequency
OUTPUT POWER (mW)
FREQUENCY (GHz)
BIAS CURRENT (mA)
0
2
4
6
8
95
100
105
0
100
200
300
400

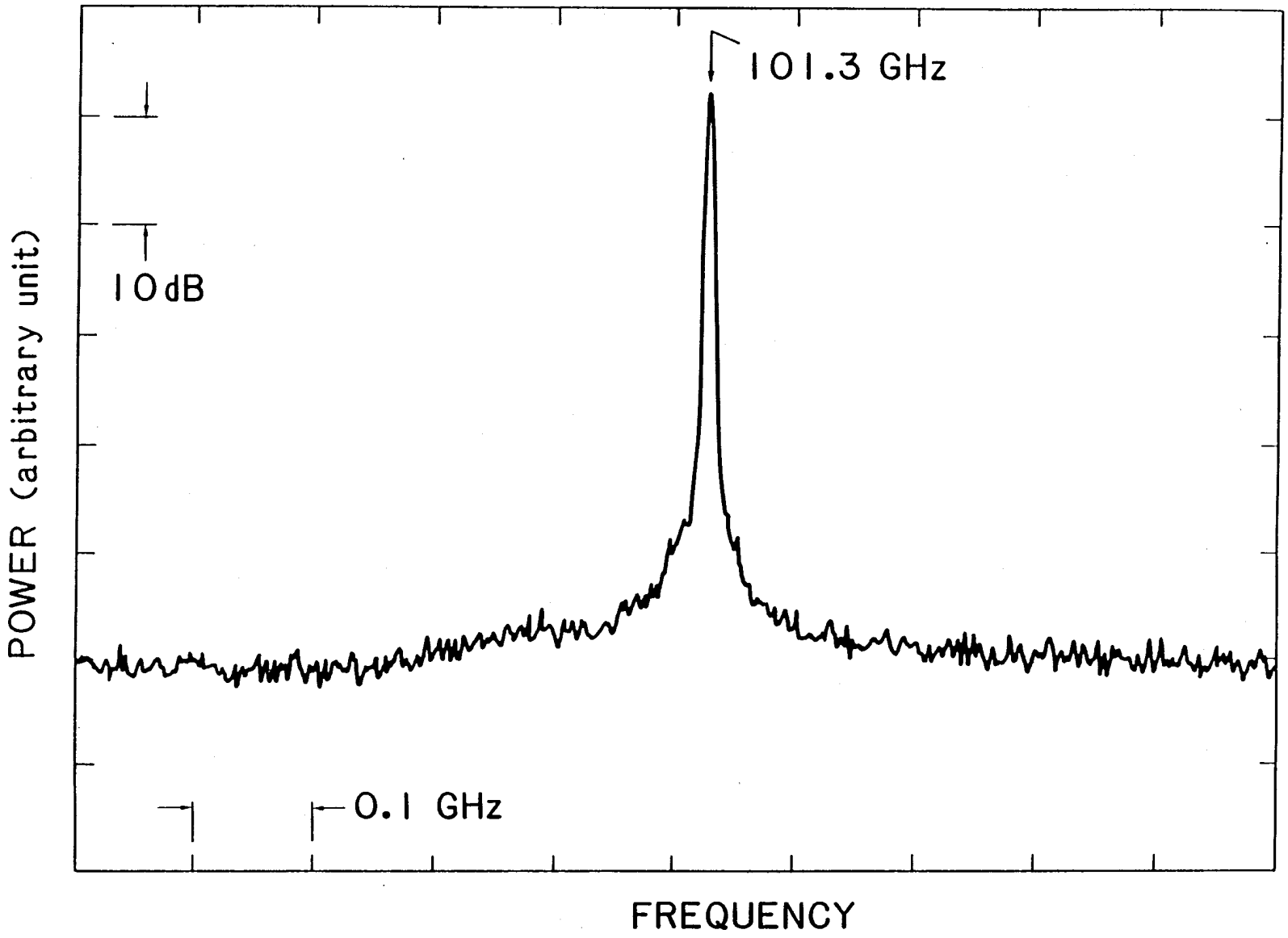
101.3 GHz
10dB
POWER (arbitrary unit)
0.1 GHz
FREQUENCY